UNIVERSITÀ DEGLI STUDI DEL MOLISE

Department of Agricultural, Environmental and Food Sciences

PhD Course in:

AGRICULTURE TECHNOLOGY AND BIOTECHNOLOGY

(CURRICULUM: **FOOD SCIENCE, TECHNOLOGY AND BIOTECHNOLOGY**)

(CYCLE XXX)

Related disciplinary scientific section: CHIM/02 (Physical Chemistry)

PhD thesis

USE OF COLLOID SYSTEMS FOR FOOD AND ENVIRONMENTAL APPLICATIONS

Coordinator of the PhD Course: Prof. Giuseppe Maiorano
Supervisor: Prof. Francesco Lopez
Co- Supervisor: Dr. Francesca Cuomo

PhD Student: Luisa Perugini
153737

ACADEMIC YEAR 2016/2017

Index

Abstract

The importance of colloids is widely recognized thanks to the meaningful contributions available in a huge number of fields that, among the others include food sciences, and optimization of analytical routes.

This thesis focuses on emulsive systems and shows the use of such systems for food and environmental analytical applications.

Regarding the food application, developed in the first part of this work the properties of edible nanoemulsions were studied and used to load and deliver the bioactive molecule curcumin through the gastrointestinal tract. Sodium caseinate represents a good candidate for food emulsion preparations because has surface-active properties and because it is perceived as a natural product by consumers. Nevertheless, it is very sensitive to acidic pH, to be used as an emulsion stabilizer. In order to prevent this drawback, sodium caseinate was used in combination with a non-ionic surfactant (Tween 20) as emulsifier of oil/water nanoemulsions. For these reasons, nanoemulsions stabilized by Tween 20, sodium caseinate and a blend of the two emulsifiers were studied and compared to their response to pH variations. Nanoemulsions were characterized by pH and for protein fluorescence. Noticeably, it was ascertained that, at pH close to caseinate isoelectric point, emulsions stabilized with the blend of caseinate and tween 20 were more stable, compared with emulsions stabilized only with sodium caseinate. The presence of Tween 20 ensured the steric stabilization thus improving the role of sodium caseinate as emulsion stabilizer.

The preparation and applicability of nanoemulsion containing curcumin were evaluated. Their suitabiliy as carrier was tested through a simulated in-vitro digestion procedure for the assessment of the bioaccessibility of ingested curcumin. Nanoemulsions stabilized by the blend of emulsifiers were able to solubilize more curcumin than nanoemulsions stabilized by caseinate only. In particular, the latter nanoemulsions, at their best, solubilized about 55 μg of curcumin per mL of nanoemulsion while, the former reached curcumin concentration around 180 μg / mL. After the simulated digestion both the nanoemulsion types gave high values of curcumin bioavailability compared to those reported in recent literature, and this represents a meaningful outcome. Nevertheless, the best solution to adsorb curcumin seems to be through the nanoemulsion stabilized by caseinate and Tween 20 together because it allowed the bioavailability of a significant amount of curcumin with a lower fat content.

In the second part of this work, the optimization of an analytical route, for an enviromental application was afforded. A number of significant applications in the pollutant determination and

removal field stress the importance of optimizing treatments by utilizing strategies that meet reliability, sensitivity and economicity. A cost-effective analytical method for the Polycyclic Aromatic Hydrocarbons (PAHs) determination in large volume of surface water was accomplished. The central role of the extraction procedure was emphasized. In particular, a new extraction procedure based on Dispersive Liquid Liquid Micro-extraction (DLLME) followed by Gas Chromatography-Mass Spectrometry (GC-MS) for minimizing the sample preparation time and simultaneously obtaining high levels of sensitivity, reproducibility and selectivity was obtained.

The important novelties of the proposed method are two: the application of the extraction technique without the addition of a dispersive solvent and the high sensitivity. The developed method is very sensitive as it allows performing PAHs determinations with a very high pre-concentration factor, up to 10,000 times. Starting from a 1 L surface water sample and reaching a final volume of 100 μL, thus allowing the PAHs determination at very low concentration. Further, it should be considered that large volume sampling can be encountered in the on-line combination of sample pre-treatment and chromatographic analysis with different and high advantages of coupling of sample pre-treatment and chromatographic analysis.

Summary

The Colloidal Science is applied to a large amount of advanced applications in the scientific research field, from biotechnology processes, to medical applications and environmental remediation. Lately, the Colloidal Science has been "restyled", integrating areas of research and development at the interface between Biology, Chemistry and Physics. Colloid suspensions are generally made by at least two phases, one made of particles of various size and shape (made of fluids or solids) dispersed in a massive phase. The main peculiarity provided by colloids is that this dispersity generates an interface between the two phases much larger than the interface that would exist if one phase were layered on the other. To give an idea of the increase of surface area generated by the use of colloids one would think, for example, of taking a cubic particle of side 1 cm and breaking it down into smaller cubes having a side of only 10 nm. The total surface area for the same amount of material then increases from 6 cm^2 to 600 m^2, a surface that would cover the area of two tennis courts.

The interface has an important role because it represents a boundary line between two compartment, for instance one made of oil and the other made of water, where a series of event occurs like chemical reactions, molecular exchange, the interface can provide protection to molecules possibly loaded into the dispersed phase etc. Consequently, the larger is the interface area, the higher is the availability for a reaction to occur, for the molecular exchange to happen, for the protection to be effective.

This thesis is characterised by two main items with the well defined common thread based on the use of colloid systems. In the first part (chapters I-V) of this investigation a compartimentalized system, considered for *food applications*, was studied and characterized to deliver a hydrophobic compound in the human body. In second part (chapters VI-VIII), the compartmentalization was applyed for the optimization of an analytical extraction route, for an *enviromental application*.

Among the colloidal dispersions, emulsions, systems made of oil dispersed in water or viceversa, are commonly used in many major chemical industries, in the pharmaceutical industry, in food chemistry and in biotechnological applications. Therefore, food grade nanoemulsions (emulsions having the oil phase dispersed finely whose size was of the order of few hundread nanometers) made of rice bran oil stabilized in water by protein (sodium caseinate), low surfactant molecule (Tween 20) or by a blend of the twe emulsifier, were characterized and evaluated for their stability to time, temperature and in particular to pH.

The other relavant issue afforded was the possibility of using some of the formulations selected from the previous stage for solubilizing hidrophobic molecules like curcumin. Hence, this compound was loaded in nanoemulsions stabilized by the proteins or by the blend of emulsifiers

through an *in-vitro* digestion procedure, to determine the influence of the different carriers on the bioavailability of curcumin.

In the second part of this thesis the development of a cost-effective, sensitive and reproducible analytical method for the polycyclic aromatic hydrocarbons (PAHs) determination in large volume of surface water was afforded. From an analytical point of view, the importance of the extraction procedure that results in the isolation of chemical compounds present in the matrix is taken for granted. The larger aromatic ring PAHs have very low water solubility and therefore extraction of large volumes of water is typically required to achieve trace level detection and quantitation. In this respect, the use of dispersive liquid–liquid microextraction (DLLME) method that is a sample-preparation technique offering high enrichment factors from liquid samples is practical creating a high surface of contact between the organic solvent for PAHs extraction and the volume of water analysed.

The present thesis is organized in chapter where the ones dedicated to *food applications* are marked with a blue page header (chapters from I to V) and the others, for *environmental applications* with a red page header (chapters from VI to VIII). Accordingly, the contents of the thesis are itemized as follows.

Chapter I illustrates the spreading of colloids from emulsion to foams, from sol to gel, in food industry.

Chapter II presents an introduction to colloid systems showing the forces that govern the colloid association and stability. A particular consideration is given to emulsions and nanoemulsions and to their formation process.

Chapter III describes the experimental techniques applied for the investigation of the food-oriented part of the study.

Chapter IV presents the part of the investigation carried out for improving the stability to acidic pH of caseinate-based nanoemulsion. An advancement on this matter was achieved by using a blend of protein and non-ionic surfactant as nanoemulsion emulsifiers. The results obtained were explained according to the composition of the emulsifiers at the oil/water interface where, at acidic pH, the presence of Tween 20 ensured the steric stabilization thus improving the role of sodium caseinate as emulsion stabilizer.

Chapter V deals with nanoemulsions made of caseinate and Tween 20 (Mix-O/W) selected from the first part of the study that were loaded with curcumin and used in comparison with caseinate O/W nanoemulsions in an in-vitro digestion model to examine the effect of the two systems on the bioaccessibility, transformation and bioavailability of curcumin.

Chapter VI is an introductive chapter on environmental applications, where the characteristics of the PAHs are illustrated together with their aspects concerning the associated toxicology and the sources of exposure.

Chapter VII describes the analytical methods used for the investigation of the environmental-oriented applications.

Chapter VIII presents the study based on the emulsification used as a method to improve the extraction procedure of PAHs from large volume of surface water. The proposed protocol works without the addition of a dispersive solvent but by means of ultrasound energy for dispersing the extraction solvent in the water sample. Breaking of emulsion with the addition of NaCl is then exploited to separate the extraction solvent, further analyzed, from water.

Chapter I

Use of colloid systems for food applications

Fig. I. Some examples of food colloids: gelatin (a); jam (b); milk (c); butter (d); mayonnaise (e); egg yolk (f); meringues (g); bread (h); ice cream (i); champagne (l); beer (m); coffee (n); chocolate (o); chocolate liquor (p).

The chemistry of foods presents many colloidal phenomena. Foods are structurally and compositionally complicated, mostly consisted of colloidal dispersions. Simple colloidal dispersions are two-phase systems, comprising a dispersed phase of small particles, droplets or bubbles, and a dispersion medium (or dispersing phase) surrounding them. Many food products contain two immiscible phases (typically oil and water) as part of the ingredients, and it is crucial to mix and stabilize them in order to produce high quality, stable, and sensory appealing products. These two immiscible phases are often incorporated into food products as emulsions, which are formed by dispersing one phase into the other in the form of small droplets [1-3]. A wide variety of food ingredients and products can be considered to consist either entirely or

partially as emulsions, or have been in an emulsified state sometime during their production, e.g., beverages, butter, cheese, colorants, cream, desserts, flavors, ice cream, margarines, milk, salad dressings, sauces, soups, and yogurts [4-8]. The emulsified components of these foods play important roles in determining their distinct functional attributes, such as appearance, texture, stability, and flavor [9-11]. Hence, the study of food colloids is an important fundamental area of research activity within the field of food science and technology. The primary objective of the food colloid researcher is to understand how the key physical properties of structure, stability, and rheology are influenced by the overall ingredient composition and formulation conditions. An essential aspect of the realization of this objective is an appreciation of how the nature of the interactions between various kinds of dispersed entities (e.g., particles, droplets, bubbles) and macromolecules (proteins and polysaccharides) affects behavior in bulk fluid phases and at solid and liquid interfaces. There are many types of colloidal systems depending on the state of the two substances mixed together. Emulsions, foams, gels, and suspensions form the basis of a wide variety of natural and manufactured materials used in the food [12, 13]; they are characterized by the nature of the continuous and a primary dispersed phases, according to the designations in Table I.

Table I. Types of colloidal dispersion.

Dispersed phase	Dispersion medium	Colloid System
Liquid	Gas	Liquid aerosol
Solid	Gas	Solid aerosol
Gas	Liquid	Foam
Liquid	Liquid	Emulsion
Solid	Liquid	Sol, suspension
Gas	Solid	Solid foam
Liquid	Solid	Gel, solid emulsion
Solid	Solid	Solid suspension

I.1 Food colloids

Table I.2 lists some of the many kinds of food colloids. Some of them are multiple dispersions. For example, ice cream is an emulsion, a foam and a suspension [14].

The food industry's emulsion, foam and suspension products can be very complex since foods contain such a wide array of components, including proteins, fats, emulsifiers, hydrocolloids and particles. Due to their intended use, food colloids need to be non-toxic, non-carcinogenic, and non-allergenic [15]. They also need to be stable for periods of months to years, including stability against such processes as aggregation, creaming, coalescence, and gelation.

Table I.2. Some food colloids: emulsions, foams, and suspensions.

O/W emulsions	Milk, ice cream, creams, coffee creamers, cream liqueurs, soft drink syrups, mayonnaise, béarnaise sauce, sausages, whippable toppings, some salad dressings, some fruit drinks
W/O emulsions	Butter, margarine, spreads, processed cheese, some salad dressings
Foams	Ice cream, whipped cream and toppings, béarnaise, souffles, mousses, aerated icing
Products made from foams	Bread, cakes, meringue, marshmallow
Suspensions	Ice cream, vegetable shortening, chocolate drinks, water ice (a semi-frozen drink)

Sols and gels

Sols and gels are both liquid loving (lyophilic) colloids. A sol is a liquid colloid or mixture in which solid particles are dispersed in a liquid phase (Table I). The disperse phase is attracted to molecules of the continuous phase. Sometimes the mixture needs to be heated and stirred. When this solution cools, the sol changes into a gel, which resembles a solid rather than a liquid (Fig. Ia). Both protein and starch can be used in the formation of a sol or gel. When a jelly is made, gelatine is dispersed into a liquid and heated to form a sol. As the sol cools, protein molecules unwind forming a network that traps water and forms a gel. If cornflour is mixed with water and heated, the starch granules absorb water until their rupture, the starch then disperses in the water and the mixture becomes more viscous and forms a gel on cooling [14]. Other types of gel are formed with pectin and agar. Pectin, a form of carbohydrate found in fruits, is used in the production of jam to help it set (Fig. Ib). Agar is a polysaccharide extracted from seaweed which is able of forming gels. If a gel is allowed to stand for a time, it starts to 'weep'. This loss of liquid is known as syneresis [14].

Emulsions

When water and oil are shaken together, they form an emulsion (Table I). Conventionally, emulsions are classified as either oil-in-water (O/W) emulsions in which oil forms the dispersed phase (oil droplets) and water the continuous phase (e.g., milk and sauces) (Fig. Ic), or water-in-oil (W/O) emulsions in which water forms the dispersed phase and oil the continuous phase (e.g., butter and margarines)[1] (Fig. Id). Oil-in-water emulsions are the most widely used in the food industry (Table I.2). Emulsions are thermodynamically unstable systems, consequently a third component, an amphiphilic compounds ("emulsifiers"), is added to the systems to facilitate emulsion formation and improve emulsion stability [1, 2, 16]. The choice of a specific emulsifier (or blend of emulsifiers) for a particular application is critical for creating successful products, and depends on product formulation, processing conditions, and the desired final properties [1, 17, 18]. Mayonnaise (Fig. Ie) is an example of a stable emulsion of oil and vinegar, when egg yolk

(lecithin) may be used as an emulsifying agent (Fig. If). More information about emulsions are described in Chapter II.

Foams

A foam is a colloidal dispersion in which a gas is dispersed in a continuous liquid phase (Table I). Foams are composed of small bubbles of gas (usually air) dispersed in a liquid, e.g. egg white foam. As liquid egg white is whisked, air bubbles are incorporated. The mechanical action causes albumen proteins to unfold and form a network, trapping the air. As for the emulsions, foams are thermodynamically unstable systems consequently, for forming a stable foam, a surface active foaming agent is essential. The foaming agent lowers the surface tension of the liquid phase and allows expansion of its surface area. The surfactant forms a closely packed film around the dispersed gas bubbles. If egg white is heated, protein coagulates and moisture is driven off. This process forms a solid foam, e.g. a meringue (Fig. Ig). Bread and ice cream are other examples of solid foams (Figs. Ih and Ii, respectively). The foaming and bubbling character of champagne and other sparkling wines have become a symbol of numerous festive events. Champagne (Fig. Il) differs from other wines because it undergoes a second fermentation to provide the carbonation needed for the bubbling and foaming properties. Unlike for champagne, whose foam film lifetimes are short (hydrodynamic control), beer foam (Fig. Im) has a slower drainage rate due to the adsorption of proteins at the interfaces and the generation of a significant disjoining pressure between bubbles [19]. A beer that has smaller bubbles of uniform size tends to have a more stable foam. The beer foam stability is generally increased by increasing concentrations of malt proteins (and/or propylene glycol alginate), metal cations (e.g., Mn^{+2}, Al^{+3}, Ni^{+2}), and hop iso-α-acids, whereas it is generally reduced by increasing amounts of lipids, protein modification, and ethanol [20]. In coffee products, such as espresso (Fig. In), a stable foam is an important aspect of overall product quality, in addition to smell, taste, colour, and body [21]. Foam layer helps trap coffee aromas, providing a more gradual release. The degree of foaming has been found to increase with the degree of roast and the amount of protein in the coffee, while the stability of the produced foam has been related to the amounts of galactomannan and arabinogalactan [21].

Suspensions

Suspensions are colloidal dispersions in which a solid is dispersed in a continuous phase that can be liquid (sol, suspension) or solid (solid suspension) (Table I). Chocolate drinks provide a related example of food suspensions. Chocolate (Fig. Io) is a solid-in-oil (S/O) suspension of non-fat particles (sugar and cocoa) in a continuous phase of cocoa butter, which is the natural fat from the cocoa bean [22]. When cocoa beans are cleaned, roasted, cracked and ground, chocolate liquor results, a suspension of cocoa powder in cocoa butter (Fig. Ip).

References

[1] McClements DJ. Food emulsions: principles, practices, and techniques: CRC press; 2015.
[2] Santana R, Perrechil F, Cunha R. High-and low-energy emulsifications for food applications: a focus on process parameters. Food Eng. Rev. 2013;5:107-22.
[3] Windhab E, Dressler M, Feigl K, Fischer P, Megias-Alguacil D. Emulsion processing—from single-drop deformation to design of complex processes and products. Chem. Eng. Sci. 2005;60:2101-13.
[4] Leal-Calderon F, Thivilliers F, Schmitt V. Structured emulsions. Curr. Opin. Colloid Interface Sci. 2007;12:206-12.
[5] McClements DJ. Emulsion design to improve the delivery of functional lipophilic components. Annu. Rev. Food Sci. Technol. 2010;1:241-69.
[6] Méndez-Velasco C, Goff HD. Enhancement of fat colloidal interactions for the preparation of ice cream high in unsaturated fat. Int. Dairy J. 2011;21:540-7.
[7] Moore R, Duncan S, Rasor A, Eigel W, O'Keefe S. Oxidative stability of an extended shelf-life dairy-based beverage system designed to contribute to heart health. J. Dairy Sci. 2012;95:6242-51.
[8] Sanguansri L, Shen Z, Weerakkody R, Barnes M, Lockett T, Augustin MA. Omega-3 fatty acids in ileal effluent after consuming different foods containing microencapsulated fish oil powder–an ileostomy study. Food Funct. 2013;4:74-82.
[9] Benjamins J, Vingerhoeds MH, Zoet FD, De Hoog EH, Van Aken GA. Partial coalescence as a tool to control sensory perception of emulsions. Food Hydrocolloids 2009;23:102-15.
[10] Chojnicka-Paszun A, De Jongh H, De Kruif C. Sensory perception and lubrication properties of milk: Influence of fat content. Int. Dairy J. 2012;26:15-22.
[11] Chung C, Olson K, Degner B, McClements DJ. Textural properties of model food sauces: Correlation between simulated mastication and sensory evaluation methods. Food Res. Int. 2013;51:310-20.
[12] Stave C, Törner M. Exploring the organisational preconditions for occupational accidents in food industry: A qualitative approach. Saf. Sci. 2007;45:355-71.
[13] McClements D, Decker E, Weiss J. Emulsion-based delivery systems for lipophilic bioactive components. J. Food Sci. 2007;72.
[14] Schramm LL. Emulsions, foams, and suspensions: fundamentals and applications: John Wiley & Sons; 2006.
[15] St Angelo A. A brief introduction to food emulsions and emulsifiers. Elsevier: New York; 1989. p. 1-8.
[16] Dickinson E. Hydrocolloids as emulsifiers and emulsion stabilizers. Food Hydrocolloids 2009;23:1473-82.
[17] Horn AF, Nielsen NS, Jacobsen C. Iron-mediated lipid oxidation in 70% fish oil-in-water emulsions: effect of emulsifier type and pH. Int. J. Food Sci. Technol. 2012;47:1097-108.
[18] Seta L, Baldino N, Gabriele D, Lupi FR, de Cindio B. The effect of surfactant type on the rheology of ovalbumin layers at the air/water and oil/water interfaces. Food Hydrocolloids 2012;29:247-57.
[19] Bergeron V. An introduction to forces and structure in individual foam and emulsion films. Foams and Emulsions: Springer; 1999. p. 45-72.
[20] Bamforth CW. Brewing and brewing research: past, present and future. J. Sci. Food Agric. 2000;80:1371-8.
[21] Nunes FM, Coimbra MA, Duarte AC, Delgadillo I. Foamability, foam stability, and chemical composition of espresso coffee as affected by the degree of roast. J. Agric. Food Chem. 1997;45:3238-43.
[22] Sherman P. Industrial rheology with particular reference to foods, pharmaceuticals, and cosmetics. 1970.

Chapter II

Colloid systems

The colloidal state was first recognized by Thomas Graham [1] in 1861. The word *colloid* derives from the Greek word *kolla* that means *glue* and *eidos* that means *shape*. Colloid science deals with systems in which one or more of the components has at least one dimension within the nanometer to micrometer scale.

The fundamental characteristic of colloidal system is *dispersity*. A colloidal dispersion has traditionally been defined as a suspension of small particles in a continuous medium. The two phases present in a colloidal system are the *dispersed phase* (the phase present in low amount) and the *dispersion medium* (the medium in which the former phase is distributed). Based on the nature of the dispersed phase and of dispersion medium, different types of colloids can be recognized, as reported in Chapter I (Table I.1).

A peculiar characteristic of dispersed systems is the presence of a border region between the two phases, called interface. In the case of emulsions, generally formed by droplets of a liquid dispersed into another, the interface is made of two immiscible liquids and, in the case of suspensions of a liquid and a solid. At the interface between the dispersed phase and the dispersion medium characteristic surface properties, such as adsorption and electric double layer effects, are evident and play a very important part in determining the physical properties of the system as a whole. It is the material within a molecular layer of the interface which exerts the greatest influence on particle-particle and particle-dispersion medium interactions.

II.1 Colloidal forces

The nature and the magnitude of the surface/interface energy are determined by the physicochemical properties of the particles and the solvent since the particles will have a tendency to undergo aggregation to reduce the surface energy. Colloidal particles in a dispersion medium are always subjected to Brownian motion with frequent collisions between them. Stability and other characteristics of dispersion are thus determined by the nature of the interactions between the particles during such collisions. When attractive forces dominate, the

particles will aggregate and the dispersion may destabilize. When repulsive forces dominate, the system will remain in a dispersed state.

Van der Waals forces

London explained the van der Waals forces (the universal attractive forces) acting between all atoms, molecules and ions on the basis of wave mechanics. These short-range forces result from the interaction between temporary dipoles on some molecules and induced dipoles on the neighboring molecules, and a quantum mechanical effect leading to attraction between nonpolar molecules. They are fairly weak and only important on small scales (crucial for molecules, very important for colloids). Most of the interpretations of London–van der Waals forces in the past have been based on the Hamaker approach [2], which involves pairwise addition of the microscopic forces acting between two bodies (Eq. II.1).

$$V_A = -\frac{AR}{2h} \qquad \text{(II.1)}$$

where: V_A is the free energy due to Van der Waals forces, R the particle radius, A the Hamaker constant and h the particle distance. These interactions are always attractive, proportional to particle size and inversely proportional to particle distance.

Electrostatic forces

When the droplets carry some electrostatic charge, it is possible a redistribution of ions in the solutions surrounding them. Like charges repel each other but the effective range of the repulsion is limited according relationship:

$$V_E = Kr\psi^2 e^{-kh} \qquad \text{(II.2)}$$

where V_E is the free energy due to electrostatic interactions, K a constant, r the particle radius, ψ the electrostatic potential, k the reciprocal Debye length, h the particle distance.

Steric and bridging forces

The total interaction between the internal droplets and the external aqueous phase is employed to determine the stability of colloid systems, and it needs a repulsive total interaction to keep the system stable. Steric repulsion can be explained in the following manner. When two particles approach each other, the entropy per adsorbed molecule decreases causing desorption and a concomitant increase in the interfacial energy. This means that additional work has to be made to bring the particles together and this manifests itself as a repulsive force. Interpenetration and aggregation is possible only if the net change in Gibbs free energy, due to the interpenetration of the polymer chains, is negative. The Gibbs free energy change is determined essentially by the change in entropy, due to the release of solvent molecules and to the decrease in randomness of

the polymer chain, and by the enthalpy of de-solvation of the polymer chains. De-solvation characteristics of the adsorbed polymer species and the dependence of it on solution properties such as temperature and ionic strength will be important in determining aggregation by this mechanism. Ottewill and Walker derived an equation (Eq. II.3) for the energy change due to an overlap of the adsorbed layers by using Flory's liquid lattice model for polymer solutions [3, 4].

$$V_{steric}(a)=\frac{4\pi kTC_V^2}{3v_1^2\varrho_2^2}\left(\psi_1-k_1\right)\left(\delta-a\right)^2\left(3R+2\delta+a/2\right) \qquad \text{(II.3)}$$

where: Cv is the concentration of material in the adsorbed layer, v_1 is the molecular volume of solvent molecules, ϱ_2 is the density of the adsorbate, ψ_1 and k_1 are the entropy and enthalpy parameters, respectively, of mixing proposed by Flory, δ is the adsorbed layer thickness, R is the particle radius and a is the distance separating the surfaces of two approaching particles.

In an emulsion system, the steric interaction depends on the separation distance between the internal aqueous droplets and the external aqueous phase, the thicknesses of the adsorbed surfactant layers and the size of the internal aqueous droplets and the oil globules. All these aspects determine the extent of the compression of the adsorbed surfactant molecules. The thickness of surfactant layers have the same effect on the steric repulsion, and stronger steric interaction can be achieved with thicker adsorbed layers, which can effectively prevent coalescence between the internal aqueous droplets and the external aqueous phase. Increasing the internal aqueous droplet size can produce stronger steric repulsion; however, larger oil globules will weaken the steric repulsion, indicating that a more stable emulsion system can be achieved by preparing the system with smaller oil globules and larger internal aqueous droplets.

Polymers can provide such bridging between particles particularly under conditions where particles are not totally coated by the polymeric species. If one wants to stabilize systems with polymers, where the surface area-to-volume A/V is high, it is important to add sufficient amount of polymer so that the surfaces of the particles become fully covered with adsorbed polymer. If not, and the polymer has a reasonably high molecular weight, there is always the risk that an adsorbed polymer molecule at a particle surface may stretch over and adsorb to another particle surface, thus creating a bridge. If the bridging force is strong enough, the outcome will be flocculation or coagulation of the dispersion. The phenomenon is generally referred to as bridging flocculation, and is consequently favored in systems with unsaturated particle surfaces and high molecular weight polymers that adsorb relatively strongly to the particles.

II.1.1 DLVO Theory

DLVO theory estimates the net interaction energy by summing the Van der Waals and electrostatic terms (Eq. II.4). This theory is represented in the Fig. II.1.

$$V=V_A+V_E \qquad \text{(II.4)}$$

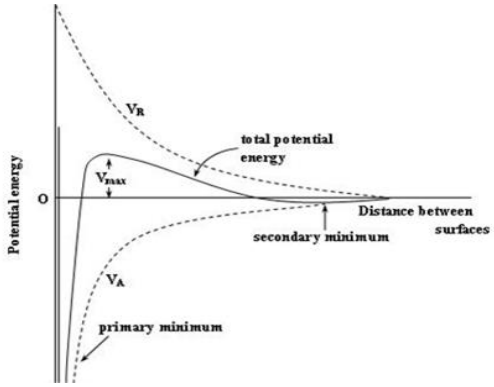

Fig. II.1. Net interaction energy by summing the Van der Waals and electrostatic forces (DLVO theory).

The net interaction is then an explicit function of particle size, separation, ionic strength and surface charge. The height of the barrier increases with surface potential and its width increases with decreasing *h*. One of the most important factors ignored in DLVO theory is steric repulsion. Many colloidal particles are surrounded by a layer of polymer (typically protein). For suspensions to be destabilized, the particles must have enough energy to surmount this barrier during collisions. In the absence of electrostatic interactions, the particles can get trapped in the secondary minimum and form loose aggregates that can usually be re-dispersed easily. The electrostatic forces however, cause the disappearance of the secondary minimum and increase the barrier to the primary minimum thereby decreasing the probability of aggregation. Thus a combination of electrostatic and steric forces is necessary for effective stabilization [5]. For systems stabilized only by electrostatic repulsion, a decrease in the energy barrier will lead to rapid coagulation. The energy barrier can be decreased by the addition of counterions that can specifically adsorb and alter the surface charge or cause double-layer compression. Adsorbed layers of surfactants and polymers can affect stability in the following manner. If they are charged they can produce, increase, or decrease the electrostatic repulsion. In the case of polymer or long-chain molecules, steric repulsion occurs when the adsorbed layers start to penetrate. The adsorbed layer has a Hamaker constant different from that of the particle and hence the van der Waals interactions are altered. DLVO theory is the simplest force-balance approach to colloidal stability. In fact there are many other types of force all with their own dependency on distance,

and structural and compositional variables. In theory it should be possible to calculate the stability of a colloid as follows:

$$V=V_A+V_E-V_{steric}+V_{other}+\ldots, \qquad (II.5)$$

but the number and extreme complexity of some of the terms render it impractical. A general understanding of the balance of forces in play provides a useful qualitative understanding of how a proposed change in the formulation will affect the stability of a colloid.

II.2 Surfactants

Probably the most important physical property of a colloidal system is its stability. The surfactant property of accumulation at surfaces or interfaces has been widely used to promote stability of dispersions [6]. Surfactants (an abbreviation for surface-active agents) are organic compounds having the ability to lower the surface tension of a liquid by facilitating surface wetting or miscibility between different liquids. Chemical compounds that exhibit surface activity, if placed in solution, migrate to the interface and this migration results in a decrease in surface tension. Surfactants are amphiphilic substances consisting of two parts: 1) hydrophobic part "tail" and 2) hydrophilic part "head". A schematic representation of a surfactant molecule is reported in Fig. II.2.

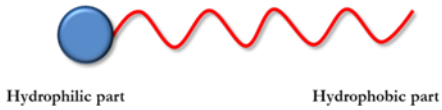

Fig. II.2. Schematic representation of a surfactant molecule.

Therefore, they are soluble in both organic solvents and water. The hydrophobic part has affinity for oil (non-polar solvents) and usually consists of some kinds of hydrocarbons. The hydrophilic part, attracted to water, usually called head group, is more varying in chemical nature. One common way to classify the more frequently used surfactants is by the charge on the head group. The hydrophilic head-group can be: non-ionic (uncharged), ionic (positive-cationic or negative-anionic), zwitterionic (containing both positive and negative charges) and ampholytic (with both acid and base-like characteristic). The hydrophobic portions of surfactants are generally linear or branched chains of hydrocarbons or steroidal structures. The class of amphiphilic compounds comprises a large category of substances. A classification can be made in base to three subcategories: 1) large molecules like proteins or other amphiphilic polymers, 2) small bio-molecules called lipids, found in e.g. all cell membrane and 3) synthetic surface active agents, normally called surfactants. These compounds possess detergent, solubilizing, foaming and

wetting properties, due to their double hydrophilic lipophilic affinity. They are used in a wide range of applications: in detergents and cosmetics, in medical and biological applications, such as controlled release systems of active ingredients. They are also used as colloid system stabilizers, such as cell membrane model systems or as nanostructure reaction micro-environments, in cultural property and environmental applications, such as in waste water treatment processes contaminated by toxic substances, e.g. aromatic or hydrocarbon compounds.

II.2.1 Nonionic surfactants

Nonionic surfactants are generally less toxic, less hemolytic and less irritating to cellular surfaces than other anionic or cationic surfactants and they tend to maintain near physiological pH in solution [7, 8]. They have uncharged hydrophilic head-groups, which make them resistant to water hardness deactivation. The hydrophilic part contains the polyoxyethylene, polyoxypropylene or polyol derivatives. The hydrophobic part contains saturated or unsaturated fatty acids or fatty alcohols. They contribute to make the surfactant system less hardness sensitive. Polysorbates 20 and 80 (Tween 20 and Tween 80) are used in the formulation of biotherapeutic products for both preventing surface adsorption and as stabilizers against protein aggregation [9].

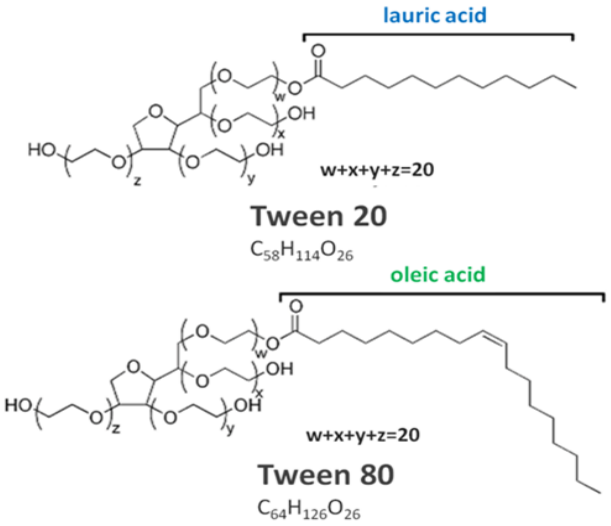

Fig. II.3. Tween 20 and Tween 80 structures.

Tween 20 and Tween 80, whose structures are reported in Fig. II.3, are non-ionic detergents with a very low critical micelle concentration (CMC), are generally gentle surfactants, do not affect protein activity and are effective in solubilization. Tween 20 exhibits a lower interfacial tension than Tween 80. This could be due to the fact that Tween 20, having lauric acid instead of oleic acid esterified, possesses lower molecular weight (1228 Da) than Tween 80 (1310 Da). Both the surfactants have Hydrophilic-Lipophilic Balance (HLB) values higher than 15. These values

indicate an increased encapsulation efficiency which could be attributed to the migration and the surface modification properties of these emulsifiers at the oil/water interface.

The HLB value of a surfactant plays a key role in defining the hydrophilic-lipophilic characteristics of an emulsifier and allows rapid selection according to the emulsion to be prepared. Each lipophilic and emulsifying substance has its HLB value. In general, if the surfactant has a low HLB form W/O emulsions, if HLB is high, form O/W emulsions. The HLB-based system is the quickest and safest way to choose the emulsifiers, but the main limit lies in the impossibility of knowing the total amount of emulsifiers to be used to obtain a stable emulsion.

II.2.2 Proteins

Proteins are monodisperse unbranched polymers consisting of uniquely defined sequences of covalently linked amino acids. The twenty normal amino acids differ by the characteristics of a side chain group and they can be classified into charged, polar, and non-polar groups [10]. Proteins are ampholytic molecules, since the charged amino acids titrate at different pKa values. The endless number of combinations of amino acids result in protein designs with various physical properties, shapes, and functions. For instance, there are fibrous proteins with regular helix structures and flexible highly soluble proteins with expanded coil structures. The native structure of protein is generally organized on different levels [10, 11]. The primary structure is the complete covalent structure of the protein, including the amino acid sequence and, if present, disulphide bridges. The secondary protein structure includes spatial arrangements of symmetric structures formed with amino acids that have positions close to each other in the backbone. The tertiary structure refers to the spatial organization of amino acids that are further apart in the primary sequence, i.e. the three dimensional structure of a globular protein monomer. It has to be noted that the diving line between secondary and tertiary structures can be ambiguous. Non-covalent aggregation of tertiary folden protein subunits into oligomers is described by the quaternary structure. The oligomers may consist of either similar or different subunits. The most important forces involved in stabilization of globular proteins are hydrophobic forces, which has the same origin as the driving force underlying micelle formation. Due to these forces, non-polar amino acids are preferably located in the interior of the protein, where water contacts are avoided. However, non-polar regions on the surface of proteins can also be found. Globular proteins are also stabilized by van der Waals interactions and, in particular, by hydrogen bonds [12]. Electrostatic interaction may both stabilize and destabilize the protein folding. On the surface of the protein, ion-pairs of oppositely charged amino acids stabilize the protein.

Electrostatic repulsions between similarly charged amino acids have an opposite effect and, usually, extreme pH conditions lead to protein denaturation. In general, globular proteins in aqueous solutions have a rather compact and well defined structure in order to function. The interior of globular proteins is semi-solid-like and it is more densely packed than that of a surfactant micelle [13]. Hence, another opposing force to protein folding is the loss of configuration freedom. The formation of disulphide bridges makes the denaturated structure less favourable, since they reduce the number of configurations available in the denaturated state compared to a molecule with no disulphide bridges.

Casein and caseinate

Casein is the main protein (24–29 g L^{-1}) in bovine milk. Casein, involved in highly hydrated micelles, is based on four major components, α_{s1}-casein (38%), α_{s2}-casein (10%), β-casein (36%) and $\varkappa$-casein (13%) and a minor constituent, γ-CN (3%). Each constituent varies in amino acid composition, molecular weight (19000–23900 Da), isoelectric point and hydrophilicity [14, 15]. Acid casein refers to precipitated casein, obtained by adjusting skim milk pH to 4.6 with mineral acids such as hydrochloric or sulphuric acid. Water-soluble caseinates can be obtained by solubilisation of caseins in alkali media such as sodium-, calcium-, potassium- or magnesium-hydroxyde, lime or borax [16]. The commercially available sodium caseinate is obtained by dissolution of acid casein in sodium hydroxide at a pH close to 7.

II.3 Emulsions

An emulsion may be defined as a biphasic system consisting of two immiscible liquids, one of which (the dispersed phase) is finely and uniformly dispersed as globules throughout the second phase (the continuous phase). Emulsions are thermodynamically unstable systems, due to free energy excess associated with the dispersed phase interfacing tension, which tends to aggregate in order to reduce the total surface area, thus leading to emulsion smearing. To reduce this phenomenon, a third component, the emulsifying agent, is added to the system. Emulsifier stabilizes the system by forming a thin film around the globules of dispersed phase. When placed at the interface between the two phases, the emulsifier lowers the interface energy and increases the stability of the system. The efficiency of the currently available emulsifiers allow stable emulsions for many months and even years. Either the dispersed phase or the continuous phase may vary in consistency from that of a mobile liquid to semisolid. Thus, emulsions range from lotions (low viscosity) to creams (high viscosity). The particle size of the dispersed phase commonly ranges from 0.1 to 100 μm [17]. The fact that the aqueous phase or oil phase becomes the dispersed phase depends on many factors, such as the relative amount of the two phases and

the emulsifying agent used, since, in the Bancroft principle, the phase in which the emulsion is more stable represent the continuous phase of the emulsion. When two immiscible liquid phases are mixed, there is an alteration of the surface separation with the formation of "liquid veins" of one phase in the other one. Continuing stirring, droplets of varying dimensions are formed, producing oil-in-water emulsions (O/W) and water-in-oil emulsions (W/O). If the oil droplets are dispersed throughout the aqueous phase, the emulsion is termed O/W as shown in Fig. II.4.

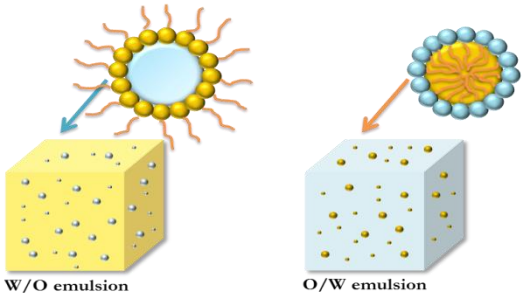

Fig. II.4. W/O and O/W emulsions; W/O emulsion is represented on the left side, O/W emulsion is represented on the right side.

Fats or oils for oral administration, either as medicaments in their own right, or as vehicles for oil soluble drugs, are always formulated as O/W emulsions. They are easily removable from the skin surface and they are used externally to provide cooling effect and internally to also mask the bitter taste of oil. Water soluble drugs are more quickly released from O/W emulsion. They give a positive conductivity test as water, the external phase is a good conductor of electricity.

A system in which water is dispersed as globules in the oil continuous phase is termed W/O emulsion (Fig. II.4). It has an effect on the absorption of drugs from W/O emulsions. They are also useful for cleansing the skin of oil soluble dirt, although its greasy texture is not always cosmetically acceptable. They are greasy and not water washable and are used externally to prevent evaporation of the moisture from the surface of skin e.g. cold cream. Oil soluble drugs are more quickly released from W/O emulsion. They are preferred for formulation meant for external use like cream W/O emulsion is not given a positive conductivity tests, because oil is the external phase which is a poor conductor of electricity [17].

In general, greater is the degree of immiscibility and greater will be the interfacial tension. The work (w) required to expand the interface of a ΔA is equal to the product of the surface tension (γ) and the increase the surface area (ΔA). If γ is low the system will have small drops and will be more stable while if γ is high the system will have big drops, consequently it will be more unstable. To produce an emulsion, energy must be provided (Eq. II.7):

$$\Delta G=\Delta A\gamma_{w/o}-T\Delta S \qquad \text{(II.7)}$$

where $\Delta A\gamma_{w/o}$ is the energy required to expand the interface due to the increase in its surface and $T\Delta S$ represents the configuration entropy resulting from the increase in the number of possible interfaces configurations. Free energy is positive because $\Delta A\gamma_{w/o}$ is always positive and higher than $T\Delta S$. Being positive ΔG, the emulsion formation is a non-spontaneous process, but it requires energy. Such energy can be mechanical and/or chemical: the first one can be supplied by agitation through any means, the latter derives from the ingredients, and it released when these ingredients come into contact. The energy required for the emulsification is given by:

$$\Delta G_{em}=\gamma 3v/R \qquad \text{(II.8)}$$

The theoretical value obtained by solving this equation is less than the real energy value needed for that process because part of the energy supplied is converted to heat (due to friction) and the energy to be supplied must be able to overcome the energy barrier against destabilization. The final structure of the emulsion, i.e. the formation of direct or inverse structures, is determined by two competitive processes: the migration of the surfactant to the interphase and the coalescence. The first stabilizes and the second destroys the emulsion. The continuous phase will be the one with the highest speed of coalescence. Another factor that affects the structure is the order in which the ingredients are mixed. To form an emulsion, it is possible to intervene on $\Delta A\gamma_{w/o}$ (interfacial energy), adding an emulsifier to the mixture, as already mentioned. The emulsifier rapidly forms a monomolecular film around the dispersed droplets, thus creating a barrier interfacial. Among the emulsifiers, the surfactants that form a mono or multi molecular layer and are able to fully coat the surface of the dispersed phase droplets are of great importance, contributing to lowering the interface and thereby decreasing the work required to disperse a liquid in another one.

A good emulsifier must:

- ✓ decrease the interfacial tension γ;
- ✓ act on free surface energy;
- ✓ prevent the film interface;
- ✓ reduce coalescence during emulsification;
- ✓ during the first stages of the emulsion forming process, it must be able to destabilize the first W/O interface.

II.3.1 Emulsion stability

As mentioned before, the emulsions are thermodynamically unstable, therefore, over time, from an homogeneous system will form an heterogeneous one in which the two phases are

macroscopically distinguishable. Fig. II.5 summarizes the different destabilization mechanisms of nanoemulsions namely flocculation, coalescence, Ostwald ripening and creaming/sedimentation. The possible "destabilization" mechanisms of an emulsion are listed and illustrated below:

1. *Sedimentation and creaming*: sedimentation occurs when the droplets of the dispersed phase move to the bottom of the emulsion; in the outcrop, the globules move to the surface of the emulsion. This phenomenon is also called "creaming" and occurs when the dispersed phase floats and it concentrates on the surface of the preparation. Both processes originate from the intervention of external forces, such as gravitational and centrifugal forces. These phenomena do not occur if the Brownian diffusion of the droplets (KT) is greater than the gravitational force in a container of height L, as expressed by the following relation:

$$KT > \frac{4}{3}\pi R^3 \Delta\varrho\, gL \qquad (II.9)$$

where $\Delta\varrho$ is the difference of density between the two phases, R is the radius of the droplets of the dispersed phase, and g is the gravitational constant. Sedimentation and creaming are not generally serious defects because the droplets are still surrounded by the emulsifying film, consequently a good agitation is necessary to bring the emulsion to its initial state.

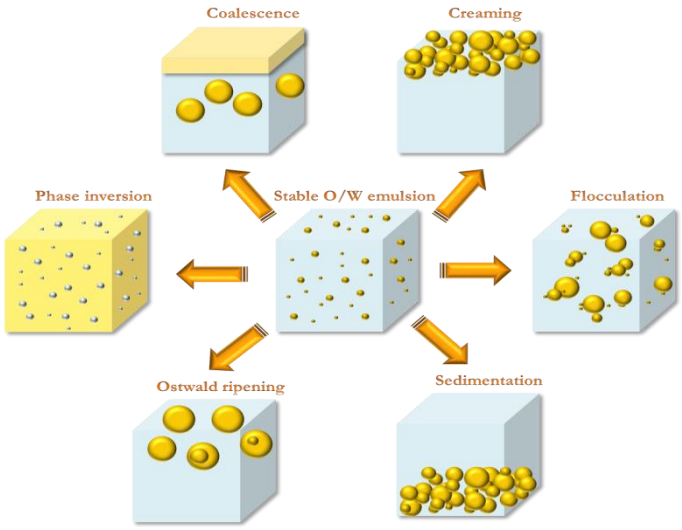

Fig. II.5. Destabilization mechanisms of an emulsion.

However, the phenomenon must be avoided because when the droplets come close each other, coalescence is facilitated, which is a serious defect in the emulsions. It gives rise to a preparation with an unacceptable aspect; moreover, if shaking is not accurate, there may be a non-homogeneous distribution of the final product. One of the strategies for

reducing the phenomenon of creaming and sedimentation is to reduce the difference of density between the two phases. This objective is achieved by producing systems that can be, as shown in Fig. II.6, water-in-oil-in-water (W/O/W) and oil-in-water-in-oil (O/W/O).

2. *Flocculation:* the phenomenon consists in the droplets aggregation, caused by Van Der Waals forces (VA), without varying their individual size. The potential of two equal particles of radius *R* at distance h is given by:

$$V_A = -\frac{AR}{2h} \qquad \text{(II.10)}$$

where *A* is the Hamaker constant, which is related to the polarizability of the molecules at the interphase. Since V_A increases decreasing *h*, in the absence of repulsive forces, large droplet aggregates are formed. Repulsive forces can be established in the presence of ionic surfactants that create a double electrical layer between the droplets or using non-ionic surfactants that are adsorbed at the interphase with the hydrophobic parts, creating a hydrophilic layer in the bulk. This layer prevent that the droplets come close each other by steric interaction.

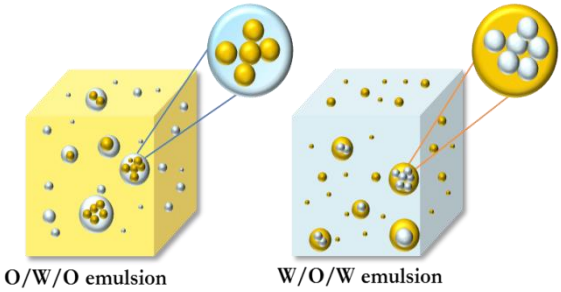

Fig. II.6. Emulsions at difference of reduced density ($\Delta\varrho$); on the left side O/W/O emulsion and on the right side W/O/W.

3. *Ostwald ripening*: is the process in which the smaller droplets are embedded in the larger ones, and it is due to the different solubility of the droplets with different radius. Particularly those with a smaller radius are more soluble than those with lower curvature. The phenomenon is described mathematically by Ostwald's relation:

$$\frac{RT}{M}\ln\frac{S_1}{S_2} = \frac{2\gamma}{\varrho}\left(\frac{1}{R_1} - \frac{1}{R_2}\right) \qquad \text{(II.11)}$$

where *S* is the solubility, *R* is the radius ($S_1 > S_2$ if $R_1 < R_2$), M is the molecular weight and ϱ is the density of the droplets. Since the force that regulates the process is γ, the addition of a surfactant reduces the process. The process is also accelerated by the phenomenon of creaming or flocculation.

4. *Coalescence*: it happens after that the films separating the droplets are thinned and broken. Two droplets coming in contact and consequently they blend. The mechanism of this phenomenon can be explained in terms of disconnection pressure, π. This pressure is the result of the summing of three contributions due to the Van der Waals forces (A), electrostatic forces (E) and steric forces (S):

$$\pi=\pi_A+\pi_E+\pi_S \quad \text{(II.12)}$$

Since electrostatic and steric forces are repulsive forces, in order to reduce coalescence, it is necessary to have a positive disconnection pressure:

$$\pi_A<\pi_E+\pi_S \quad \text{(II.13)}$$

II.4 Macroemulsions, Microemulsions and Nanoemulsions

Emulsions are categorized based on their particle diameter and thermodynamic stability as conventional emulsions and microemulsions [18]. Conventional emulsions are thermodynamically unstable systems, consequently they separate into oil and water phases with time. However, the stability of the two phases could be controlled kinetically such that conventional emulsions can be stabilized for a long period of time from few days to several months [19]. IUPAC defines microemulsion as dispersion made of water, oil, and surfactant(s) that is an isotropic and thermodynamically stable system with dispersed domain diameter varying approximately from 1 to 100 nm, usually 10 to 50 nm [20, 21], whereas a conventional emulsion has a broader range of droplet radii from few hundred nanometers to several micrometers (100 nm-100 μm) [18]. A new class of emulsion, called nanoemulsion had taken form in the recent years which are claimed to possess much improved stability as compared to conventional emulsions [22]. Nanoemulsions are very similar to microemulsions in terms of particle diameter but they are obtained by mechanical force unlike to microemulsions which forms spontaneously [23, 24]. By definition nanoemulsions are emulsions with droplet radii less than 100 nm [18]. However, this range of droplet size is arbitrary and some authors consider the upper range to be 200 nm [25]. The major differences between conventional emulsions, microemulsions and nanoemulsions are shown in Fig. II.8. Both conventional emulsions and nanoemulsion are metastable systems, meaning they have a tendency to break down over time due to a variety of destabilization mechanisms, such as gravitational separation, coalescence, flocculation, and Ostwald ripening [26] cited above. However, the small sized droplets (radius less than 100 nm) of nanoemulsions display number of potential advantages over the conventional emulsions, e.g., higher stability to droplet aggregation and gravitational separation, high optical clarity, ability to modulate product texture, and increase

bioavailability [22]. These advantages bring in potential applications of nanoemulsions; these are described in the paragraph II.4.2.

	macroemulsions	nanoemulsions	microemulsions
	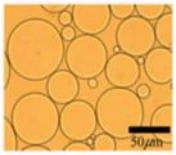	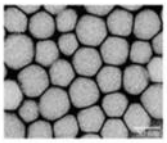	
size	1-100 µm	20-500 nm	10-100 nm
shape	spherical	spherical	spherical, lamellar
stability	thermodynamically unstable, weakly kinetically stable	thermodynamically unstable, kinetically stable	thermodynamically stable
method of preparation	high & low energy methods	high & low energy methods	low energy method
polydispersity	often high (>40%)	typically low (<10-20%)	typically low (<10%)

Fig. II.8. Comparison of macroemulsions, nanoemulsions (also referred to as miniemulsions) and microemulsions with respect to size, shape, stability, method of preparation, and polydispersity. Nanoemulsions and microemulsions have a larger surface area per unit volume than do macroemulsions because of their size. In addition, due to a strong kinetic stability, nanoemulsions are less sensitive to physical and chemical changes. Copyright (2006) by IOP Publishing.

II.4.1 Nanoemulsions preparation

Preparation of nanoemulsions may involve single step or multiple steps depending on the type and nature of the ingredients present in oil and aqueous phases [26]. As the two phases in emulsions are immiscible, external energy is required to disperse one phase as droplets into the other. The free energy (ΔG) required to form a nanoemulsion is given by the equation II.8 cited in the paragraph II3. This free energy can be provided by mechanical devices or by the chemical potential of the system [27]. A number of different approaches can be employed to form an emulsion, but these can be broadly categorized as high-energy and low-energy approaches [26]. In high-energy methods, the free energy comes from mechanical forces applied to the system (such as shear, turbulence, or cavitation), while in low-energy methods, the majority of the free energy associated with emulsion formation comes from physicochemical processes rather than the application of mechanical forces.

Low energy methods

In low energy methods, the smaller droplets are formed when the system undergoes a phase inversion in response to changes in composition or temperature, and passes through a state of low interfacial tension. The two most widely used low energy methods are emulsion inversion point (EIP) [28, 29] and phase inversion temperature (PIT) [30]. EIP is sometimes referred to as phase inversion composition (PIC). Low energy methods begin with a W/O macroemulsion

which is then transformed into an O/W nanoemulsion. In EIP, a W/O macroemulsion is prepared at room temperature and is then diluted slowly with water. During this dilution process, the system passes through an inversion point where the transformation from W/O to O/W emulsion takes place. At this inversion point, the interfacial tension of the oil–water interface is very low and thus small droplets can be formed without a significant energy penalty [29]. In PIT, on the other hand, the W/O macroemulsion is prepared at a temperature higher than the phase inversion temperature (T_{HLB}) of the mixture. When the oil–water–surfactant mixture is cooled down to room temperature, it passes through the inversion temperature at which the transformation of the mixture from a W/O to an O/W emulsion takes place. As with EIP, the interfacial tension of the oil–water interface near the inversion point is very low, and small droplets with high specific surface area can be generated with low energy requirements [30].

High energy methods

High energy methods require a change in temperature to induce the formation of a nanoemulsion. In contrast to low energy methods, high energy methods begins preparing an O/W macroemulsion, which is usually accomplished by mixing oil, water and surfactant in a simple batch stirrer system for a sufficient period of time; in the second step, the macroemulsion is converted into a nanoemulsion. These methods utilize mechanical devices that are capable of generating intensive disruptive forces that produce oil droplets of smaller size. Examples of these devices include the high pressure valve homogenizers, microfluidizers, sonicators etc. In a high pressure homogenization (HPH), a high pressure pump pushes the macroemulsion through a narrow gap (gap height is on the order of a few microns [31]) where the large droplets break into smaller droplets as they are subjected to extreme elongational and shear stress [31, 32]. The homogenization process is typically repeated multiple times (referred to as the number of passes) until the droplet size becomes constant [33]. In an ultrasonicator, high energy shock waves create turbulence (due to cavitation) which ruptures the droplets. It is the most commonly and widely used method to prepare nanoemulsions, because they are capable of producing desired small droplets required for nanoemulsions. If employed, these methods are also able to produce on a large scale for industries [34].

Disadvantages of low energy methods

Although low-energy methods have some advantages over high energy methods (low cost, low energy, low temperature), the types of oils and emulsifiers that can be used often limit them. Currently, low-energy methods have only been shown to work with synthetic surfactants such as Tweens and Spans, consequently it will be not possible employing these methods in applications that use natural emulsifiers, such as phospholipids, proteins, or polysaccharides, due to the nature

of the physicochemical mechanisms involved in nanoemulsion formation by low-energy methods. Moreover, low-energy methods are unsuitable for the formation of food, products that contain relatively high levels of fat, such as salad dressings or mayonnaise, because there would be high levels of surfactant present in the final product. However, this limitation can be overcome in applications where the nanoemulsions are used in a highly diluted form, such as in soft drinks and fortified waters, because the total amount of surfactant in the final product is then relatively low, even though the surfactant-to-oil ratio is high [35].

II.4.2 Nanoemulsions applications

Nanoemulsions have unique properties, such as small droplet size, exceptional stability and tunable rheology that make them an attractive candidate for applications in the food, cosmetic, pharmaceutical industries and in drug delivery applications.

Nanoemulsions in drug delivery

The lyphophilic nature of nanoemulsions allows them to be used in most forms of drug delivery, namely topical, ocular, intravenous, internasal and oral delivery. The nanoemulsions are able to solvate water-insoluble drugs in order to formulate aqueous solutions that can be easily delivered to patient. A considerable number of studies focused on using nanoemulsions for topical drug delivery [36], [37, 38]. Some studies claim that, due to the relatively small size and low ζ-potential of nanoemulsion formulations, hydrophobic drugs are delivered more efficiently than the suspensions of these drugs [39, 37].

Nanoemulsions in food industry

Nanoemulsions are used in the food industry to improve the bioavailability of food ingredients. An example is curcumin, a bioactive agent possessing health benefits, whose biovailability is limited due to its low-water solubility in gastrointestinal fluids. Yu and Huang [40] have explored the possible application of nanoemulsions in improving the digestibility of food. The researchers showed that O/W nanoemulsions are able to solubilize curcumin in the oil phase thus allowing to increase the digestion of curcumin than when it is taking in directly. Other studies on nanoemulsions in the food industry have discovered the preparation and stability of flavored nanoemulsions using low energy methods [41-45].

Nanoemulsions in pharmaceutical industry

Pharmacy is the field where nanoemulsion formulations are studied for their application as nanocarriers which allow the treatment of a variety of diseases.

Eral et al. [46, 47] proposed an approach for producing size-controlled crystals of poorly water-soluble pharmaceutical compounds The researchers dissolved the active pharmaceutical ingredient (API) in nanosized droplets of anisole in an aqueous medium containing alginate (a biopolymer) and F68 (a biocompatible polymeric surfactant); and cross-linked the continuous phase leaving a droplets trapped in a hydrogel. Through evaporation of the composite hydrogel, authors showed that crystals of controlled size and loading can be produced.

References

[1] Graham T. Liquid diffusion applied to analysis. Philos. Trans. R. Soc. London 1861;151:183-224.
[2] Hamaker HC. Rec. Trav. Chim. 1936:55-63.
[3] Flory P, Volkenstein M. Statistical mechanics of chain molecules. Wiley Online Library; 1969.
[4] Slater R, Kitchener J. Characteristics of flocculation of mineral suspensions by polymers. Discuss. Faraday Soc. 1966;42:267-75.
[5] Goddard ED, Vincent B. Polymer adsorption and dispersion stability: ACS Publications; 1984.
[6] Vaisman L, Wagner HD, Marom G. The role of surfactants in dispersion of carbon nanotubes. Adv. Colloid Interface Sci. 2006;128:37-46.
[7] J. J. Polyoxyethylated nonionicsurfactants and their applications in topical ocular drug delivery. Adv. Drug. Deliv. Dev. 2008;60:1666-73.
[8] DG. H. Thermodynamics of micelle formation New York 1987.
[9] Kerwin BA. Polysorbates 20 and 80 used in the formulation of protein biotherapeutics: structure and degradation pathways. J. Pharm. Sci. 2008;97:2924-35.
[10] Havel TF, Kuntz ID, Crippen GM. The combinatorial distance geometry method for the calculation of molecular conformation. I. A new approach to an old problem. J. Theor. Biol. 1983;104:359-81.
[11] Metzler DE. Biochemistry: the chemical reactions of living cells: Academic Press; 2003.
[12] Dill KA, Fiebig KM, Chan HS. Cooperativity in protein-folding kinetics. Proc. Natl. Acad. Sci. 1993;90:1942-6.
[13] Klapper MH. On the nature of the protein interior. Biochimica et Biophysica Acta (BBA)-Protein Structure 1971;229:557-66.
[14] Kinsella JE, Morr CV. Milk proteins: physicochemical and functional properties. Crit. Rev. Food Sci. Nutr. 1984;21:197-262.
[15] Kinsella J, Whitehead D, Brady J, Bringe N. Milk proteins: possible relationships of structure and function. Dev. Dairy Chem. 1989;4:55-95.
[16] Southward C, Walker N. The manufacture and industrial use of casein. N. Z. J. Dairy Sci. Technol. 1980;15:201-17.
[17] Khan BA, Akhtar N, Khan HMS, Waseem K, Mahmood T, Rasul A, et al. Basics of pharmaceutical emulsions: A review. Afr. J. Pharm. Pharmacol. 2011;5:2715-25.
[18] McClements DJ. Nanoemulsions versus microemulsions: terminology, differences, and similarities. Soft Matter 2012;8:1719-29.
[19] Mason T, Wilking J, Meleson K, Chang C, Graves S. Nanoemulsions: formation, structure, and physical properties. J. Phys.: Condens. Matter 2006;18:R635.
[20] Yaqoob Khan A, Talegaonkar S, Iqbal Z, Jalees Ahmed F, Krishan Khar R. Multiple emulsions: an overview. Curr. Drug delivery 2006;3:429-43.
[21] Kumar P, Mittal KL. Handbook of microemulsion science and technology: CRC press; 1999.
[22] Rao J, McClements DJ. Food-grade microemulsions and nanoemulsions: Role of oil phase composition on formation and stability. Food Hydrocolloids 2012;29:326-34.
[23] Tang J-l, Sun J, He Z-G. Self-emulsifying drug delivery systems: strategy for improving oral delivery of poorly soluble drugs. Curr. Drug Ther. 2007;2:85-93.
[24] Talegaonkar S, Azeem A, Ahmad FJ, Khar RK, Pathan SA, Khan ZI. Microemulsions: a novel approach to enhanced drug delivery. Recent Pat. Drug Delivery & Formulation 2008;2:238-57.
[25] Gutiérrez J, González C, Maestro A, Sole I, Pey C, Nolla J. Nano-emulsions: New applications and optimization of their preparation. Curr. Opin. Colloid Interface Sci. 2008;13:245-51.
[26] McClements DJ. Food emulsions: principles, practices, and techniques: CRC press; 2015.
[27] Solans C, Izquierdo P, Nolla J, Azemar N, Garcia-Celma M. Nano-emulsions. Curr. Opin. Colloid Interface Sci. 2005;10:102-10.

[28] Forgiarini A, Esquena J, González C, Solans C. Studies of the relation between phase behavior and emulsification methods with nanoemulsion formation. Trends in colloid and interface science XIV 2000:36-9.
[29] Forgiarini A, Esquena J, Gonzalez C, Solans C. Formation of nano-emulsions by low-energy emulsification methods at constant temperature. Langmuir 2001;17:2076-83.
[30] Izquierdo P, Esquena J, Tadros TF, Dederen C, Garcia M, Azemar N, et al. Formation and stability of nano-emulsions prepared using the phase inversion temperature method. Langmuir 2002;18:26-30.
[31] Floury J, Bellettre J, Legrand J, Desrumaux A. Analysis of a new type of high pressure homogeniser. A study of the flow pattern. Chem. Eng. Sci. 2004;59:843-53.
[32] Meleson K, Graves S, Mason TG. Formation of concentrated nanoemulsions by extreme shear. Soft Mater. 2004;2:109-23.
[33] Mason T, Graves S, Wilking J, Lin M. Extreme emulsification: formation and structure of nanoemulsions. Condens. Matter Phys. 2006.
[34] Tadros T, Izquierdo P, Esquena J, Solans C. Formation and stability of nano-emulsions. Adv. Colloid Interface Sci. 2004;108:303-18.
[35] Komaiko JS, McClements DJ. Formation of Food-Grade Nanoemulsions Using Low-Energy Preparation Methods: A Review of Available Methods. Compr. Rev. Food Sci. Food Saf. 2016;15:331-52.
[36] Baboota S, Shakeel F, Ahuja A, Ali J, Shafiq S. Design, development and evaluation of novel nanoemulsion formulations for transdermal potential of celecoxib. Acta Pharm. 2007;57:315-32.
[37] Tagne J-B, Kakumanu S, Ortiz D, Shea T, Nicolosi RJ. A nanoemulsion formulation of tamoxifen increases its efficacy in a breast cancer cell line. Mol. Pharmaceutics 2008;5:280-6.
[38] Calderilla-Fajardo S, Cazares-Delgadillo J, Villalobos-Garcia R, Quintanar-Guerrero D, Ganem-Quintanar A, Robles R. Influence of sucrose esters on the in vivo percutaneous penetration of octyl methoxycinnamate formulated in nanocapsules, nanoemulsion, and emulsion. Drug Dev. Ind. Pharm. 2006;32:107-13.
[39] Tagne J-B, Kakumanu S, Nicolosi RJ. Nanoemulsion preparations of the anticancer drug dacarbazine significantly increase its efficacy in a xenograft mouse melanoma model. Mol. Pharmaceutics 2008;5:1055-63.
[40] Yu H, Huang Q. Improving the oral bioavailability of curcumin using novel organogel-based nanoemulsions. J. Agric. Food Chem. 2012;60:5373-9.
[41] Ostertag F, Weiss J, McClements DJ. Low-energy formation of edible nanoemulsions: factors influencing droplet size produced by emulsion phase inversion. J. Colloid Interface Sci. 2012;388:95-102.
[42] Rao J, McClements DJ. Formation of flavor oil microemulsions, nanoemulsions and emulsions: influence of composition and preparation method. J. Agric. Food Chem. 2011;59:5026-35.
[43] Troncoso E, Aguilera JM, McClements DJ. Fabrication, characterization and lipase digestibility of food-grade nanoemulsions. Food Hydrocolloids 2012;27:355-63.
[44] Jafari SM, He Y, Bhandari B. Optimization of nano-emulsions production by microfluidization. Eur. Food Res. Technol. 2007;225:733-41.
[45] Lee SJ, McClements DJ. Fabrication of protein-stabilized nanoemulsions using a combined homogenization and amphiphilic solvent dissolution/evaporation approach. Food Hydrocolloids 2010;24:560-9.
[46] Eral HB, López-Mejías V, O'Mahony M, Trout BL, Myerson AS, Doyle PS. Biocompatible alginate microgel particles as heteronucleants and encapsulating vehicles for hydrophilic and hydrophobic drugs. Cryst. Growth Des. 2014;14:2073-82.
[47] Eral HB, O'Mahony M, Shaw R, Trout BL, Myerson AS, Doyle PS. Composite Hydrogels Laden with Crystalline Active Pharmaceutical Ingredients of Controlled Size and Loading. Chem. Mater. 2014;26:6213-20.

Chapter III

Experimental techniques

III.1 Dynamic Light Scattering (DLS)

Dynamic Light Scattering (DLS), Photon Correlation Spectroscopy (PCS) or Quasi-Elastic Light Scattering (QELS) is a technique for measuring the size of particles in the sub-micron region [1], [2]. DLS measures Brownian motion and relates this to the size of the particles. Brownian motion is the random movement of particles due to the bombardment by the solvent molecules that surround them. Normally DLS is concerned with measurement of particles suspended within a liquid. Smaller particles are "kicked" further by the solvent molecules and move more rapidly. On the contrary, larger particles will move slower. An accurately known temperature is necessary for DLS because knowledge of the viscosity is required (the viscosity of a liquid is related to its temperature). The velocity of the Brownian motion is defined by a property known as the translational diffusion coefficient (D)[3].

The Hydrodynamic diameter

The size of a particle is calculated from the translational diffusion coefficient by using the Stokes-Einstein equation;

$$d(H)=\frac{KT}{3\pi\eta D} \qquad \text{(III.1)}$$

where: *d(H)* is the hydrodynamic diameter; *D* is the translational diffusion coefficient; *k* is the Boltzmann's constant; *T* is the absolute temperature and η is the viscosity.

The diameter obtained by this technique is the diameter of a sphere that has the same translational diffusion coefficient as the particle. The translational diffusion coefficient will depend not only on the size of the particle "core", but also on any surface structure, as well as the concentration and type of ions in the medium.

Ionic Strength of Medium

The ions in the medium and the total ionic concentration can affect the particle diffusion speed by changing the thickness of the electric double layer called the Debye length (K^{-1}). Thus a low

conductivity medium will produce an extended double layer of ions around the particle, reducing the diffusion speed and resulting in a larger, apparent hydrodynamic diameter. Conversely, higher conductivity media will suppress the electrical double layer and the measured hydrodynamic diameter.

Surface structure

Any change to the surface of a particle that affects the diffusion speed will correspondingly change the apparent size of the particle. The nature of the surface and the polymer, as well as the ionic concentration of the medium can affect the polymer conformation, which in turn can change the apparent size by several nanometers.

Non-spherical particles

The sphere is the only object whose size can be unambiguously described by a single figure. Different techniques are sensitive to different properties of the particle, e.g. projected area, density, scattering intensity, and in general will produce different mean sizes and size distributions for any given sample. The conformation of proteins and macromolecules are usually dependent on the exact nature of the dispersing medium. As conformational changes will usually affect the diffusion speed, DLS is a very sensitive technique for detecting these changes [3].

III.1.1 Light Scattering Theories [4]

Rayleigh Scattering

If the particles are small, compared to the wavelength of the laser used (typically less than d =λ/10 or around 60nm for a He-Ne laser), then the scattering from a particle illuminated by a vertically polarized laser will be essentially isotropic, i.e. equal in all directions. The Rayleigh approximation is given by $I \propto d^6$ and also that $I \propto \frac{1}{\lambda^4}$, where *I* is the intensity of light scattered, *d* is the particle diameter and *λ* is the laser wavelength. The d^6 term explains that a 50nm particle will scatter 10^6 or one million times as much light as a 5 nm particle. Hence there is a risk that the light from the larger particles will swamp the scattered light from the smaller ones. This d^6 factor also means it is difficult with DLS to measure a mixture of 1000 nm and 10 nm particles because the contribution to the total light scattered by the small particles will be extremely small. The inverse relationship to λ^4 means that a higher scattering intensity is obtained as the wavelength of the laser used decreases.

Mie theory

When the size of the particles becomes roughly equivalent to the wavelength of the illuminating light, then a complex function of maxima and minima with respect to angle is observed. Fig. III.1

shows the theoretical plot screening the log of the relative scattering intensity versus particle size at angles of 173° (the detection angle of the Zetasizer Nano S and Nano ZS in aqueous media) and 90° (the detection angle of the Nano S90 and Nano ZS90) assuming a laser wavelength of 633 nm, real refractive index of 1.59 and an imaginary refractive index of 0.001.

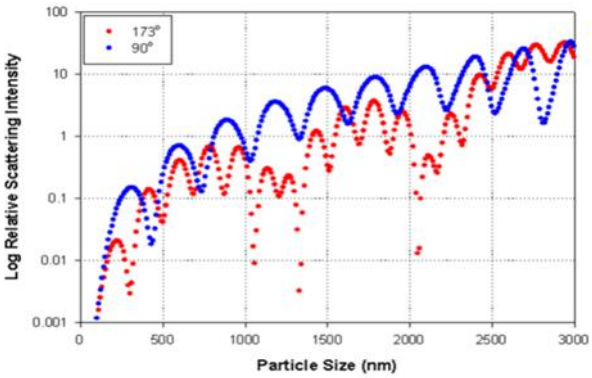

Fig. III.1. Theoretical plot of the log of the relative intensity of scattering versus particle size at angles of 173° and 90° assuming a laser beam at a wavelength of 633 nm, real refractive index of 1.59 and an imaginary refractive index of 0.001.

Mie theory is the only theory that explains correctly the maxima and minima in the plot of intensity with angle and will give the correct answer over all wavelengths, sizes and angles. This theory is used in the Nano software for conversion of the intensity distribution into volume.

III.1.2 How DLS works

In dynamic light scattering is measured the speed at which the particles are diffusing due to Brownian motion**.** This measure is obtained by determining the rate at which the intensity of the scattered light fluctuates. How do these fluctuations in the intensity of scattered light arise?

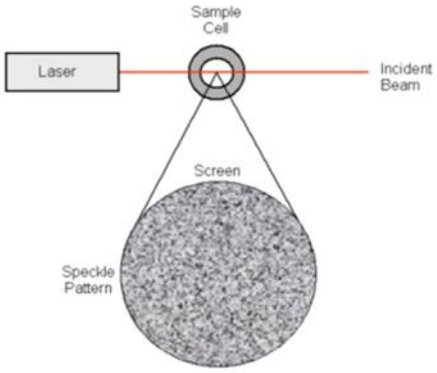

Fig. III.2. Schematic representation of a speckle pattern.

Imagine if a cuvette, containing particles which are stationary, is illuminated by a laser and a frosted glass screen is used to view the sample cell. A classical speckle pattern would be seen (Fig.

III.2) that will be stationary both in speckle size and position because the whole system is stationary. The dark spaces are where the phase additions of the scattered light are mutually destructive and cancel each other out (Fig. III.3A). The bright blobs of light in the speckle pattern are where the light scattered from the particles arrives with the same phase and interfere constructively to form a bright patch (Fig. III.3B). For a system of particles undergoing Brownian motion, a speckle pattern is observed where the position of each speckle is seen to be in constant motion. It happens because the phase addition from the moving particles is constantly evolving and forming new patterns. The rate at which these intensity fluctuations occur will depend on the size of the particles.

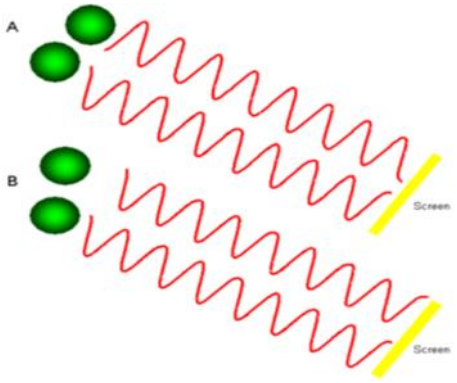

Fig. III.3. The observed signal depends on the phase addition of the scattered light falling on the detector. In example A, two beams interfere and 'cancel each other out' resulting in a decreased intensity detected. In example B, two beams interfere and 'enhance each other' resulting in an increased intensity detected.

Fig. III.4 schematically illustrates typical intensity fluctuations arising from a dispersion of large particles and a dispersion of small particles.

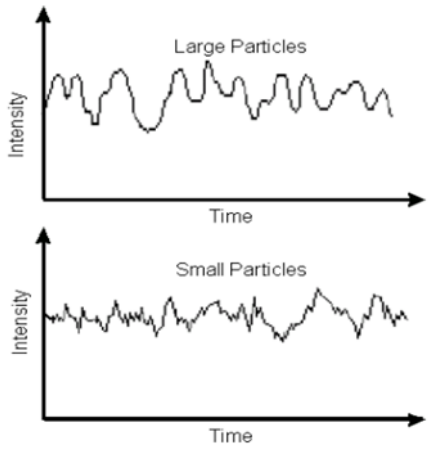

Fig. III.4. Typical intensity fluctuations for large and small particles.

The small particles cause the intensity to fluctuate more rapidly than the large ones. It is possible to directly measure the spectrum of frequencies contained in the intensity fluctuations arising

from the Brownian motion of particles, but it is inefficient to do so. The best way is to use a device called a digital auto correlator.

How a correlator works

A correlator is basically a signal comparator. It is designed to measure the degree of comparison between two signals, or one signal with itself at varying time intervals. If the intensity of a signal is compared with itself at a particular point in time and a time much later, then for a randomly fluctuating signal it is obvious that the intensities are not going to be related in any way, i.e. there will be no correlation between the two signals (Fig. III.5). Knowledge of the initial signal intensity will not allow the signal intensity at time t = infinity to be predicted. This will be true of any random process such as diffusion.

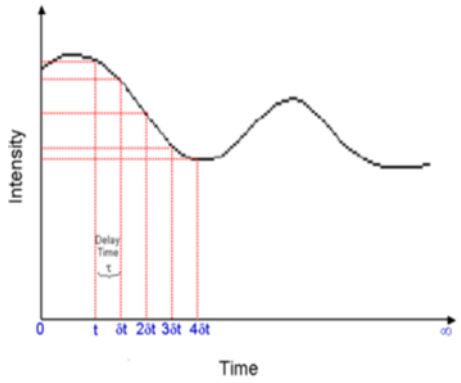

Fig. III.5. Schematic showing the fluctuation in the intensity of scattered light as a function of time.

However, if the intensity of signal at time = t is compared to the intensity a very small time later $(t+\delta t)$, there will be a strong relationship or correlation between the intensities of two signals. The two signals are strongly or well correlated. If the signal, derived from a random process such as Brownian motion, at t is compared to the signal at $t+2\delta t$, there will be a reasonable comparison or correlation between the two signals, but it will not be as good as the comparison at t and $t+\delta t$. The correlation is reducing with time. The period of time δt is usually very small, maybe nanoseconds or microseconds and is called the sample time of the correlator. $t = \infty$ maybe of the order of a millisecond or tens of milliseconds. If the signal intensity at t is compared with itself, then there is perfect correlation as the signals are identical. Perfect correlation is indicated by unity (1.00) and no correlation is indicated by zero (0.00). The time at which correlation begins to decline is an indication of the average size. If the particles are large the signal will be changing slowly and the correlation will persist for a long time (Fig. III.6A). If the particles are small and moving rapidly then correlation will reduce more quickly (Fig. III.6B). The time at which the correlation starts to significantly decay is an indication of the mean size of the sample. The

steeper the line, the more monodisperse the sample is. Conversely, the more extended the decay becomes, the greater the sample polydispersity.

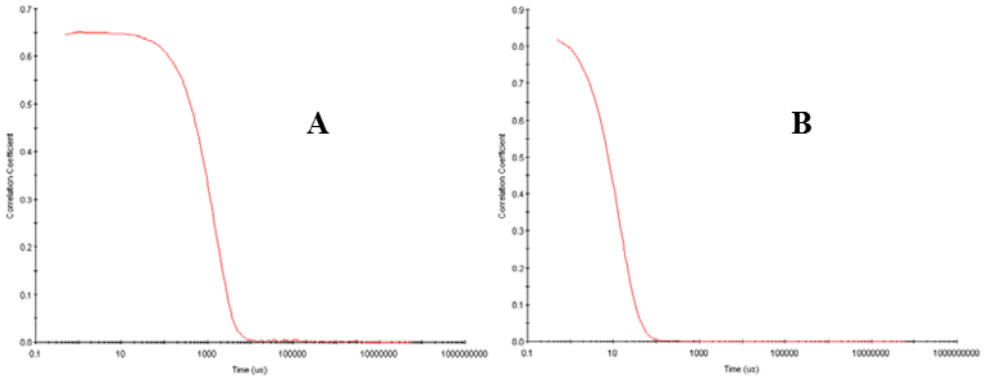

Fig. III.6. Typical correlogram from a sample containing large particles in which the correlation of the signal takes a long time to decay (A); typical correlogram from a sample containing small particles in which the correlation of the signal decays more rapidly (B).

The correlation function

The correlator used in a PCS instrument will construct the correlation function *G(τ)* of the scattered intensity (Eq. III.2):

$$G(\tau)=\langle I(t).I(t+\tau)\rangle \qquad \text{(III.2)}$$

where τ is the time difference (the sample time) of the correlator.

For a large number of monodisperse particles in Brownian motion, the correlation function (*G*) is an exponential decaying function of the correlator time delay τ (Eq. III.3):

$$G(\tau)=A\left[1+B\exp(-2\Gamma\tau)\right] \qquad \text{(III.3)}$$

where *A* is the baseline of the correlation function, *B* is the intercept of the correlation function.

$\Gamma = Dq^2$

where *D* is the translational diffusion coefficient and *q* is $(4\ \pi n/\lambda o)\ \sin(\theta/2)$

where *n* is the refractive index of dispersant, λo is the wavelength of the laser and θ is the scattering angle.

For polydisperse samples, the equation can be written as:

$$G(\tau)=A\left[1+Bg_1(\tau)^2\right] \qquad \text{(III.4)}$$

where $g_1(\tau)$ is the sum of all the exponential decays contained in the correlation function.

Obtaining Size information from the correlation function

Size is obtained from the correlation function by using various algorithms. There are two approaches that can be taken:

- fit a single exponential to the correlation function to obtain the mean size (z-average diameter) and an estimate of the width of the distribution (polydispersity index); this is called the Cumulants analysis.
- fit a multiple exponential to the correlation function to obtain the distribution of particle sizes.

The size distribution obtained is a plot of the relative intensity of light scattered by particles in various size classes and is therefore known as an intensity size distribution. If the distribution by intensity is a single fairly smooth peak, then there is little point in doing the conversion to a volume distribution using the Mie theory. If the optical parameters are correct, this will just provide a slightly different shaped peak. However, if the plot shows a substantial tail, or more than one peak, then Mie theory can make use of the input parameter of sample refractive index to convert the intensity distribution to a volume distribution. This will then give a more realistic view of the importance of the tail or second peak present. In general terms it will be seen that:

$$d(\text{intensity}) > d(\text{volume}) > d(\text{number})$$

A very simple way of describing the difference between intensity, volume and number distributions is to consider two populations of spherical particles of diameter 5 nm and 50 nm present in equal numbers (Fig. III.7).

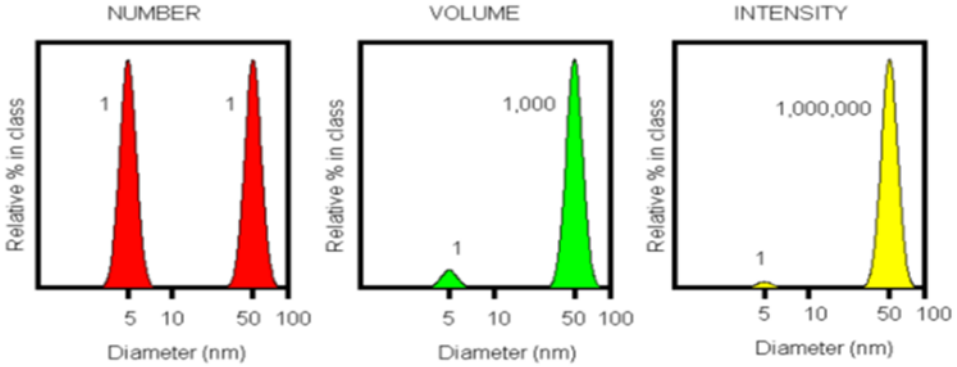

Fig. III.7. Number, volume and intensity distributions of a bimodal mixture of 5 and 50 nm lattices present in equal numbers.

If a number distribution of these two particle populations is plotted, a plot consisting of 2 peaks (positioned at 5 and 50 nm) of a 1 to 1 ratio would be obtained. If this number distribution was converted into volume, then the two peaks would change to a 1:1000 ratio because the volume of a sphere is equal to $4/3\pi^3$. If this was further converted into an intensity distribution, a 1:1000000 ratio between the two peaks would be obtained because the intensity of scattering is proportional to d^6 (from Rayleighs approximation).

Optical configuration of a Dynamic Light Scattering instrument

The optical configuration of a Dinamic Light Scattering instrument is shown in Fig. III.8. Firstly, a laser (1) provides a light source to illuminate the sample contained in a cell (2). For dilute concentrations, most of the laser beam passes through the sample, but some is scattered by the particles within the sample at all angles. A detector (3) is used to measure the scattered light. In the Zetasizer Nano series, the detector position will be at either 173° or 90°, depending upon the particular model.

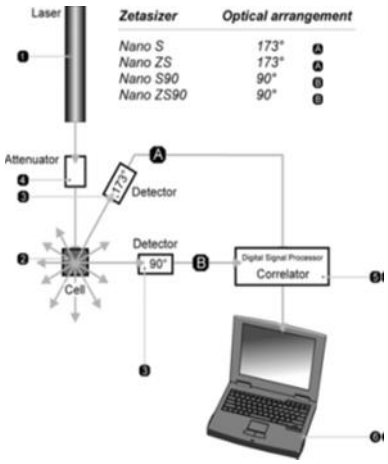

Fig. III.8. Optical configurations of the Zetasizer Nano series for dynamic light scattering measurements. A typical dynamic light scattering system comprises of six main components.

The intensity of scattered light must be within a specific range for the detector to successfully measure it. If too much light is detected, then the detector will become saturated. To overcome this, an attenuator (4) is used to reduce the intensity of the laser source and hence reduce the intensity of scattering. For samples that do not scatter much light, such as very small particles or samples of low concentration, the amount of scattered light must be increased. In this situation, the attenuator will allow more laser light through to the sample. For samples that scatter more light, such as large particles or samples at higher concentration, the intensity of scattered light must be decreased. The appropriate attenuator position is automatically determined by the Nano software and covers a transmission range of 100% to 0.0003%. The scattering intensity signal from the detector is passed to a digital processing board called a correlator (5). The correlator compares the scattering intensity at successive time intervals to derive the rate at which the intensity is varying. This correlator information is then passed to a computer (6), where the Nano software will analyze the data and derive size information.

III.2 ζ-potential

Zeta potential is a physical property showed by any particle in suspension. It can be used to optimize the formulations of suspensions and emulsions. Knowledge of the zeta potential can

reduce the time needed to produce trial formulations. It is also an aid in predicting long-term stability. As cited in the paragraph II.1.4 of the chapter II, the DLVO suggests that the stability of a particle in solution is dependent upon its total potential energy function V_T. V_A and V_R are the attractive and repulsive contributions. They potentially are much larger and operate over a much larger distance (Eq. III.5);

$$V_A = -A/(12\pi D^2) \qquad \text{(III.5)}$$

where A is the Hamaker constant and D is the particle separation. The repulsive potential V_R is a far more complex function (Eq. III.6);

$$V_R = 2\pi\varepsilon a\zeta^2 \exp^{(-kD)} \qquad \text{(III.6)}$$

Where a is the particle radius, π is the solvent permeability, $\varkappa$ is a function of the ionic composition and ζ is the zeta potential [5]. It has long been recognized that the ζ-potential is a very good index of the interaction degree between colloidal particles and measurements of zeta potential are commonly used to assess the stability of colloidal systems [6]. Most colloidal dispersions in aqueous media carry an electric charge. There are many origins of this surface charge depending upon the nature of the particle and also the surrounding medium. Dissociation of acidic groups on the surface of a particle will give rise to a negatively charged surface. Conversely, a basic surface will take on a positive charge (Fig. III.9). In both cases, the magnitude of the surface charge depends on the acidic or basic strengths of the surface groups and on the pH of the solution. The surface charge can be reduced to zero suppressing the surface ionization by decreasing the pH in case of negatively charged particles (Fig. III.9A) or by increasing the pH in the case of positively charged particles [7] (Fig. III.9B).

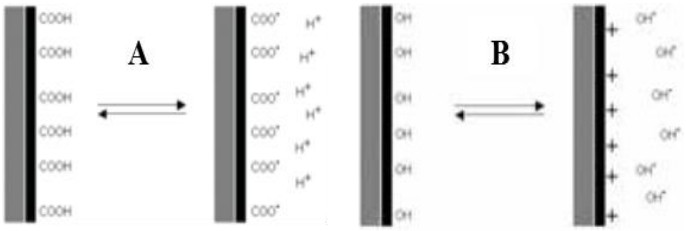

Fig. III.9. Origin of surface charge by ionization of acidic groups to give a negatively charged surface (A); origin of surface charge by ionization of basic groups to give a positively charged surface (B).

The electrical double layer

The development of a net charge at the particle surface affects the distribution of ions in the surrounding interfacial region, resulting in an increased concentration of counter ions, ions of opposite charge to that of the particle, close to the surface. Thus, an electrical double layer exists round each particle. The liquid layer surrounding the particle exists as two parts; an inner region (Stern layer) where the ions are strongly bound and an outer (diffuse) region where they are less

firmly associated. Within the diffuse layer there is a notional boundary inside which the ions and particles form a stable entity. When a particle moves (e.g. due to gravity), ions within the boundary move it. Those ions beyond the boundary stay with the bulk dispersant. The potential at this boundary (surface of hydrodynamic shear) is the ζ-potential (Fig. III.10).

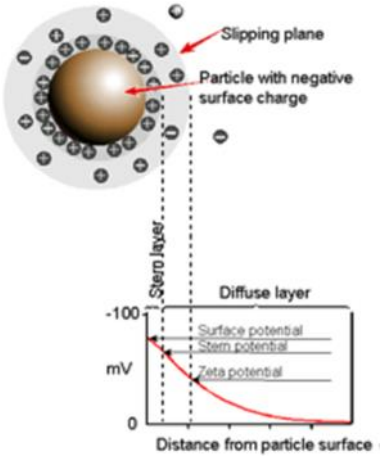

Fig. III.10. Schematic representation of zeta potential.

The magnitude of the ζ-potential gives an indication of the potential stability of the colloidal system. If all the particles in suspension have a large negative or positive ζ-potential then they will tend to repel each other and there will be no tendency for the particles to come together. However, if the particles have low ζ-potential values then there will be no force to prevent the particles coming together and flocculating. The general dividing line between stable and unstable suspensions is generally taken at either +30 or -30 mV. Particles with ζ-potentials more positive than +30 mV or more negative than -30 mV are normally considered stable. However, if the particles have a density different form the dispersant, they will eventually sediment forming a close packed bed (i.e. a hard cake) [8,9]. The most important factor that affects ζ-potential is pH. Imagine a particle in suspension with a negative zeta potential.

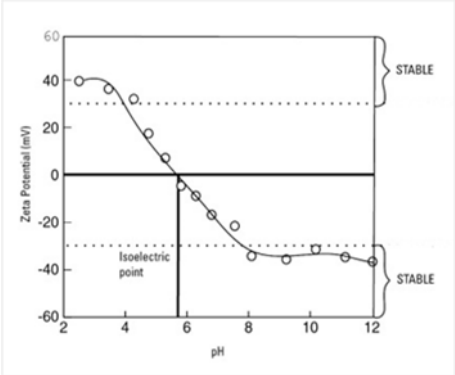

Fig. III.11. Typical plot of ζ-potential versus pH showing the position of the isoelectric point and the pH values where the dispersion would be expected to be stable.

If more alkali is added to this suspension then the particles tend to acquire more negative charge. If acid is added to this suspension then a point will be reached where the charge will be neutralised. Further addition of acid will cause a build up of positive charge. Therefore a ζ-potential versus pH curve will be positive at low pH and lower or negative at high pH (Fig. III.11).

Electrokinetic effects

An important consequence of the existence of electrical charges on the surface of particles is that they interact with an applied electric field. These effects are collectively defined as electrokinetic effects [10]. There are four distinct effects depending on the way in which the motion is induced. These are:

- **Electrophoresis:** the movement of a charged particle relative to the liquid is suspended in under the influence of an applied electric field
- **Electro-osmosis:** the movement of a liquid relative to a stationary charged surface under the influence of an electric field
- **Streaming potential:** the electric field generated when a liquid is forced to flow past a stationary charged surface
- **Sedimentation potential:** the electric field generated when charged particles sediment.

III.3 Rheometry

Rheometry refers to the experimental technique used to determine the rheological properties of materials; it is defined as the study of the flow and deformation of matter which describes the interrelation between force, deformation and time. Rheology describes the deformation of a body under the influence of stresses. "Bodies" in this context can be either solids, liquids or gases [11].

Viscosity

There are two basic types of flow, these being shear flow and extensional flow. In shear flow, fluid components shear past one another while, in extensional flow, fluid component flowing away or towards from one other [12].

Shear flow

Shear flow can be depicted as layers of fluid sliding over one another with each layer moving faster than the one beneath it. The uppermost layer has maximum velocity while the bottom layer is stationary. For shear flow to take place a shear force must act on the fluid. This external force

takes the form of a *shear stress* (τ) which is defined as the force (F) acting over a unit area (A) as shown in Fig. III.12. In response to this force the upper layer will move a given distance x, while the bottom layer remains stationary. Hence we have a displacement gradient across the sample (x/h) termed the *shear strain* (γ). For a solid which behaves like a single block of material, the strain will be finite for an applied stress – no flow is possible. However, for a fluid where the constituent components can move relative to one another, the shear strain will continue to increase for the period of applied stress. This creates a velocity gradient termed the *shear rate* or *strain rate* ($\dot{\gamma}$) which is the rate of change of strain with time ($d\gamma/dt$).

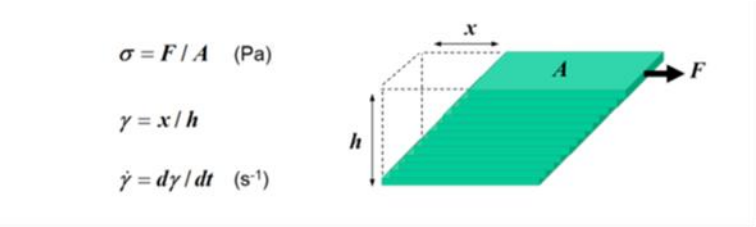

Fig. III.12. Quantification of shear rate and shear stress for layers of fluid sliding over one another.

When we apply a shear stress to a fluid we are transferring momentum, indeed the shear stress is equivalent to the *momentum flux* or *rate of momentum transfer* to the upper layer of fluid. That momentum is transferred through the layers of fluid by collisions and interactions with other fluid components giving a reduction in fluid velocity and kinetic energy. The coefficient of proportionality between the shear stress and shear rate is defined as the *shear viscosity* or *dynamic viscosity* (η), which is a quantitative measure of the internal fluid friction and associated with damping or loss of kinetic energy in the system (Eq. III.7).

$$\eta=\tau/\dot{\gamma} \qquad \text{(III.7)}$$

In SI the viscosity is expressed in Pa s (Nm^{-2} s). It should be noted that fluid viscosity is both pressure and temperature dependent, with viscosity generally increasing with increased pressure and decreasing temperature. Temperature is more critical than pressure in this regard with higher viscosity fluids, such as asphalt or bitumen, much more temperature dependent than low viscosity fluids such as water [13].

Fluids flow behavior

From the rheological point of view, fluids can be distinguished in Newtonians and non Newtonians [13]. These various types of flow behavior are shown in Fig. III.13.

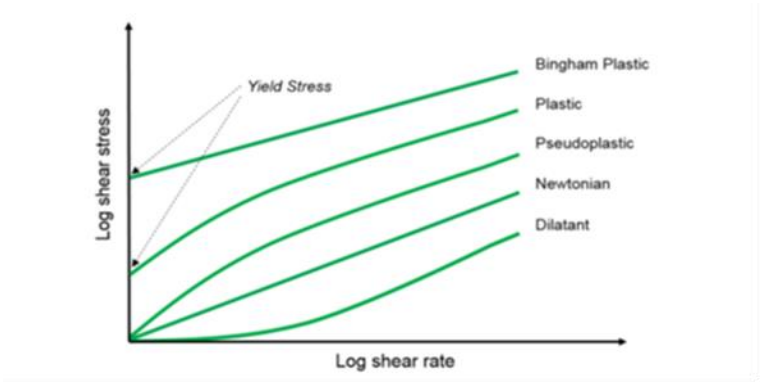

Fig. III.13. Shear stress/shear rate plots depicting various types of flow behavior.

Newtonian fluids

Newtonian fluids are fluids in which the shear stress is linearly related to the shear rate and hence the viscosity is invariable with shear rate or shear stress. For the Newtonian fluids, the η doesn't change varying τ. Typical Newtonian fluids include water, simple hydrocarbons and dilute colloidal dispersions. The angular coefficient of the curve is called dynamic viscosity (η). The equation describing the rheological behavior of Newtonian fluids is:

$$\tau=\eta\dot{\gamma} \qquad \text{(III.8)}$$

The shear rate $(dv/dz)=\dot{\gamma}$ is expressed in s^{-1} (Eq. III.9).

$$\frac{m}{s}\frac{1}{m}=\frac{1}{s} \qquad \text{(III.9)}$$

Non Newtonian fluids

Non-Newtonian fluids are those where the viscosity varies as a function of the applied shear rate or shear stress. These fluids are particularly interesting in the food sector because biological fluids, such as solutions and suspensions of protein or polysaccharide macromolecules, present these behaviors. For the *pseudoplastic fluids* (shear thinning), the viscosity, defined by the tangent to the curve in each single point, is called *apparent viscosity* and decreases increasing the shear gradient.

Increasing the applied shear stress, the macromolecules orient themselves in the direction of the motion, consequently they offer less resistance to sliding liquid. This behavior is mathematically expressed by Ostwald's power equation:

$$\tau=K\dot{\gamma}^{n} \qquad \text{(III.10)}$$

with n<1, denominated *index of rheological behavior* and k = constant named *consistence index* (Pa s^n). Consistence index is dependent from temperature, according to the Arrhenius law (Eq. III.11);

$$\ln\frac{k_1}{k_2}=\frac{Ea}{R}\left(\frac{1}{T_1}-\frac{1}{T_2}\right) \qquad \text{(III.11)}$$

where *Ea* is the activation energy (J/mol K), *R* is the gas constant (8.314 J/mol K) and *T* is the temperature expressed in K.

For *plastic fluids* the fluid sliding occur only when the applied shear stress exceed the *yeld stress* (τ_0), the limit shear stress value. Thus, before they flow, plastic fluids require an yeld stress to be applied. Depending on the flow behavior, there are two types of plastic fluid: 1) bingham plastic fluid or Casson plastic fluid (Fig. III.13). An ideal plastic fluid is like toothpaste. Before it starts to flow (deform) you need to provide some yield stress, after you push the toothpaste comes out of the tube. A typical food product that acts as a plastic fluid is ketchup. Like toothpaste, ketchup also require a force to be applied (yeld stress) in order to get the ketchup out of the bottle.

For the mathematical interpretation of plastic fluids we use the Herschel-Bulkley model:

$$\tau=\tau_0+K\dot{\gamma}^n \qquad \text{(III.12)}$$

Finally, the dilating fluids (shear thickening) are characterized by an apparent viscosity which increases to the increasing of shear rate. This behavior is rare in food fluids, while it is found in products such as varnishes etc. In this case, mathematic representation is also provided by Ostwald power equation (III.10) with n>1 [13].

III.3.1 Rotational rheometer

The fluids viscosity measurement is carried out with the viscometers, instruments using to establish the correlation between the shear stress and the shear rate. An example of viscosity measuring system is shown in Fig. III.14. A single head (stress controlled) rotational rheometer with parallel plate measuring systems (PP MS) is used to measure the viscosity. The sample is loaded between the plates at a known gap (*h*). Single head rheometers are able to work in controlled stress or controlled rate mode, consequently it is possible to apply a torque and measure the rotational speed or alternatively apply a rotational speed and measure the torque required to maintain that speed. In controlled stress mode a torque is requested from the motor which translates to a force (*F*) acting over the surface area of the plate (*A*) to give a shear stress (*F*/*A*). In response to an applied shear stress, a liquid will flow with a shear rate dependent on its viscosity.

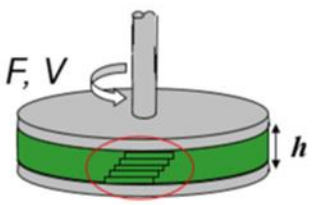

Fig. III.14. Illustration showing a sample loaded between parallel plates and shear profile generated across the gap.

If the measurement gap (h) is accurately known, then the shear rate (V/h) can be determined from the measured angular velocity (ω) of the upper plate, which is determined by high precision position sensors, and its radius (r), since $V = r\,\omega$.

Other measuring systems including cone-plate and concentric cylinders are commonly used for measuring viscosity. The type of measuring system used and its dimensions is dependent on the sample type and its viscosity [14].

III.4 Fluorescence spectroscopy

Luminescence is the emission of light from any substances, and occur from electronically excited states. Luminescence is formally divided in two categories: 1) fluorescence and 2) phosphorescence, depending on the nature of the excited state. Fluorescence is the property of some substances to re-emit the received radiation at a lower frequency, particularly absorbing ultraviolet light and emitting it visible, as is the case of the highlighters. This phenomenon was discovered from fluorite, calcium and fluoride mineral, that is fluorescent. Fluorescence typically occurs from aromatic molecules, fluorescent substances (fluorophores). It is based on the emission of a photon from the excited state to the fundamental one. Such photon emission occurs with a precise energy (E) that can be followed at a specific wavelength (λ_{em}). The emission intensity by a population of excited fluorophors will be:

$$I=nE \qquad \text{(III.13)}$$

The transition from different vibrational levels occurs spontaneously with the energy emission at lower intensity than that of excitation by generating a fluorescence spectrum with a maximum corresponding to the emission transition. The typical fluorescence lifetime is in the order of pico/nanoseconds, therefore it represents a very rapid process. For this reason, to observe fluorescence phenomenon, the fluorophore must be continually excited. Intensity, position of the wavelength and lifetime are some of the observable parameters that characterize a fluorophore; these parameters may be influenced by the temperature and/or viscosity of the medium. Fluorescence spectral data are generally presented as emission spectra. A fluorescence emission spectrum is a plot of the fluorescence intensity versus wavelength (nanometers) or wavenumber (cm^{-1}). The processes that occur between the absorption and emission of light are usually illustrated by the Jablonski [15] diagram (Fig. III.15). Jablonski diagrams are often used as the starting point for discussing light absorption and emission.

The singlet ground, first, and second electronic states are depicted by S_0, S_1, and S_2, respectively.

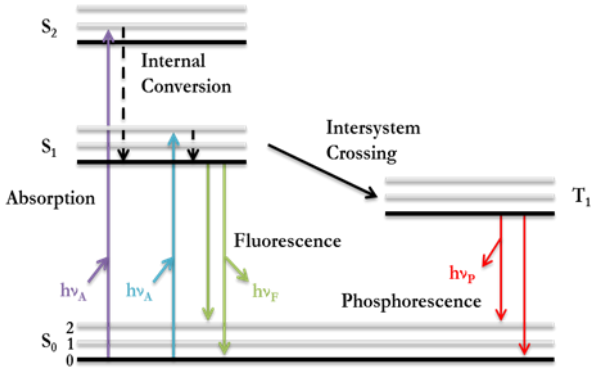

Fig. III.15. One form of a Jablonski diagram.

At each of these electronic energy levels, the fluorophores can exist in a number of vibrational energy levels, represented by 0, 1, 2, etc. The transitions between states are shown as vertical lines to illustrate the instantaneous nature of light absorption. Transitions occur in about 10^{-15} s, a time too short for significant displacement of nuclei. This is the Franck-Condon principle. Absorption and emission occur mostly from molecules with the lowest vibrational energy. The absorption of luminous energy by a fluorophore leads to the promotion of an electron to one of the vibrational levels of the electronic excited states S_1 or S_2. With a few rare exceptions, molecules in condensed phases rapidly relax reaching the lowest vibrational level of S_1. This process is called *internal conversion* and generally occurs within 10^{-12} s or less. Since fluorescence lifetimes are typically near 10^{-8} s, internal conversion is generally complete prior to emission. Hence, fluorescence emission generally results from a thermally equilibrated excited state, that is, the lowest energy vibrational state of S_1. Return to the ground state typically occurs to a higher excited vibrational ground state level, which then quickly (10^{-12} s) reaches thermal equilibrium (Fig. III.15). Molecules in the S_1 state can also undergo a spin conversion to the first triplet state T_1. Emission from T_1 is termed phosphorescence, and is generally shifted to longer wavelengths (lower energy) relative to the fluorescence. Conversion of S_1 to T_1 is called intersystem crossing. Transition from T_1 to the singlet ground state is forbidden, and as a result the rate constants for triplet emission are several orders of magnitude smaller than those for fluorescence. Examination of the Jablonski diagram (Fig. III.15) reveals that the energy of the emission is typically less than that of absorption. Fluorescence typically occurs at lower energies or longer wavelengths. This phenomenon was first observed by Sir. G. G. Stokes in 1852 at the University of Cambridge [16]. Energy losses between excitation and emission are observed universally for fluorescent molecules in solution. One common cause of the Stokes shift is the rapid decay to the lowest vibrational level of S_1. Furthermore, fluorophores generally decay to higher vibrational levels of S_0 (Fig. III.15), resulting in further loss of excitation energy by thermalization of the excess vibrational energy. In addition

to these effects, fluorophores can display further Stokes shifts due to solvent effects, excited-state reactions, complex formation, and/or energy transfer. Another general property of fluorescence is that the same fluorescence emission spectrum is generally observed irrespective of the excitation wavelength. This is known as Kasha's rule [17] although Vavilov reported in 1926 that quantum yields were generally independent of excitation wavelength [18]. Upon excitation into higher electronic and vibrational levels, the excess energy is quickly dissipated, leaving the fluorophore in the lowest vibrational level of S_1. This relaxation occurs in about 10^{-12} s, and is presumably a result of a strong overlap among numerous states of nearly equal energy. Because of this rapid relaxation, emission spectra are usually independent of the excitation wavelength. The generally symmetric nature of these spectra is a result of the same transitions being involved in both absorption and emission, and the similar vibrational energy levels of S_0 and S_1. In most fluorophores these energy levels are not significantly altered by the different electronic distributions of S_0 and S_1. Suppose the absorption spectrum of a fluorophore shows distinct peaks due to the vibrational energy levels. These peaks are due to transitions from the lowest vibrational level of the S_0 state to higher vibrational levels of the S_1 state. Upon return to the S_0 state the fluorophore can return to any of the ground state vibrational levels. These vibrational energy levels have similar spacing to those in the S_1 state. The emission spectrum shows the same vibrational energy spacing as the absorption spectrum (Fig. III.16).

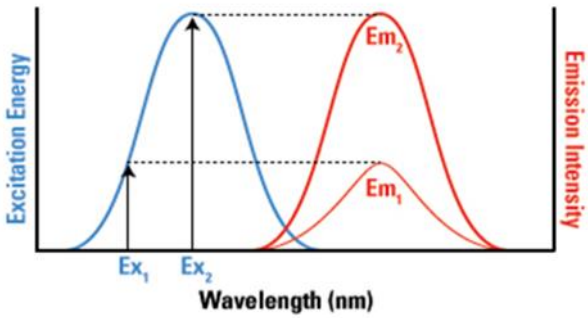

Fig. III.16. Excitation and emission spectrum

The fluorescence lifetime and quantum yield are perhaps the most important characteristics of a fluorophore. Quantum yield is the number of emitted photons relative to the number of absorbed photons. Substances with the largest quantum yields display the brightest emissions. The lifetime is also important, as it determines the time available for the fluorophore to interact with or diffuse in its environment, and hence the information available from its emission.

III.4.1 Intrinsic or natural fluorophores

Fluorophores can be broadly divided into two main classes: 1) intrinsic and 2) extrinsic. Intrinsic fluorophores are those that occur naturally. These include the aromatic amino acids, NADH, flavins, derivatives of pyridoxyl, and chlorophyll. Extrinsic fluorophores are added to the sample to provide fluorescence when none exists, or to change the spectral properties of the sample. Extrinsic fluorophores include dansyl, fluorescein, rhodamine, and numerous other substances. Intrinsic protein fluorescence originates from the aromatic amino acids [19], [20] tryptophan (trp), tyrosine (tyr), and phenylalanine (phe) (Fig. III.17).

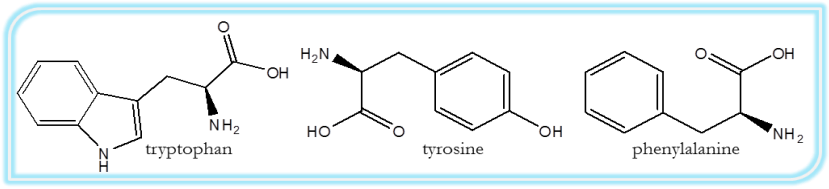

Fig. III.17. Tryptophan, tyrosine and phenylalanine structures.

The indole groups of tryptophan residues are the dominant source of UV absorbance and emission in proteins. Tyrosine has a quantum yield similar to tryptophan but its emission spectrum is more narrowly distributed on the wavelength scale. This gives the impression of a higher quantum yield for tyrosine. In native proteins the emission of tyrosine is often quenched, which may be due to its interaction with the peptide chain or energy transfer to tryptophan. Denaturation of proteins frequently results in increased tyrosine emission. Like phenol, the Pk_A of tyrosine decreases dramatically upon excitation, and excited state ionization can occur. Emission from phenylalanine is observed only when the sample protein lacks both tyrosine and tryptophan residues, which is a rare occurrence. The emission of tryptophan is highly sensitive to its local environment, and is thus often used as a reporter group for protein conformational changes. Spectral shifts of protein emission have been observed as a result of several phenomena, including binding of ligands, protein–protein association, and protein unfolding. The emission maxima of proteins reflect the average exposure of their tryptophan residues to the aqueous phase. Fluorescence lifetimes of tryptophan residues range from 1 to 6 ns. Tryptophan fluorescence is subject to quenching by iodide, acrylamide, and nearby disulfide groups. Tryptophan residues can be quenched by nearby electron-deficient groups like NH_3^+, $–CO_2H$, and protonated histidine residues. The presence of multiple tryptophan residues in proteins, each in a different environment, is one reason for the multi-exponential intensity decays of proteins.

References

[1] ISO13321 I. Methods for determination of particle size distribution part 8: Photon correlation spectroscopy. International Organization for Standardization (ISO) 1996.
[2] Dahneke BE. Measurement of suspended particles by quasi-elastic light scattering: John Wiley & Sons 1983.
[3] Zero K, Pecora R. Dynamic depolarized light scattering: Plenum Press: New York 1985.
[4] Washington C. Particle Size Analysis In Pharmaceutics And Other Industries: Theory And Practice: Theory And Practice: CRC Press 2005.
[5] Verwey EJW, Overbeek JTG. Theory of the stability of lyophobic colloids. J. Colloid Sci. 1955;10:224-5.
[6] Hunter RJ. Zeta potential in colloid science: principles and applications: Academic press 2013.
[7] Shaw DJ, Costello B. Introduction to colloid and surface chemistry: Butterworth-Heinemann, Oxford, 1991, ISBN 0 7506 1182 0, 306 pp,£ 14.95. Elsevier 1993.
[8] Everett DH. Basic principles of colloid science: R. Soc. Chem. 2007.
[9] Ross S, Morrison E. Colloidal systems and interfaces 1988.
[10] Lyklema J. Fundamentals of interface and colloid science: soft colloids: Academic press 2005.
[11] Barnes HA. A handbook of elementary rheology 2000.
[12] Shaw MT, MacKnight WJ. Introduction to polymer viscoelasticity: John Wiley & Sons 2005.
[13] Larson RG. The structure and rheology of complex fluids: Oxford university press New York 1999.
[14] Larsson M, Duffy J, AB MIN. An overview of measurement techniques for determination of yield stress. Annu. Trans. Nord. Rheol. Soc. 2013;21:125-38.
[15] Jabłoński A. Über den mechanismus der photolumineszenz von farbstoffphosphoren. Zeitschrift für Physik A Hadrons and Nuclei 1935;94:38-46.
[16] Stokes GG. On the change of refrangibility of light. Philos. Trans. R. Soc. London 1852;142:463-562.
[17] Kasha M. Characterization of electronic transitions in complex molecules. Discuss. Faraday Soc. 1950;9:14-9.
[18] Valeur B, Berberan-Santos MN. Molecular fluorescence: principles and applications: John Wiley & Sons 2012.
[19] Demchenko AP. Ultraviolet spectroscopy of proteins: Springer Science & Business Media; 2013.
[20] Permyakov EA. Luminescent spectroscopy of proteins: CRC press 1992.

Chapter IV

Effect of the coexistence of sodium caseinate and Tween 20 as stabilizers of food emulsions at acidic pH

IV.1 Introduction

In the last few years functional foods or nutraceuticals are gaining increasing attention due to the raise in the development and consumption of these products. The interest is not only related to the growing of the market trend but also to the tremendous need to exploit natural foods potentially able to prevent carcinogenic, cardiovascular and respiratory diseases. When nutraceutical molecules have low water solubility, the use of a compartmentalized system, like emulsions, represents one of the choices to improve both the bioactive compound addition in food preparation and the nutraceutical delivery in the human body [1]. Emulsion, indeed, offers a suitable way to reduce fat in food without compromising their organoleptic properties and to assure the appropriate availability.

Emulsions are commonly used in many major chemical industries, in the pharmaceutical industry, in food chemistry and in biotechnological applications [2-7]. One of the issues related to the use of emulsion is the stability to environmental stress and its effect on the physico-chemical characteristics. Surfactants are generally used to improve the stability of food emulsions [8, 9]. The two most important types of surface-active materials in food are proteins and low molecular weight surfactants [10]. The importance of emulsifier food additives in the manufacture of food products such as creamy sauces, candy, packaged processed foods, margarine and confections is well established for almost a century [11-14].

Among the proteins, sodium caseinate is largely used as food ingredient in food industry. Sodium caseinate derives from casein that is the principal protein component of milk. It is formed by different protein fractions (α_{s1}-,α_{s2}-, β- and *k*-casein in weight ratio of 0.4:0.08:0.4:0.1) [15, 16]. Thanks to its composition, sodium caseinate is characterized by good solubility and suitable surface-active properties. It is, in fact, composed of hydrophilic and hydrophobic domains distributed in various sequences and fractions [17]. These characteristics and the fact that it is a

natural diary product make caseinate a good emulsifier for food emulsion preparation. Together with the strengths that come with the use of sodium caseinate, the issue related to effects induced by pH fluctuation of the medium should be handled with the utmost care. As well known, sodium caseinate has an isoelectric point at pH 4.6, that is the pH value at which the overall charge of the protein is zero (a neutral charge) . In these conditions, sodium caseinate loses the repulsive forces that support the protein solubilization and as a consequence it precipitates. When this happens to caseinate in food emulsion, i.e., to caseinate forming a thin layer that stabilizes oil droplets in an aqueous phase, it generates the emulsion destabilization. This last aspect is a drawback when caseinate is used as stabilizer of preparations characterized by acidic pH [18].

Several cases of coexistence of proteins and surfactants at the oil/water (*O/W*) interface have been reported, i.e. for the case of oil or water soluble surfactants [19-21]. The behavior of mixed systems containing surfactants is strongly related to the presence of surfactant-protein association structures and interfacial interactions [22]. Low molecular weight surfactants decrease the surface or interfacial tension to a greater extent compared with macromolecular surfactants. This difference is mainly related to differences in orientation and configuration at the interface. Generally, low molecular mass surfactants rapidly adsorb and orient themselves properly between the two phases facilitating a maximum reduction of interfacial tension. Proteins are less surface active compared to low molecular mass surfactants, because proteins lower the interfacial tension by forming a continuous viscoelastic membrane around droplets that like a film stabilize the dispersed phase. Low molecular mass surfactants do not form such a viscoelastic films. The behavior of mixed systems depends on the nature of the interactions between proteins and emulsifiers at the oil-water interface. For emulsions containing both low molecular and macromolecular surfactants, the stability is mainly dependent on protein films adsorbed at the interfaces [23]. However simple non-ionic emulsifiers displace milk proteins from the interface because at high surfactant concentrations they produce a lower interface tension [24]. Dickinson well highlighted the importance of ionic emulsifiers and particularly the role of sodium caseinate [25]. Recently Su and coworkers, highlighted that sodium caseinate can be used in a mixed system to partially replace synthetic surfactants for nanoemulsions fabrications using the PIT (phase inversion temperature) method [26]. Zou et al. reported that using mixed colloidal dispersions the bioaccessibility of hydrophobic bioactive agents like curcumin can be enhanced [27].

Furthermore, it is well established that parameters like pH, ionic strength and temperature has to be considered pivotal for demulsification and thus for the emulsions stability [28]. For O/W emulsions stabilized by polystyrene latex particles with ionizable amino surface groups, the role of pH and temperature for the demulsification process was defined [29]. Since emulsions or

nanoemulsions stabilized by caseinate lose their stability in correspondence of the protein isoelectric point, this aspect could make caseinate unappealing for applications where the stability is required. For this reason, this study focuses on the preparation and the characterization of stable nanoemulsions made by using a blend of caseinate with a non-ionic surfactant in an attempt of finding the optimal formulation to produce stable nanoemulsions for food and healthcare applications.

IV.2 Materials and Methods

Materials

Tween 20 (polyoxyethylene 20 monolaureate), sodium caseinate, sodium bicarbonate, sodium carbonate, citric acid monohydrate, trisodium citrate dihydrate, sodium phosphate dibasic, sodium phosphate monobasic and hydrochloric acid were purchased from Sigma-Aldrich and used without further purification. Rice bran oil was from a local supermarket. All other chemicals were of analytical grade. Ultrapure water was used to prepare all solutions and nanoemulsions.

O/W Nanoemulsion preparation

Nanoemulsions were prepared by mixing the previously aqueous phase prepared by dissolving Tween 20 or sodium caseinate in ultrapure water with 5% (w/w) rice bran oil. Fine emulsions were then obtained by mixing the two phases through an Ultrasonic Homogenizer (Model 300 VT) for 2 minutes. All the nanoemulsions were prepared with 5% oil content and in the range of emulsifier concentrations (0.5, 1.0, 1.5, 2.0 % w/w). Tween 20, sodium caseinate or a 1:1 (w/w) blend of the two emulsifier were used as emulsifiers.

Nanoemulsion Characterization

The mean particle diameters (Z-average) and the polydispersity index (PDI) of the oil dispersed phase were determined through Dynamic Light Scattering (DLS) using a Malvern UK Zetasizer-Nano ZS90 instrument operating with a 4 mW He-Ne laser (633 nm wavelength). The average aggregate size and the PDI values were estimated with a fixed detector angle of 90° by a cumulant analysis of the autocorrelation function using the software provided by the manufacturer. Samples were properly diluted with ultrapure water prior to measurements to avoid multiple scattering effects according to previous studies [30, 31]. Effects of different processing conditions on the nanoemulsion stability were analyzed by changing parameters such as incubation time, temperature and pH. Particle size distribution and stability were analyzed after sample preparation, after 4 days at 25°C and after heating the samples at 37 °C for 4 days. ζ-potential measurements (angle of detection 17°) were carried out through the electrophoretic

mobilities of the dispersed phase as determined by laser Doppler velocimetry. The ζ-potential was calculated from the Smoluchowski approximation of the Henry equation. Samples were placed into dedicated disposable capillary cells. All measurements were performed at 25 °C.

Rheology measurements of nanoemulsions were carried out using a Haake MARS III rheometer (Thermo Scientific) equipped with a parallel plate geometry probe with a plate diameter of 60 mm. This geometry solution provided narrow gap and large surface area suited for low viscosity samples [32]. The temperature was controlled by a Phoenix II cooling and heating system in combination with a Peltier heating system. The samples (2.9 mL) were carefully poured into the surface of the lower plate and the upper plate was lowered until reached a 1 mm gap distance. Before testing samples were left to rest for 10 minutes in order to allow temperature equilibration. Flow curves were made in CR (control rate) mode varying the shear rate (0.1- 150 s^{-1}) at 25°C. Apparent viscosity was measured at fixed shear rate of 100 s^{-1} at 25°C.

Fluorescence measurements were performed using a Varian Eclipse spectrofluorimeter in a 1 cm quartz fluorescence cuvette. The measurements were carried out after an incubation time of 5 min. The excitation and the emission slit widths were 5 nm. The excitation wavelength was 290 nm.

IV.3 Results and discussion

In this investigation 5% (w/w) rice bran oil nanoemulsions stabilized by non-ionic surfactant (Tween 20), protein (Caseinate) and a blend of the two emulsifiers in a 1:1 weight ratio (Mix) were analyzed and compared. The overall amount of surface-active molecules varied in the range of 0.5-2% (w/w). Henceforth, it will be referred to *Tw20-O/W* (nanoemulsions stabilized by Tween 20), *Cas-O/W* (nanoemulsions stabilized by caseinate) and *Mix-O/W* (nanoemulsions stabilized by both the emulsifiers).

The size of the oil droplets immediately after the nanoemulsion preparation obtained by means of DLS analysis is reported in Fig. IV.1A. Samples were properly diluted according to other authors [30, 31]. At first glance, it appeared that increasing the concentration of the emulsifier resulted in a decrease of the oil droplet size present in the dispersed phase when Tween 20 took part to the nanoemulsion, i.e. for *Tw20-O/W* and *Mix-O/W* nanoemulsions. Conversely, the amount of protein in *Cas-O/W* did not seem influencing the aggregates diameters of the dispersed phase which varied from about 390 to 450 nm.

The effect of time on the samples was studied by performing the measurements after a period of 4 days (Fig. IV.1B). As can be seen, this storage time slightly affected the droplet size for *Tw20-O/W* nanoemulsions, while the dispersed phase size decreased for low protein concentration in

Cas-O/W nanoemulsions and increased for *Mix-O/W* which lost the early resemblance to Tween 20 stabilized nanoemulsion in term of size and gained an higher similarity to *Cas-O/W*.

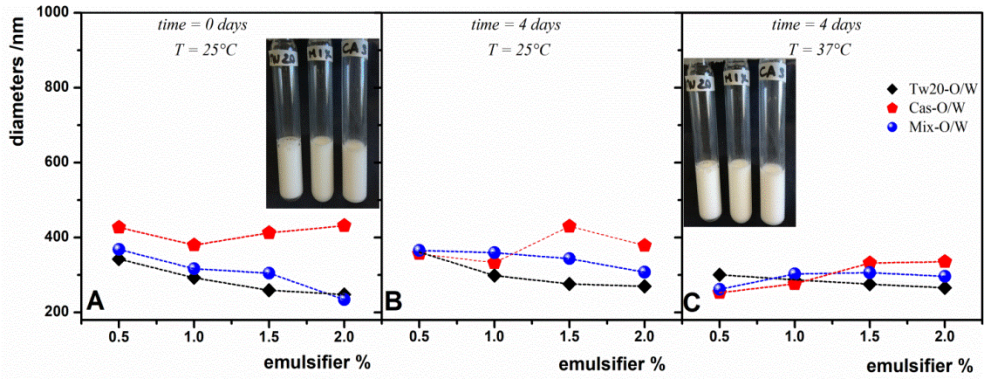

Fig. IV.1. Oil droplet size as function of emulsifier percentage immediately after nanoemulsion preparation (A); after 4 days storage at 25°C (B); after 4 days storage at 37 °C (C). *Tw20-O/W*: full black diamonds; *Cas-O/W*: full red pentagons ; *Mix-O/W:* full blue circles. Inset of panel A and C: pictures (from left to right: *Tw20-O/W*, *Mix-O/W* and *Cas-O/W* nanoemulsions) of just prepared and stored at 37°C nanoemulsions respectively.

The effect of storage under heating, was evaluated by keeping the samples at 37 °C for the same period of time (4 days). As can be inferred from Fig. IV.1C, in these conditions, sizes of dispersed phase for all the nanoemulsions became approximately close each other for all the analysed systems. Comparing these results with those of the samples stored at 25 °C *Cas-O/W* showed the higher variation. Insets of Fig. IV.1A and IV.1C showed pictures of the three different nanoemulsions freshly prepared and after 4 days storage at 37 °C. As shown, from a macroscopic point of view the samples appeared stable and substantially unchanged.

In order to improve the nanoemulsions characterization, samples were tested for their rheological behavior. The flow curves and the relative viscosity curves of the different types of nanoemulsions are illustrated in Fig. IV.2. As reported, for all the emulsifiers content the best fitting of shear stress as function of shear rate is given by Herschel Bulkley model (Eq. IV.1) that is applied on fluids with a non linear behavior and yield stress:

$$\tau = \tau_0 + K\dot{\gamma}^n \qquad \text{(IV.1)}$$

where τ_0 is the yield stress value, *K* indicated as consistency index, reflect the viscosity of the fluid and *n* is the flow behavior index. When *n* is close to 1 the fluid tends to pass from a shear thinning to a shear thickening behavior, when *n* is above 1, the fluid has shear thickening properties. The parameters obtained from the experimental data fitting to Eq. IV.1 are reported in Table IV.1. According to the Herschel Bulkley model and to the viscosity data flow all the nanoemulsions here considered, regardless of the type and concentration of emulsifier, behaved as non-newtonian fluids, and considering that the obtained *n* values are all close each other, all nanoemulsions exhibited similar flow behavior.

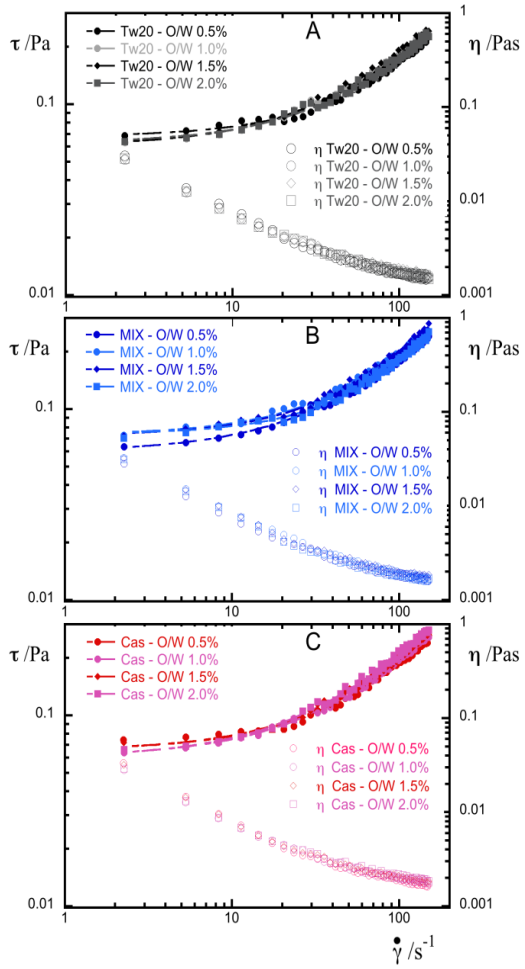

Fig. IV.2. Flow curves of nanoemulsions (full symbols) and relative viscosity as function of shear rate (empty symbols). A: Tween 20 stabilized nanoemulsions; B: Mix stabilized nanoemulsions; C: Sodium caseinate stabilized nanoemulsions.

Table IV.1. Yield stress (τ_0), consistency index (K) and flow behavior index (n) obtained from fitting the experimental data to Eq. 4.1.

	τ_0 (Pa)		K (Pas^n)		n	R^2
Tw20 – O/W 0.5%	6.80 x 10^{-2}	± 2.5 x 10^{-3}	7.00 x 10^{-4}	± 1.70 x 10^{-4}	1.078 ± 4.7 x 10^{-2}	0.99504
Tw20 – O/W 1.0%	6.05 x 10^{-2}	± 3.0 x 10^{-3}	1.39 x 10^{-3}	± 3.0 x 10^{-4}	0.964 ± 4.1 x 10^{-2}	0.99097
Tw20 – O/W 1.5%	6.07 x 10^{-2}	± 3.1 x 10^{-3}	1.41 x 10^{-3}	± 3.1 x 10^{-4}	0.971 ± 4.1 x 10^{-2}	0.99098
Tw20 – O/W 2.0%	6.29 x 10^{-2}	± 3.1 x 10^{-3}	1.07 x 10^{-3}	± 2.6 x 10^{-4}	1.008 ± 4.6 x 10^{-2}	0.98929
MIX – O/W 0.5%	5.97 x 10^{-2}	± 3.3 x 10^{-3}	1.46 x 10^{-3}	± 3.2 x 10^{-4}	0.962 ± 4.2 x 10^{-2}	0.99531
MIX – O/W 1.0%	7.34 x 10^{-2}	± 3.0 x 10^{-3}	9.70 x 10^{-4}	± 2.30 x 10^{-4}	1.045 ± 4.4 x 10^{-2}	0.99524
MIX – O/W 1.5%	7.26 x 10^{-2}	± 2.8 x 10^{-3}	8.30 x 10^{-4}	± 1.70 x 10^{-4}	1.090 ± 4.0 x 10^{-2}	0.99629
MIX – O/W 2.0%	7.38 x 10^{-2}	± 2.7 x 10^{-3}	5.20 x 10^{-4}	± 1.30 x 10^{-4}	1.156 ± 4.9 x 10^{-2}	0.99499
Cas – O/W 0.5%	6.59 x 10^{-2}	± 3.5 x 10^{-3}	1.12 x 10^{-3}	± 2.9 x 10^{-4}	1.020 ± 4.9 x 10^{-2}	0.99415
Cas – O/W 1.0%	6.08 x 10^{-2}	± 3 x 10^{-4}	1.47 x 10^{-3}	± 2.8 x 10^{-4}	0.982± 3.6 x 10^{-2}	0.99661
Cas – O/W 1.5%	6.61 x 10^{-2}	± 2 x 10^{-4}	1.13 x 10^{-3}	± 2.4 x 10^{-4}	1.041± 4.1 x 10^{-2}	0.99599
Cas – O/W 2.0%	6.01 x 10^{-2}	± 3.4 x 10^{-3}	1.73 x 10^{-3}	± 3.3 x 10^{-4}	0.972 ± 3.7 x 10^{-2}	0.99647

The apparent viscosity varied according to the type of emulsifier already at low concentration, as shown in Fig. IV.3. Low concentration of Tween 20 (0.5%) had apparent viscosity value very similar to that of water and linearly and slightly increased while increasing the surfactant concentration. In the same way, *Cas-O/W* and *Mix-O/W* nanoemulsions had growing values of apparent viscosity according to the rise of concentration. Although increasing the apparent viscosity values remained low and were typical of liquid feeds or beverages [33].

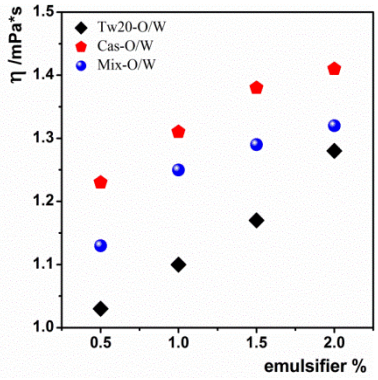

Fig. IV.3. Nanoemulsions apparent viscosity measured at shear rate of 100 s^{-1} as a function of emulsifier type and concentrations.

Apparent viscosity values were collected at a shear rate of 100 s^{-1}, such kind of shear rate value is typical for food processes such as mastication, flow through a pipe or stirring [34].

In order to consider a wide range of applications, the pH of the nanoemulsions was changed from the native values, which were for all slightly acidic (between pH 6.0 and 6.5), to acidic pHs, lower than 3 and alkaline values. Considering that ζ-potential gives information on nanoemulsion stability and that the surface charge of protein is influenced by pH, the surface charge of the nanoemulsion droplet was determined according to pH variations (Fig. IV.4). As indicated, at native pH all the nanoemulsions, regardless of the emulsifier type and concentration gave negative values of surface charge. More negative values were found for *Cas-O/W* nanoemulsions, while less negative surface charge values were found for *Tw20-O/W* nanoemulsions. *Mix-O/W* nanoemulsions gave intermediate surface charge values between the two other systems, because ζ-potential values strongly depend on the interface layer composition [35].

From the ζ-potential profiles, it emerged that *Cas-O/W* and *Mix-O/W* nanoemulsions were characterized by three main surface charge zones, according to variations of pH values. When the pH was lower than the pI value of caseinate (pH 4.6), the surface became positively charged, approaching the pI value the surface charge turned close to zero, moving toward higher pH the ζ-potential value was even more negative.

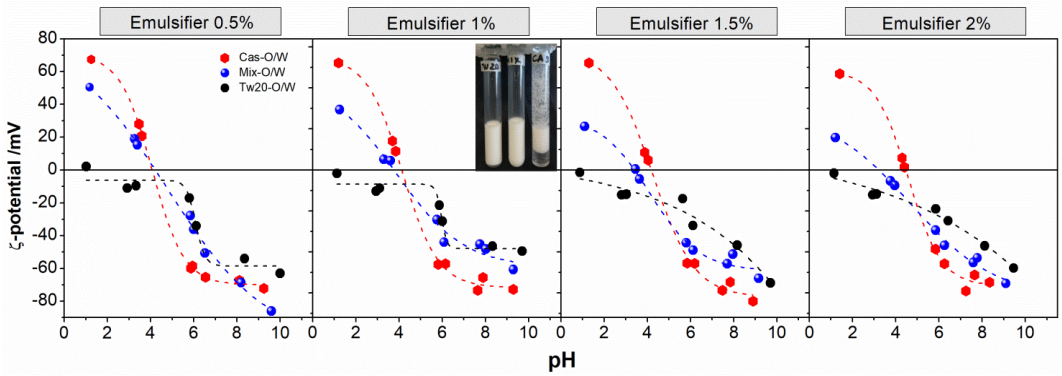

Fig. IV.4. ζ-potential as function of pH for nanoemulsions stabilized with different percentages of emulsifier. Red dots indicate *Cas-O/W*; black dots are for *Tw20-O/W* and blue dots for *Mix-O/W*. Inset: picture of acidified nanoemulsions, from left to right: *Tw20-O/W*, *Mix-O/W* and *Cas-O/W* nanoemulsions.

Taking into account the ζ-potential profiles of Tween 20, the negative surface charge of the O/W nanoemulsion may be attributed to the adsorption of OH^- species from the aqueous phase [34, 36]. Size distributions of the nanoemulsions dispersed phases were measured according to variations of pH. By means of this approach, it was verified that the *Cas-O/W* nanoemulsion were destabilized at pH values close to the pI. A direct evidence of this behavior is given in the inset of Fig. IV.4 where pictures of the acidified nanoemulsions highlighted the flocculation occurring when only caseinate was used as emulsion stabilizer. On the contrary, *Mix-O/W* and *Tw20-O/W* nanoemulsions remain stable also at acidic pH. Size distributions of the dispersed phase for *Cas-O/W* 0.5 and 2%, respectively, were reported in Fig. IV.5A and IV.5C, as function of pH. As can be seen, for low caseinate concentration (0.5%) the size distribution was at least bimodal for pH close to 4, while for the same pH at higher caseinate concentration (2%) no size distribution was detected because the nanoemulsion was fully destabilized and flocculated. By comparing the *Cas-O/W* with the *Mix-O/W* nanoemulsions, whose droplet size distributions are reported in Fig. IV.5B and D (for emulsifier concentration of 0.5 and 2% respectively), two main aspects can be highlighted: i) *Mix-O/W* nanoemulsions gave size distributions characterized by low dispersity; ii) *Mix-O/W* nanoemulsions showed stability at pH values close to 4. On the contrary, *Cas-O/W* nanoemulsions were destabilized. The presence of caseinate affected the *Mix-O/W* nanoemulsion at high emulsifier concentration (2%) where the size distribution was centered on higher diameter values.

In view of these results, it was most likely that the 1:1 (w/w) blend of emulsifiers stabilized the nanoemulsion also at acidic pH conditions, even though the overall ζ-potential profiles of *Mix-O/W*, that in absolute terms presented lower values compared to *Cas-O/W*, would suggest a lower stability. The stabilizing effect, that was more evident in the *Mix-O/W* with low emulsifier content, indicated that in the *Mix-O/W* nanoemulsion, the droplet interface hosted both the emulsifiers and benefited of two mechanism of stabilization; on one side there was the

predominant role of Tween 20 that provided a steric stabilization and, on the other caseinate, that at low pH, gave electrostatic repulsion to the dispersed phase.

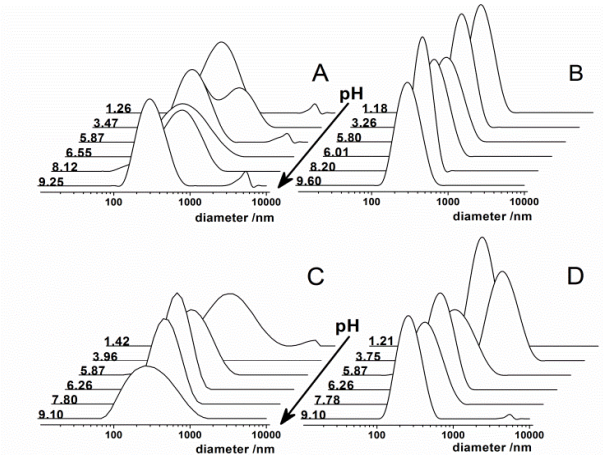

Fig. IV.5. Oil droplet size distribution as function of pH for *Cas-O/W* nanoemulsions 0.5% (A), 2% (C) and for *Mix-O/W* nanoemulsions 0.5% (B), 2% (D).

In order to understand if the stabilizing effect was due to the interactions between caseinate and Tween 20, experiments of acidification were also carried out on simple suspensions (without oil) of caseinate and Mix (caseinate/Tw-20 1:1 w/w). The different response to acidic pH values observed for the nanoemulsions, was not confirmed in the absence of oil. Indeed, at pH values close to 4 precipitation was observed in either the suspension of caseinate or the 1:1 blend of non-ionic surfactant and caseinate (data not shown).

Reckoning in that caseinate is made of different protein fractions (α_{s1}-, α_{s2}-, β-, and k-caseins), that the higher part of them is mainly hydrophobic (α_{s1}- and β-casein represent above 70% of protein), that the pI of protein depends mostly on charged aminoacids (water soluble) some hypothesis related to the surface arrangement of the protein, protein/Tween 20 can be made.

Fluorescence spectra reported in Fig. IV.6 compared the emission from caseinate suspension with the one of *Cas-O/W* nanoemulsion (Fig. IV.6A) and caseinate/Tween 20 blend (without oil) with Mix-O/W nanoemulsion. The oil content, in this case, was lowered to 0.1% (w/w) to avoid scattering interferences during the spectrofluorimetric measurements. The fluorescence of proteins is related to tryptophan, tyrosine and phenylalanine residues [16]. These amino acids generally self-assemble in hydrophobic portion of the proteins to shield from water contact. From the spectra reported in Fig. IV.6, as can be seen, no differences were detected for the caseinate emission in suspension with or without Tween 20. The emission spectra were, in fact, identical in absence of oil. On the other hand, both caseinate and Mix induced a red shift of the emission when emulsified with oil. When a red shift is observed, it means that the fluorescent

residues are more exposed to aqueous environment [37] as consequence of a conformational change of caseinate occurring at the o/w interface with or without Tween 20.

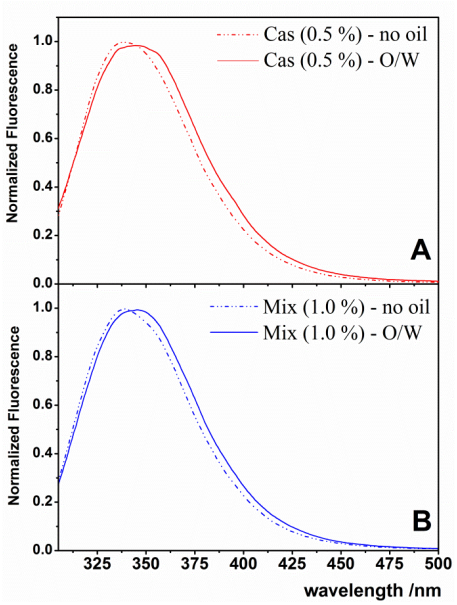

Fig. IV.6. Fluoresce emission spectra (λ_{ex} =290 nm) of caseinate suspension, *Cas-O/W* nanoemulsion (A) and mix suspension, *Mix-O/W* nanoemulsion (B) at 25°C.

Needless, this indication does not explain the different response of the *Cas-O/W* and *Mix-O/W* nanoemulsion at pH values close to 4. Nevertheless, this evidence proves that Tween 20 does not displace caseinate from interface, although small non-ionic surfactant are reported to dislocate protein at the o/w interface [23]. In light of these results, it is reasonable to speculate that, due to relatively large hydrophilic (polyoxyethylene) head groups of adsorbed Tween molecules, droplet flocculation was controlled in the *Mix-O/W* nanoemulsion and it is possible that the surfactant, in some way, segregated and protected the charged aminoacids thus preventing the protein precipitation and nanoemulsion destabilization.

IV.4 Conclusions

The present study was focused on improving the stability of a caseinate-based nanoemulsion to allow this protein to be used as food emulsifier of liquid preparations [38]. Sodium caseinate is sensitive to pH, in particular near its isoelectric point (pH 4.6), where, the overall charge of the protein is close to zero. The lack of electrostatic repulsion causes the protein precipitation and if the protein is located at the nanoemulsion o/w interface, the nanoemulsion loses stability. In order to improve the nanoemulsion stability the o/w interface was stabilized by a blend of protein and non-ionic surfactant. The results obtained through DLS demonstrated that the diameters of the dispersed phase in the blend stabilized nanoemulsions were smaller then those

of the *Cas-OW* nanoemulsion, indicating that the mixed system was more stable and that the ability of the blend of emulsifier in stabilizing the nanoemulsion was also proven at pH close to caseinate isoelectric point. The combination of ζ-potential and DLS data as function of pH demonstrated that in nanoemulsions stabilized by a blend of caseinate and Tween 20, the presence of Tween 20 ensured the steric stabilization.

As a whole the results obtained allow to draw the conclusion that promoting the use of sodium caseinate as emulsion stabilizer, the studied nanoemulsions could represent suitable tools in the field of manufacture of food products [38].

References

[1] Zou L, Zheng B, Liu W, Liu C, Xiao H, McClements DJ. Enhancing nutraceutical bioavailability using excipient emulsions: Influence of lipid droplet size on solubility and bioaccessibility of powdered curcumin. J. Funct. Foods 2015;15:72-83.
[2] Cinelli G, Cuomo F, Hochkoeppler A, Ceglie A, Lopez F. Use of Rhodotorula minuta live cells hosted in water-in-oil macroemulsion for biotrasformation reaction. Biotechnol. Prog. 2006;22:689-95.
[3] De Leonardis A, Cuomo F, Macciola V, Lopez F. Influence of free fatty acid content on the oxidative stability of red palm oil. RSC Adv. 2016;6:101098-104.
[4] Friberg S, Larsson K, Sjoblom J. Food emulsions: CRC Press; 2003.
[5] Lopez F, Cinelli G, Colella M, De Leonardis A, Palazzo G, Ambrosone L. The role of microemulsions in lipase-catalyzed hydrolysis reactions. Biotechnol. Prog. 2014;30:360-6.
[6] Patravale VB, Date AA, Kulkarni RM. Nanosuspensions: A promising drug delivery strategy. J. Pharm. Pharmacol. 2004;56:827-40.
[7] Sjöblom J. Encyclopedic Handbook of Emulsion Technology. New York: Marcel Dekker; 2001.
[8] Baldauf L, Schechter R, Wade W, Graciaa A. The relationship between surfactant phase behavior and the creaming and coalescence of macroemulsions. J. Colloid Interface Sci. 1982;85:187-97.
[9] Kralova I, Sjöblom J. Surfactants used in food industry: A review. J. Dispersion Sci. Technol. 2009;30:1363-83.
[10] Dickinson E. Introduction to food colloids: Oxford University Press; 1992.
[11] De Leonardis A, Pizzella L, Macciola V. Evaluation of chlorogenic acid and its metabolites as potential antioxidants for fish oils. Eur. J. Lipid Sci. Technol. 2008;110:941-8.
[12] Dickinson E. Food emulsions and foams: Stabilization by particles. Curr. Opin. Colloid Interface Sci. 2010;15:40-9.
[13] Hasenhuettl GL. Overview of food emulsifiers. Food Emulsifiers and Their Applications: Second Edition2008. p. 1-9.
[14] Mosca M, Diantom A, Lopez F, Ambrosone L, Ceglie A. Impact of antioxidants dispersions on the stability and oxidation of water-in-olive-oil emulsions. Eur. Food Res. Technol. 2013;236:319-28.
[15] Fox PF. Milk proteins: general and historical aspects. Adv. Dairy Chem.—1 Proteins: Springer; 2003. p. 1-48.
[16] Lopez F, Cuomo F, Nostro PL, Ceglie A. Effects of solvent and alkaline earth metals on the heat-induced precipitation process of sodium caseinate. Food Chem. 2013;136:266-72.
[17] Dickinson E. Milk protein interfacial layers and the relationship to emulsion stability and rheology. Colloids Surf., B 2001;20:197-210.
[18] Pallandre S, Decker EA, McClements DJ. Improvement of Stability of Oil-in-Water Emulsions Containing Caseinate-Coated Droplets by Addition of Sodium Alginate. J. Food Sci. 2007;72.
[19] Dickinson E, Tanai S. Protein displacement from the emulsion droplet surface by oil-soluble and water-soluble surfactants. J. Agric. Food Chem. (USA) 1992.
[20] Doxastakis G, Sherman P. The interaction of sodium caseinate with monoglyceride and diglyceride at the oil-water interface and its effect on interfacial rheological properties. Colloid Polym. Sci. 1986;264:254-9.
[21] Fang Y, Dalgleish DG. Casein adsorption on the surfaces of oil-in-water emulsions modified by lecithin. Colloids Surf., B 1993;1:357-64.
[22] Dickinson E, Hong S-T. Influence of an anionic surfactant on the rheology of heat-set β-lactoglobulin-stabilized emulsion gels. Colloids Surf., A 1997;127:1-10.
[23] Damodaran S. Food Proteins and Their Applications: Taylor & Francis; 1997.
[24] Chen J, Dickinson E. Viscoelastic properties of protein-stabilized emulsions: Effect of protein−surfactant interactions. J. Agric. Food Chem. 1998;46:91-7.

[25] Dickinson E. Properties of Emulsions Stabilized with Milk Proteins: Overview of Some Recent Developments. J. Dairy Sci. 1997;80:2607-19.
[26] Su D, Zhong Q. Lemon oil nanoemulsions fabricated with sodium caseinate and Tween 20 using phase inversion temperature method. J. Food Eng. 2016;171:214-21.
[27] Zou L, Zheng B, Zhang R, Zhang Z, Liu W, Liu C, et al. Enhancing the bioaccessibility of hydrophobic bioactive agents using mixed colloidal dispersions: Curcumin-loaded zein nanoparticles plus digestible lipid nanoparticles. Food Res. Int. 2016;81:74-82.
[28] Sari TP, Mann B, Kumar R, Singh RRB, Sharma R, Bhardwaj M, et al. Preparation and characterization of nanoemulsion encapsulating curcumin. Food Hydrocolloids 2015;43:540-6.
[29] Ngai T, Behrens SH, Auweter H. Novel emulsions stabilized by pH and temperature sensitive microgels. Chem. Commun. 2005:331-3.
[30] Guttoff M, Saberi AH, McClements DJ. Formation of vitamin D nanoemulsion-based delivery systems by spontaneous emulsification: Factors affecting particle size and stability. Food Chem. 2015;171:117-22.
[31] Qian C, McClements DJ. Formation of nanoemulsions stabilized by model food-grade emulsifiers using high-pressure homogenization: Factors affecting particle size. Food Hydrocolloids 2011;25:1000-8.
[32] Dolz M, Hernández MJ, Delegido J. Creep and recovery experimental investigation of low oil content food emulsions. Food Hydrocolloids 2008;22:421-7.
[33] Taherian AR, Fustier P, Britten M, Ramaswamy HS. Rheology and stability of beverage emulsions in the presence and absence of weighting agents: A review. Food Biophys. 2008;3:279-86.
[34] McClements DJ. Food emulsions: principles, practices, and techniques: CRC press; 2015.
[35] Russo Krauss I, Imperatore R, De Santis A, Luchini A, Paduano L, D'Errico G. Structure and dynamics of cetyltrimethylammonium chloride-sodium dodecylsulfate (CTAC-SDS) catanionic vesicles: High-value nano-vehicles from low-cost surfactants. J. Colloid Interface Sci. 2017;501:112-22.
[36] Anarjan N, Tan CP. Effects of selected polysorbate and sucrose ester emulsifiers on the physicochemical properties of astaxanthin nanodispersions. Mol. 2013;18:768-77.
[37] Vivian JT, Callis PR. Mechanisms of Tryptophan Fluorescence Shifts in Proteins. Biophys. J. 2001;80:2093-109.
[38] Perugini L, Cinelli G, Cofelice M, Ceglie A, Lopez F, Cuomo F. Effect of the coexistence of sodium caeinate and Tween 20 as stabilizers of food emulsions at acidic pH. Colloids Surf., B 10.1016/j.colsurfb.2018.02.003 (*in press*).

Chapter V

Effect of nanoemulsion stabilizers on the *in-vitro* digestion of curcumin

V.1 Introduction

Rhizome turmeric (*Curcuma longa*), containing high levels of curcumin, is used in numerous food products as a spice and pigment because of its characteristic flavor profile and yellow color [1], [2]. Curcuminoids are a group of highly hydrophobic molecules found in the spice turmeric, with the three dominant forms being curcumin, demethoxycurcumin and bisdemethoxycurcumin [3]. In traditional Chinese and Indian medicine, turmeric and curcuminoids have been used for the cure of numerous ailments, including anemia, bacterial infection, colds, coughs, eczema, fevers, inflammation, jaundice, liver, skin and urinary diseases, viral infections and wounds [2]. Curcumin, whose structure is shown in Fig. V.1, has been reported to have the highest bioactivity among the curcuminoids and to have low oral toxicity, even when ingested at relatively high doses (12 g per day) [4]. It contains three closely related lipophilic molecules having a number of phenolic groups and conjugated double bonds [5].

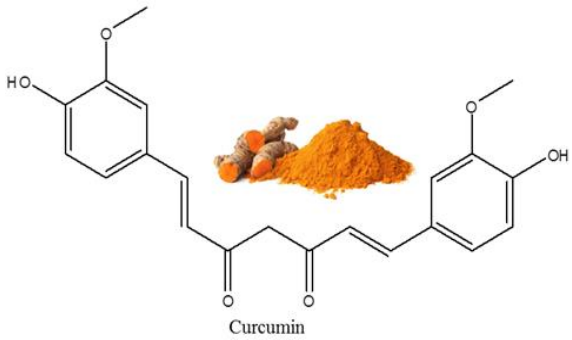

Fig. V.1. Curcumin structure.

Curcumin is considered highly effective against colorectal [6] and pancreatic cancer [7] thanks to its ability to interfere with various biochemical pathways. The health benefits of the nutraceutical

agent have been attributed to numerous different pharmacological effects, including antibacterial, antifungal, anti-inflammatory, antioxidant, anti-tumor and anti-viral activities [8]. These potential health benefits, as well as its good safety profile, have led to interest in its application as a bioactive agent in functional food, supplements and pharmaceuticals [9]. Nevertheless, the physicochemical characteristics that currently limit its incorporation into many food products are its low water-solubility, chemical instability and low oral bioavailability. The low-water solubility makes it difficult the integration into many functional food and beverages, while its low oral bioavailability may reduce its biological activity [4, 10,11]. The main factors limiting the bioavailability of curcumin are its low solubility in gastrointestinal fluids and its propension to undergo chemical transformation within the gastrointestinal tract [3]. These limits may be overcome by encapsulating curcumin within food-grade delivery systems such as liposomes [12], nanocomplexes [13, 14], colloidosomes [15], emulsions [16, 17], nanoemulsions [18, 19], or biopolymer nanoparticles [20, 21]. Nanoemulsion delivery systems are particularly effective at increasing the bioavailability of hydrophobic nutraceuticals because they are rapidly digested in the gastrointestinal tract (GIT), and therefore allow the rapid formation of mixed micelles that can solubilize the nutraceuticals [22]. Proteins represent a class of common ingredients found in functional food products [23], and therefore it is important to study how they may influence curcumin bioavailability. The presence of proteins in a food matrix may alter the oral bioavailability of nutraceuticals by altering their bioaccessibility, absorption or transformation in the GIT through various mechanisms, such as binding interactions, alteration of diffusion processes, interference with active or passive transport mechanisms and antioxidant activity [24]. The water-solubility and/or chemical stability of curcumin has been reported to improve when it binds to soy protein [25], whey protein [26], and caseinate [27]. As reported in chapter IV, the instability of the caseinate stabilized nanoemulsions at acidic pH was overcome using a mixed system, containing a combination of a non-ionic surfactant (Tween 20) and the protein. For this reason nanoemulsions made of caseinate and Tween 20 (*Mix-O/W*) were selected for being loaded with curcumin and, in this chapter, they are used in comparison with caseinate O/W nanoemulsions in an *in-vitro* digestion model to examine the effect of the two systems on the bioaccessibility, transformation and bioavailability of curcumin. In detail, the solubility of curcumin was evaluated according to the variation of type and concentration of emulsifier and according to different temperature of incubation (25, 30 and 100°C) to mimic the fact that an emulsion-based functional food may be consumed at room temperature (e.g. salad dressings) or after heating (e.g. cooking sauces). The outcomes of this study provide useful information on the

relationship between surface composition of the oil droplets, the curcumin solubility and bioavailability provided by the proposed nanoemulsion systems.

V.2 Materials and Methods

Materials

Rice bran oil was from a local supermarket. The following chemicals were purchased from the Sigma Chemical Company (St. Louis, MO): curcumin, mucin from porcine stomach, pepsin from porcine gastric mucosa, lipase from porcine pancreas pancreatin, porcine bile extract, Tween 20 (polyoxyethylene 20 monolaureate) and NaCas (sodium caseinate). All other chemicals were of analytical grade. Ultrapure water was used to prepare all solutions and emulsions.

O/W Nanomulsion preparation

Nanoemulsions were prepared by mixing the aqueous phase previously prepared by dissolving Tween 20 and sodium caseinate or only caseinate in ultrapure water with 5% (w/w) rice bran oil. Fine emulsions were then obtained by mixing the two phases through an Ultrasonic Homogenizer (Model 300 VT) for 2 minutes. Samples of nanoemulsions were all prepared with 5% oil content and increasing emulsifier concentrations (0.5, 1.0, 1.5 % w/w). Sodium caseinate or a 1:1 (w/w) blend of two emulsifier, Tween 20 and caseinate, were used as emulsifiers. Curcumin was added either in the oil phase before the nanoemulsion preparation or to the O/W nanoemulsion. The resulting mixtures were then incubated at 25 and 30 °C for 30 min and 100 °C for 15 min [28].

Curcumin solubility in O/W emulsion

The solubility of curcumin in each O/W nanoemulsion was measured using a UV-visible spectrophotometer based on the method previously proposed with some modifications [29]. The method is described as follows and it is shown in Fig. V.2.

Briefly, 5 mL of O/W emulsion were centrifuged at 2000 rpm for 10 minutes at room temperature to remove undissolved curcumin. After centrifugation, 1 mL of supernatant was mixed with 1 mL of chloroform and 1 mL of ultrapure water, vortexed for 2 minutes and centrifuged at 4000 rpm for 10 minutes.

The bottom layer (chloroform), containing the solubilized curcumin, was collected, while the top layer was further mixed with other chloroform (1 mL) and the same procedure was repeated until all the curcumin was extracted from the O/W emulsion. The chloroform collected was spectrophotometrically analyzed at 419 nm. The concentration of curcumin extracted from each mixture was calculated from a calibration curve (Fig. V.3). The solubility of curcumin in each

mixture was then calculated as the concentration of curcumin extracted from each mixture multiplied by the dilution factor.

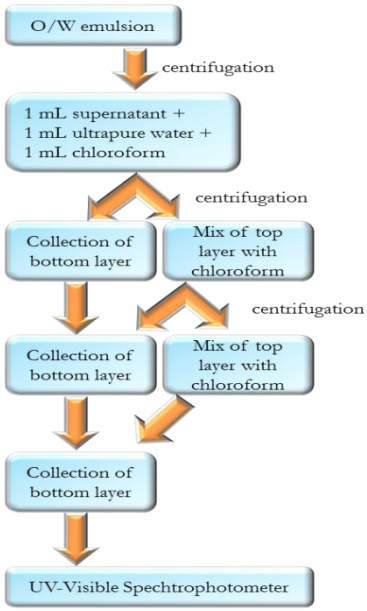

Fig. V.2. Flowchart of curcumin extraction procedure from O/W nanoemulsions.

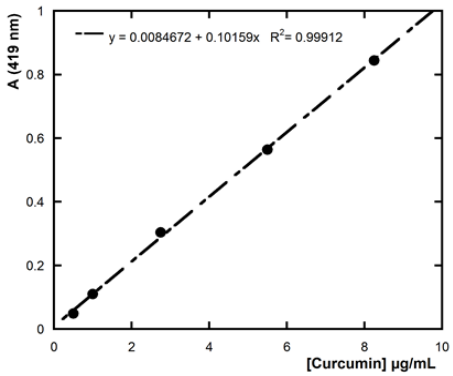

Fig. V.3. Calibration curve of curcumin in chloroform carried out through UV-Vis spectrophotometry.

V.2.1 Simulated Gastrointestinal Digestion

The potential gastrointestinal (GIT) fate of the samples was analyzed by passing them through an in vitro model that consisted of mouth, stomach and small intestine phases [30, 31]. The digestion process is simulated in a simplified manner by applying physiologically based conditions, i.e. chemical composition of digestive fluids, pH and residence time periods for each compartment. The model introduced by Oomen et al. (2003) [32] was used as starting point with some modifications [28, 29 33-35]. The digestive fluids were prepared according to Table V.1 showing the constituents and concentrations of the various synthetic fluids representing fed conditions.

Table V.1. Constituents and concentrations of the various synthetic juices of the in vitro digestion model representing fed conditions.

	Saliva	Gastric juice	Duodenal juice	Bile juice
Inorganic solution	10 mL KCl 89.6 g/L 10 mL KSCN 20 g/L 10 mL NaH_2PO_4 88.8 g/L 10 mL $NaSO_4$ 57 g/L 1.7 mL NaCl 175.3 g/L 20 mL $NaHCO_3$ 84.7 g/L	15.7 mL NaCl 175.3 g/L 3 mL NaH_2PO_4 88.8 g/L 9.2 mL KCl 89.6 g/L 18 mL $CaCl_2$ 2H20 22.2 g/L 10 mL NH_4Cl 30.6 g/L 6.5 mL HCl 37% g/g	40 mL NaCl 175.3 g/L 40 mL $NaHCO_3$ 84.7 g/L 10 mL KH_2PO_4 8 g/L 6.3 mL KCl 89.6 g/L 10 mL $MgCl_2$ 5 g/L 180 µL HCl 37% g/g	30 mL NaCl 175.3 g/L 68.3 mL $NaHCO_3$ 84.7 g/L 4.2 mL KCl 89.6 g/L 150 µL HCl 37% g/g
Organic solution	8 mL urea 25 g/L	10 mL glucose 65 g/L 10 mL glucuronic acid 2 g/L 3.4 mL urea 25 g/L 10 mL glucoseamine hydrochloride 33 g/L	4 mL urea 25 g/L	10 mL urea 25 g/L
Add to mixture organic + inorganic solution	290 mg α-amylase 25 mg mucin	1 g BSA 2.5 g pepsin 3 g mucin	9 mL $CaCl_2$ $2H_2O$ 22.2 g/L 1 g BSA 9 g pancreatin 1.5 g lipase	10 mL $CaCl_2$ $2H_2O$ 22.2 g/L 1.8 g BSA 30 g Bile
pH	6.8 ± 0.2	1.30 ± 0.02	8.1 ± 0.2	8.2 ± 0.2

The in vitro digestion model used in this study is described as follow and is shown in the Fig. V.4.

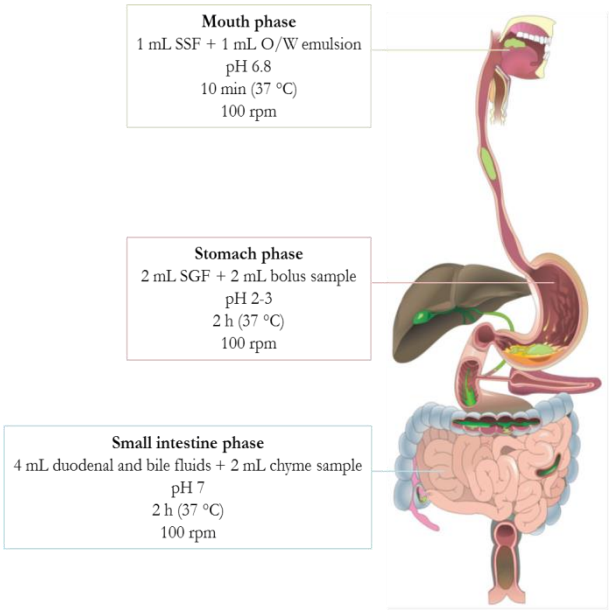

Fig. V.4. Schematic representation of the model used to simulate the in vitro digestion of curcumin.

Initial system: all the O/W nanoemulsions and the digestive fluids were placed in a shaking incubator at 100 rpm and 37°C for 15 min.

Mouth phase: a preheated simulated saliva fluid (SSF) (1 mL) was mixed with the preheated O/W nanoemulsion (1 mL) at 1:1 mass ratio. The mixture was then adjusted to pH 6.8 and placed in a shaking incubator at 100 rpm and 37°C for 10 minutes to mimic oral conditions.

Stomach phase: a preheated simulated gastric fluid (SGF) (2 mL) was mixed with the bolus sample from the mouth phase (2 mL) at 1:1 mass ratio. The mixture was then adjusted to pH 2-3 and placed in a shaking incubator at 100 rpm and 37°C for 2 h to mimic stomach digestion.
Small intestine phase: finally a mixture (4 mL) of duodenal and bile fluids was mixed with the chyme sample from the stomach phase (4 mL) at 1:1 mass ratio. The mixture was then adjusted to pH 7 and placed in a shaking incubator at 100 rpm and 37°C for 2 h [34].

Curcumin concentration, bioaccessibility and bioavailability after digestion

After in vitro digestion, 3 mL of "raw digesta" of each mixture were collected for the following extraction in chloroform and 5 mL were centrifuged at 10.000 rpm at 5°C for 1 h. The clear supernatant was collected and assumed to be the "micelle fraction" in which the curcumin was solubilized. Aliquots of 2 mL of "raw digesta" or "micelle fraction" were mixed with 2 mL of chloroform, vortexed for 2 min and centrifuged at 2000 rpm at 25°C for 10 min. The bottom layer, containing the solubilized curcumin, was collected while the top layer was mixed with other chloroform (2 mL) and the same procedure was repeated again until all the curcumin was extracted. The collected chloroform layers were mixed together and analyzed by a UV-VIS spectrophotometer at 419 nm. Anhydrous sodium sulphate was added to chloroform when it was opalescent to remove chloroform-solubilized water. The curcumin concentrations in the overall "raw digesta" and in the "mixed micelle phase" were calculated from the absorbance measurements using a standard curve and the known dilution factor [4].
The bioavailability (*BA*) of nutraceuticals is a function of other parameters such as Transformation (*T*) and Bioaccessibility (*B*) within the gastro-intestinal tract, for these reasons *B* and T were determined. *T* was calculated as the ratio of the curcumin concentration in raw digesta to that of the initial curcumin concentration as reported in Eq. V.1:

$$T = \frac{C_{digesta}}{C_{initial}} \times 100 \qquad (V.1)$$

The bioaccessibilily is the amount of active compound accessible for absorption. *B* is calculated as the ratio between curcumin in the micellar phase to the curcumin concentration in raw digesta (Eq. V.2):

$$B = \frac{C_{micelle}}{C_{digesta}} \times 100 \qquad (V.2)$$

The bioavailability, *BA*, is given by *B* x *T*, so it is the ratio between the curcumin in micellar phase to the initial curcumin concentration.

V.3 Results and discussion

V.3.1. Curcumin solubility in O/W nanoemulsions

In this study, 5 % O/W nanoemulsion have been considered, stabilized by protein (Sodium Caseinate) or a 1:1 w/w blend of protein and non ionic surfactant (Sodium Caseinate and Tween 20). In the following discussion the former nanoemulsion will be indicated with the code *Cas-O/W* and the latter with *Mix-O/W*. In the first stages curcumin solubility was determined in oil and in nanoemulsions. Spectrophotometric measurements reveals that by dispersing an access of curcumin powder at 25 °C in rice bran oil, the maximal amount of about 190 μg/mL of the drug can be solubilized. However, for a 5% O/W nanoemulsion, an amount of about 8 μg/mL of curcumin was found. With the purpose of increasing the amount of curcumin delivered with the nanoemulsions, an excess of powder was added to the nanoemulsion during the homogenization phase and successively the dispersed systems were incubated at 25 and 30 °C for 30 minutes and at 100 °C for 15 minutes. After incubation the nanoemulsions were left cooling at room temperature and subjected to centrifugation in order to remove the non-solubilized curcumin on the bottom of the test tubes. An example of the sample appearance is shown in Fig. V.5. Visual inspection of the samples in Fig. V.5A showed that the nanoemulsion delivery systems had a uniform yellow appearance with a more intense yellow color at high incubation temperature (from left to right the incubation temperature are 25, 30 and 100 °C). Fig. V.5B showed the samples after centrifugation; for all the samples curcumin crystals were deposited at the bottom of the test tubes.

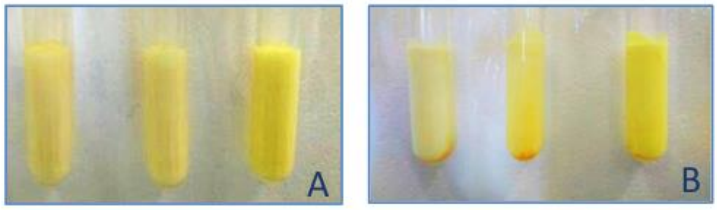

Fig. V.5. O/W nanoemulsion before (A) and after (B) centrifugation. From left to right in both panels O/W nanoemulsion containing excess of curcumin incubated at 25 and 30°C for 30 min and at 100°C.

The curcumin solubility in nanoemulsions at different emulsifier concentration determined after the treatment (temperature and time) as function of the incubation temperature is reported in Fig. V.6.

As can be seen in Fig. V.6, the solubility of the hydrophobic bioactive compound for *Mix-O/W* nanoemulsions increased with the increase of temperature and emulsifier content. Moreover, a small increase of temperature (from 25 to 30 °C) influenced the solubility of curcumin significantly for both protein and mixed protein/surfactant stabilized nanoemulsions.

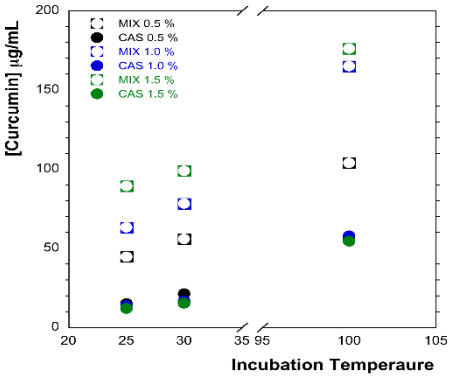

Fig. V.6. Curcumin concentration as function of incubation temperature according to different emulsifier type (sodium caseinte is represented with full dots, and mix emulsifier with empty dots) and concentration for *Cas-O/W* and *Mix-O/W* naoemulsions.

On the other side, *Cas-O/W* nanoemulsions increased the concentration of solubilized curcumin with the temperature, regardless the amount of protein used as interface stabilizer. Finally, the amount of curcumin solubilized through *Mix-O/W* nanoemulsion was always higher than that solubilized by *Cas-O/W* nanoemulsion. One possible explanation for this evidence would be that curcumin interacts with caseinate at the oil-water interface. At this juncture, if the surface of the oil droplets is already saturated of protein (concentration of 0.5%), the fact that curcumin concentration does not increase when increasing caseinate concentration will be explained. In order to corroborate this hypothesis curcumin solubility was also evaluated for emulsion with different oil concentrations than the 5% used (2.5 and 10%). Experiments were performed on samples with oil concentrations of 2.5 (lower) and 10% (higher) and with caseinate concentrations of 0.5, 1 and 1.5%. For nanoemulsion prepared with 2.5% oil content, the concentration of curcumin solubilized was around 11 µg/mL for all the caseinate concentrations considered. On the other side, in nanoemulsions prepared with 10% oil content, an excess of oil (stratified on top of nanoemulsion) was observed for 0.5% caseinate and the amount of curcumin solubilized was of about 15 µg/mL. No oil separation was observed in nanoemulsion stabilized by 1.0 and 1.5% of caseinate where curcumin concentration was of about 22 µg/mL for both the nanoemulsions. The present data confirmed that curcumin solubility in nanoemulsions stabilized by caseinate was dependent on the oil solubilized that varied according to the amount of caseinate.

V.3.2 *In-vitro* digestion of curcumin loaded nanoemulsions

With the purpose of having information on curcumin bioadsorption, *Mix-O/W* and *Cas-O/W* nanoemulsions, containing the bioactive component, were passed through a simulated gastrointestinal tract. The *in-vitro* digestion model here applied simulated the digestion in the human gastrointestinal tract in a simplified manner mimicking a three-phase process. In detail,

mouth, stomach and small intestine are simulated since it is in the latter that the absorption of many food components occurs. After the intestinal phase, curcumin concentration was determined both in raw digesta and in the micellar phase.

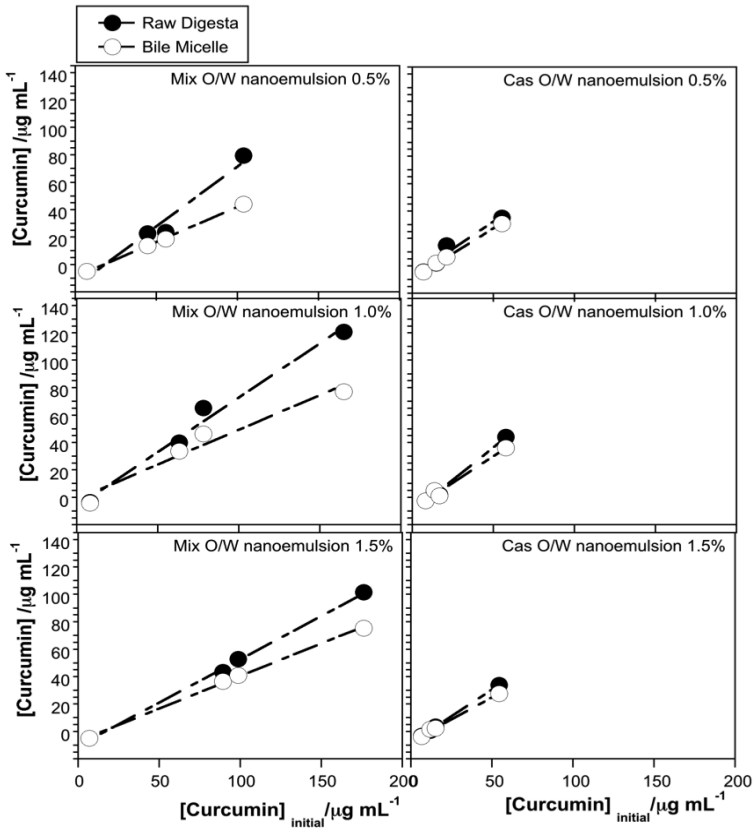

Fig. V.7. Curcumin concentration in raw digesta (full dots) and in bile micelle (empty dots) from nanoemulsions stabilized by Mix emulsifier (panels on the left, from top to bottom at increasing emulsifier concentration) or by sodium caseinate (panels on the right, from top to bottom at increasing emulsifier concentration) as function of initial curcumin concentration.

Raw digesta is the whole sample coming from the complete digestion (after the intestinal phase) while the micellar phase is obtained after centrifugation of the raw digesta at high speed and represents the micelle fraction where curcumin as well as lipophilic compounds are solubilized. Fat digestion starts in the stomach and continues in the small intestine where fat absorption also occurs. In the stomach, lipids are emulsified because of the shearing actions of mouth and stomach. When the emulsified lipids move to the intestine they are digested by pancreatic lipases and bile salt. Protein digestion starts with the gastric fluid as well, where the action of pepsin hydrolyzes the proteins to small peptides and follows in the small intestine by the action of the enzyme trypsin. The digestion route of proteins and fats will influence the fate of curcumin delivered by systems made of those ingredients.

In determining the amount of curcumin in raw digesta and bile micelle a linear correlation with the amount of solubilized curcumin was detected, as in Fig. V.7. Moreover, it was evident that

the difference in curcumin concentration in the two fractions was higher for the *Mix-O/W* nanoemulsions, while, the two concentrations were very similar for curcumin delivered with *Cas-O/W* nanoemulsions.

Samples passed through a simulated GIT and after exposure to each GIT stage bioaccessibility, transformation and bioavailability of curcumin were calculated. The overall bioavailability (BA) of a nutraceutical depends on its bioaccessibility (B) and transformation (T) within the GIT, and therefore the comprehension of the factors that impact these different contributions to the overall BA is important. Curcumin transformation and bioaccessibility were calculated according to eq.V.1 and V.2 respectively.

Curcumin Transformation

The transformation of a compound is referred to the amount of compound that remains in a bioactive form in the intestinal phase.

The amount of curcumin that is determined in the raw digesta has resisted to a series of variations in the route from the mouth to the intestine like ionic strenght changes, enzymatic activity and pH variations (from 7.0 in the mouth to 1.5–3.0 in the stomach and 6.0–7.5 in the intestine). Considering that curcumin is practically water insoluble at acidic or neutral pH, but it is relatively soluble at alkaline pH [36] where it rapidly undergoes hydrolytic degradation, generating feruloyl methane, ferulic acid and other minor components as degradation products [37], it would be difficult to find it in the bioactive form after its passage through GIT without a protection, such as the one offered by encapsulation strategies. The concentration of curcumin in the raw digesta to the initial curcumin concentration for all the nanoemulsions considered is illustrated by Fig. V.8 where a bar chart representing the parameter *T* is shown as function of the emulsifier percentage and according to variation of incubation temperature.

From the Fig. V.8, it appears that a trend can be defined for *Cas-O/W* nanoemulsions where the overall amount of curcumin seems decreasing with the emulsifier content, but increasing with the temperature of incubation. It is noteworthy that nanoemulsions where kept at 25, 30 and 100°C only for a limited time (30 or 15 min) and then cooled at room temperature that was close to 25°C. Accordingly, it seems that the incubation temperature affected the nanoemulsion structure and the curcumin transformation especially in the presence of caseinate as emulsifier.

On the contrary, *Mix-O/W* nanoemulsions did not present a marked trend with the emulsifier content and all in all offered a better protection to loaded curcumin, maybe because the presence of non-ionic surfactant and proteins at the oil droplet interface minimized the effect of the GIT route and of the temperature treatment which leads to a relatively high amount of curcumin remaining in an active form in the small intestine.

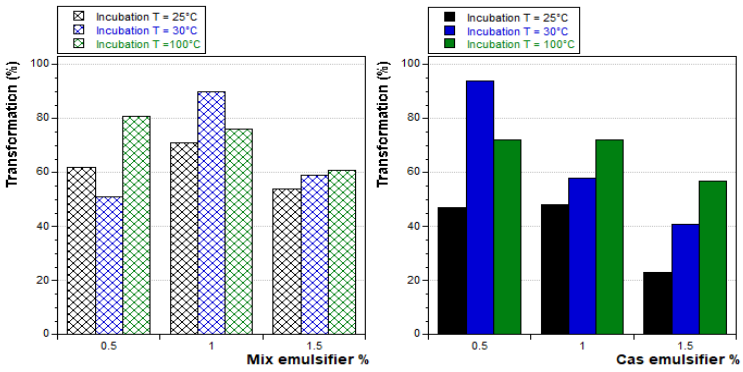

Fig. V.8. Transformation of curcumin as function of emulsifier percentage from *Mix-O/W* nanoemulsions (left panel) and *Cas-O/W* nanoemulsions (right panel) incubated at 25, 30 and 100°C.

These data showed that curcumin was well protected in this investigation and they were in agreement with previous studies where it was demonstrated that both lipids and proteins may shield curcumin from hydrolysis [38]. The fact that we observed a small difference between samples containing only sodium caseinate as emulsifier and samples containing both the stabilizers, caseinate and Tween 20, suggests that the curcumin was protected to a similar degree.

Curcumin Bioaccessibility

The Bioaccessibility of a compound is given by the amount of compound that is transferred to the micellar phase from the raw digesta. The content of curcumin in the bile salt micelle is influenced by the process of bile micelle formation from the nanoemulsions coming from the gastric phase. Because bile salts have strong surface-active properties, they partially or completely displace original emulsifiers from the oil/water interface [39, 40] thus forming bile salt micelle or mixed micelles containing oil and curcumin that will be further available for being adsorbed. Fig. V.9 shows the bioaccessibility of curcumin (i.e., the fraction of curcumin in the small intestine that was solubilized in the mixed micelle phase) for the systems, *Mix-O/W* and *Cas-O/W*, at different emulsifier percentages and after incubation at different temperatures.

As can be seen, *Cas-O/W* nanoemulsion showed higher bioaccessibility values than those obtained with the *Mix-O/W* systems. This would suggest that the micelle formation was eased by the presence of protein only.

Nevertheless, the calculated bioaccessibility was high enough for both the systems with values ranging from 60 to about 85 % for *Mix-O/W* nanoemulsions and from 80 (exception is 0.5% incubated at 30°C) to 100% for *Cas-O/W* nanoemulsions. In this case, a trend in decreasing with the increasing of incubation temperature was detected, in particular, for *Mix-O/W* nanoemulsions. In reasoning on the Transformation parameter, the effect of temperature were seen influencing the caseinate stabilized nanoemulsions more than the *Mix-O/W* nanoemulsions.

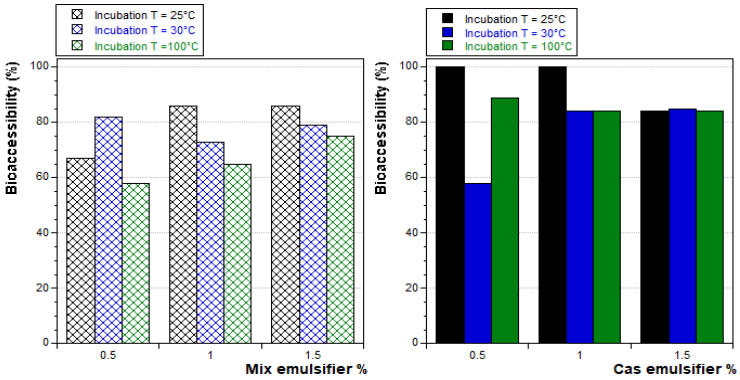

Fig. V.9. Bioaccessibility of curcumin as function of emulsifier percentage from *Mix-O/W* nanoemulsions (left panel) and *Cas-O/W* nanoemulsions (right panel) incubated at 25, 30 and 100°C.

For this reason, the trend observed for the latter regarding the Bioaccessibility should be correlated with the very high curcumin concentration solubilized as consequence of the temperature treatment, maybe too high for being completely adsorbed according to the conditions imposed in the present study.

Curcumin Bioavailability

The most interesting parameter obtained from an *in-vitro* digestion study is the Bioavailability *i.e.* the fraction of ingested curcumin present in the mixed micellar phase respect to the initial curcumin concentration. The compound concentration found in micellar phase is the part that eventually ends up in the systemic circulation. The Bioavailability values calculated for *Mix-O/W* and *Cas-O/W* nanoemulsion are illustrated in Fig. V.10. *Mix-O/W* nanoemulsions made the curcumin Bioavailability almost constant with values varying from about 42 to about 60% with the higher values given by the nanoemulsion stabilized by 1% of emulsifier. *Cas-O/W* nanoemulsions, in turn, gave similar values of Bioavailability, but for the 1.5% characterized by lower curcumin availability, as if a high concentration of caseinate reduced bioavailability, with an increasing trend depending on the incubation temperature and therefore on the initial concentration.

In a recent study, it was reported that curcumin powder was dissolved in the lipid phase of 10% oil in water nanoemulsion delivery system or directly mixed with an excipient nanoemulsion (nanoemulsion stabilized by surfactant without curcumin). The influence of thermal treatment and caseinate addition on curcumin bioavailability was evaluated and the obtained values were lower than 40% [38]. In another study [28], it was evaluated the impact of oil type (coconut, sunflower, corn, flax seed, or fish oils) on curcumin loaded in o/w emulsions. The best outcomes were obtained by fish oil that allowed curcumin bioavailability of about 38 %. Compared to those

references, the values of curcumin Bioavailability here detected represent a step forward in the formulation of curcumin rich food supplement, or pharmaceutical applications.

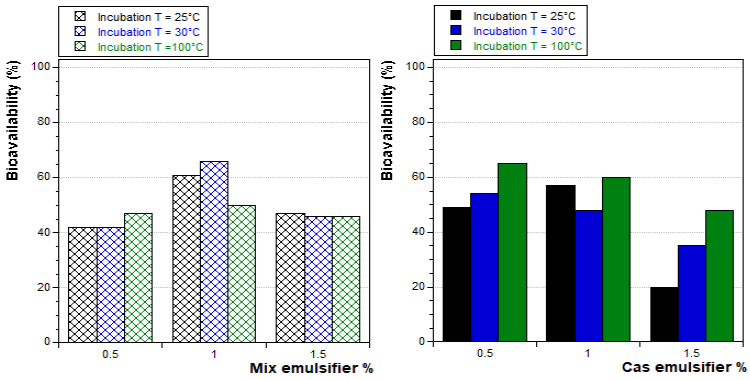

Fig. V.10. Bioavailability of curcumin as function of emulsifier percentage from *Mix-O/W* nanoemulsions (left panel) and *Cas-O/W* nanoemulsions (right panel) incubated at 25, 30 and 100°C.

Finally, representing the Bioavailability of curcumin as function of the initial concentration of compound loaded in the nanoemulsion, as shown in Fig. V.11, some consideration should be made.

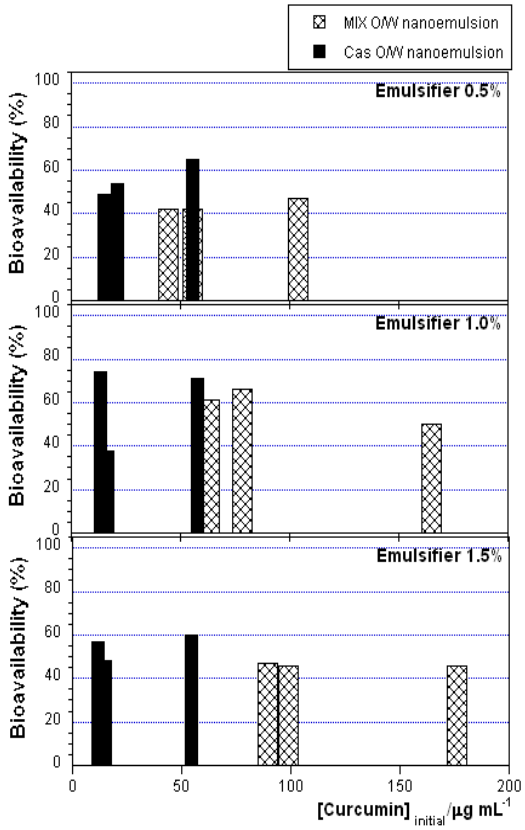

Fig. V.11. Bioavailability (C) of curcumin as function of initial curcumin concentration for Cas-O/W nanoemulsions (black bars) and Mix-O/W nanoemulsions (crossed fill pattern bars).

Although the bioavailability values are quite similar for the nanoemulsions stabilized with only caseinate or with the protein and surfactant blend, the different concentration of initial curcumin can not be ignored. Considering this aspect, in fact, some calculations can be made.

Regardless the incubation temperature taking into account, for example, the nanoemulsions with 1.0% of emulsifier, caseinate or emulsifiers blend, the amounts of curcumin solubilized were 55 and 165 μg/mL, respectively. Consequently, 10 mL of nanoemulsion (5% oil) will provide about 380 μg of curcumin bioavailable for adsorption from Cas-O/W nanoemulsion and about 825 μg from Mix-O/W nanoemulsion (values obtained multiplying the initially solubilized curcumin concentration by the bioavailability percentage and by the volume - 10 mL - of nanoemulsion considered). This result indicated that the blend stabilized nanoemulsions provided more than twice the curcumin provided by the former nanoemulsion.

V.4 Conclusions

Based on the previous investigation [40, 41] made on the nanoemulsion stability at acidic pH, the nanoemulsions stabilized by caseinate and non ionic surfactant (Tween 20) were selected for their stability characteristics, and used in the present study to load and deliver curcumin through the gastrointestinal tract. The results carried out on *Mix-O/W* nanoemulsions were compared to those obtained on *Cas-O/W* nanoemulsions. Starting from the load ability the two systems showed a noticeable difference with the *Mix-O/W* nanoemulsions able to solubilize more curcumin than *Cas-O/W* nanoemulsions. In particular, *Cas-O/W* nanoemulsions, at their best, solubilized about 55 μg of curcumin per mL of nanoemulsion and *Mix-O/W* nanoemulsions reached a curcumin concentration around 180 μg/mL.

After the simulated digestion both the nanoemulsion types gave high values of curcumin bioavailability compared to those reported in recent literature [28, 38] and this represented a meaningful outcome. Nevertheless the best solution to adsorb curcumin seems to be through *Mix-O/W* nanoemulsion because it allows the introduction of a significant amount of curcumin together with a low fat content.

References

[1] Prasad S, Gupta SC, Tyagi AK, Aggarwal BB. Curcumin, a component of golden spice: from bedside to bench and back. Biotechnol. Adv. 2014;32:1053-64.
[2] Syed HK, Liew KB, Loh GOK, Peh KK. Stability indicating HPLC–UV method for detection of curcumin in Curcuma longa extract and emulsion formulation. Food Chem. 2015;170:321-6.
[3] Heger M, van Golen RF, Broekgaarden M, Michel MC. The molecular basis for the pharmacokinetics and pharmacodynamics of curcumin and its metabolites in relation to cancer. Pharmacol. Rev. 2014;66:222-307.
[4] Anand P, Kunnumakkara AB, Newman RA, Aggarwal BB. Bioavailability of curcumin: problems and promises. Mol. Pharmaceutics 2007;4:807-18.
[5] Zhang Z, Zhang R, Zou L, Chen L, Ahmed Y, Al Bishri W, et al. Encapsulation of curcumin in polysaccharide-based hydrogel beads: Impact of bead type on lipid digestion and curcumin bioaccessibility. Food Hydrocolloids 2016;58:160-70.
[6] Carroll RE, Benya RV, Turgeon DK, Vareed S, Neuman M, Rodriguez L, et al. Phase IIa clinical trial of curcumin for the prevention of colorectal neoplasia. Cancer Prev. Res. 2011;4:354-64.
[7] Dhillon N, Aggarwal BB, Newman RA, Wolff RA, Kunnumakkara AB, Abbruzzese JL, et al. Phase II trial of curcumin in patients with advanced pancreatic cancer. Clin. Cancer Res. 2008;14:4491-9.
[8] Wilken R, Veena MS, Wang MB, Srivatsan ES. Curcumin: A review of anti-cancer properties and therapeutic activity in head and neck squamous cell carcinoma. Mol. Cancer 2011;10:12.
[9] Schneider C, Gordon ON, Edwards RL, Luis PB. Degradation of curcumin: from mechanism to biological implications. J. Agric. Food Chem. 2015;63:7606-14.
[10] Jitoe-Masuda A, Fujimoto A, Masuda T. Curcumin: from chemistry to chemistry-based functions. Curr. Pharm. Des. 2013;19:2084-92.
[11] Fu S, Shen Z, Ajlouni S, Ng K, Sanguansri L, Augustin MA. Interactions of buttermilk with curcuminoids. Food Chem. 2014;149:47-53.
[12] Chen X, Zou L-Q, Niu J, Liu W, Peng S-F, Liu C-M. The stability, sustained release and cellular antioxidant activity of curcumin nanoliposomes. Mol. 2015;20:14293-311.
[13] Chen F-P, Li B-S, Tang C-H. Nanocomplexation between curcumin and soy protein isolate: influence on curcumin stability/bioaccessibility and in vitro protein digestibility. J. Agric. Food Chem. 2015;63:3559-69.
[14] Wang Y-H, Wang J-M, Yang X-Q, Guo J, Lin Y. Amphiphilic zein hydrolysate as a novel nano-delivery vehicle for curcumin. Food Funct. 2015;6:2636-45.
[15] Shah BR, Li Y, Jin W, An Y, He L, Li Z, et al. Preparation and optimization of Pickering emulsion stabilized by chitosan-tripolyphosphate nanoparticles for curcumin encapsulation. Food Hydrocolloids 2016;52:369-77.
[16] Aditya N, Aditya S, Yang H-J, Kim HW, Park SO, Lee J, et al. Curcumin and catechin co-loaded water-in-oil-in-water emulsion and its beverage application. J. Funct. Foods 2015;15:35-43.
[17] Sari T, Mann B, Kumar R, Singh R, Sharma R, Bhardwaj M, et al. Preparation and characterization of nanoemulsion encapsulating curcumin. Food Hydrocolloids 2015;43:540-6.
[18] Ahmed K, Li Y, McClements DJ, Xiao H. Nanoemulsion-and emulsion-based delivery systems for curcumin: encapsulation and release properties. Food Chem. 2012;132:799-807.
[19] Patel A, Velikov KP. Colloidal delivery systems in foods: A general comparison with oral drug delivery. LWT-Food Sci. Technol. 2011;44:1958-64.
[20] Xiao J, Nian S, Huang Q. Assembly of kafirin/carboxymethyl chitosan nanoparticles to enhance the cellular uptake of curcumin. Food Hydrocolloids 2015;51:166-75.
[21] Hu K, Huang X, Gao Y, Huang X, Xiao H, McClements DJ. Core–shell biopolymer nanoparticle delivery systems: Synthesis and characterization of curcumin fortified zein–pectin nanoparticles. Food Chem. 2015;182:275-81.

[22] McClements DJ, Xiao H. Potential biological fate of ingested nanoemulsions: influence of particle characteristics. Food Funct. 2012;3:202-20.
[23] Damodaran S, Parkin KL, Fennema OR. Fennema's Food Chem.: CRC press; 2007.
[24] McClements DJ, Xiao H. Excipient foods: designing food matrices that improve the oral bioavailability of pharmaceuticals and nutraceuticals. Food Funct. 2014;5:1320-33.
[25] Chen F-P, Li B-S, Tang C-H. Nanocomplexation of soy protein isolate with curcumin: influence of ultrasonic treatment. Food Res. Int. 2015;75:157-65.
[26] Li M, Cui J, Ngadi MO, Ma Y. Absorption mechanism of whey-protein-delivered curcumin using Caco-2 cell monolayers. Food Chem. 2015;180:48-54.
[27] Pan K, Zhong Q, Baek SJ. Enhanced dispersibility and bioactivity of curcumin by encapsulation in casein nanocapsules. J. Agric. Food Chem. 2013;61:6036-43.
[28] Zou L, Zheng B, Zhang R, Zhang Z, Liu W, Liu C, et al. Influence of lipid phase composition of excipient emulsions on curcumin solubility, stability, and bioaccessibility. Food Biophys. 2016;11:213-25.
[29] Zou L, Zheng B, Liu W, Liu C, Xiao H, McClements DJ. Enhancing nutraceutical bioavailability using excipient emulsions: Influence of lipid droplet size on solubility and bioaccessibility of powdered curcumin. J. Funct. Foods 2015;15:72-83.
[30] Cuomo F, Cofelice M, Venditti F, Ceglie A, Miguel M, Lindman B, et al. In-vitro digestion of curcumin loaded chitosan-coated liposomes. Colloids Surf., B 2017.
[31] Versantvoort CH, Oomen AG, Van de Kamp E, Rompelberg CJ, Sips AJ. Applicability of an in vitro digestion model in assessing the bioaccessibility of mycotoxins from food. Food Chem. Toxicol. 2005;43:31-40.
[32] Oomen A, Rompelberg C, Bruil M, Dobbe C, Pereboom D, Sips A. Development of an in vitro digestion model for estimating the bioaccessibility of soil contaminants. Arch. Environ. Contam. Toxicol. 2003;44:0281-7.
[33] Minekus M, Alminger M, Alvito P, Ballance S, Bohn T, Bourlieu C, et al. A standardised static in vitro digestion method suitable for food–an international consensus. Food Funct. 2014;5:1113-24.
[34] Zou L, Zheng B, Zhang R, Zhang Z, Liu W, Liu C, et al. Enhancing the bioaccessibility of hydrophobic bioactive agents using mixed colloidal dispersions: Curcumin-loaded zein nanoparticles plus digestible lipid nanoparticles. Food Res. Int. 2016;81:74-82.
[35] Pinheiro AC, Coimbra MA, Vicente AA. In vitro behaviour of curcumin nanoemulsions stabilized by biopolymer emulsifiers–Effect of interfacial composition. Food Hydrocolloids 2016;52:460-7.
[36] Tønnesen HH, Karlsen J. Studies on curcumin and curcuminoids. Zeitschrift für Lebensmittel-Untersuchung und Forschung 1985;180:402-4.
[37] Tønnesen HH, Másson M, Loftsson T. Studies of curcumin and curcuminoids. XXVII. Cyclodextrin complexation: solubility, chemical and photochemical stability. Int. J. Pharm. 2002;244:127-35.
[38] Zou L, Zheng B, Zhang R, Zhang Z, Liu W, Liu C, et al. Food matrix effects on nutraceutical bioavailability: impact of protein on curcumin bioaccessibility and transformation in nanoemulsion delivery systems and excipient nanoemulsions. Food biophys. 2016;11:142-53.
[39] Maldonado-Valderrama J, Wilde P, Macierzanka A, Mackie A. The role of bile salts in digestion. Adv. Colloid Interface Sci. 2011;165:36-46.
[40] Li J, Ye A, Lee SJ, Singh H. Influence of gastric digestive reaction on subsequent in vitro intestinal digestion of sodium caseinate-stabilized emulsions. Food Funct. 2012;3:320-6.
[41] Perugini L, Cinelli G, Cofelice M, Ceglie A, Lopez F, Cuomo F. Effect of the coexistence of sodium caeinate and Tween 20 as stabilizers of food emulsions at acidic pH. Colloids Surf., B 10.1016/j.colsurfb.2018.02.003 (*in press*).

Chapter VI

Environmental pollution by organic chemical compounds

The intensive development of civilization, together with evolution of industry, has caused profound changes in the quality of the environment in which human beings live. Our world is full of synthetic chemicals which pollute air, water, soil and food. In urban areas, large concentrations of chemical compounds are emitted into the atmosphere by industries, vehicles and other human activities [1]. Since the late 1800s the range of synthesized chemicals, such as pesticides, plastics, hydrocarbons fuels, soaps, detergents and other useful substances, has increased dramatically. Importantly there were no reliable techniques available to chemically analyze environmental samples and to evaluate the occurrence of these substances. Improvements in techniques for chemical analysis have had a major effect on the development of environmental chemistry [2]. Prior to 1952 no reliable methods for analysis of organic compounds in environmental samples existed. Only in the 1952 gas-liquid chromatography, an analytical technique for the separation of organic chemicals on a small scale, was developed. Between 1957 and 1958 detectors, like flame ionization and electron capture, able to detect trace amount of organic chemicals, were discovered. These detectors, coupled with gas-liquid chromatography, resulted in a powerful technique for the analysis of chemicals present in trace in environmental samples. Finally, in 1960 gas chromatography, coupled to more performing sensitive detectors and to mass spectrometers, provided a powerful tool to detect and identify trace chemicals in environmental samples at very low levels. The various types of organic pollutant can be placed into three general classes: 1) hydrocarbons, 2) oxygen, nitrogen and phosphorus compounds and 3) organometallic compounds. Probably the major category is represented by the hydrocarbons and related compounds, which contains such compounds as Dichlorodiphenyltrichloroethane (DDT), the dioxins and the polycyclic aromatic hydrocarbons (PAHs) [2]. These compounds are mainly made of carbon and hydrogen but often containing chlorine and oxygen as well. Due to presence of mostly apolar chemical bonds (C-H, C-C, C-Cl, C=C and aromatic C=C), the resulting chemical species are extremely stable and poorly soluble in water. These characteristics are due to the presence of bonds with relatively high levels of polarity, represented by carbon and other

atoms being attached to oxygen, nitrogen or phosphorus conferring a high level of polarity onto the related compounds. Due to their low persistence, low accumulation in sediments and low bioaccumulation capacity in organisms, the substances in this group only rarely form residues in the environment and are mainly found in ground and open water. Finally, the organometallic group is probably the least important from an environmental perspective and includes compounds made of metals, such as lead and tin, in combination with carbon based molecules [2]. On the other hand, particular environmental problems are caused by chemical substances having fat solubility, potential bioaccumulation and environmental persistence as well as usage patterns. These are referred to as Persistent Organic Pollutants (POPs) and these substances are often distributed over long distances up to a global scale. POPs are commonly members of the hydrocarbon and related compounds group. There is a growing concern about POPs including Polycyclic Aromatic Hydrocarbons (PAHs) [3]. PAHs are one of the typical POPs featured in regional and global cycling and they are the most toxic among the hydrocarbon families [4]. The last century of industrial development caused a significant increase of PAHs concentrations in the natural environment [5, 6]. Investigation in the content of these compounds in ice cores from Greenland showed that the current level of these compounds is about 50 times higher than in preindustrial periods; these results suggest that the sources of PAHs shifted from biomass burning to fossil fuel combustion in the last 200 years . The general trends in PAHs concentration in the ice core were in agreement with the historical record of world Petroleum production [7]. PAHs are widespread environmental contaminants that have been studied due to their carcinogenicity, mutagenicity and teratogenicity. For this reasons, the PAHs levels monitoring in the environment is of paramount importance [8, 9].

VI.1 Polycyclic Aromatic Hydrocarbons (PAHs)

In recent years PAHs have become one of the most widely investigated compounds in medical sciences, biology, organic chemistry, physics and material sciences [10-12]. PAHs are the first chemical carcinogens discovered, they were found around the 19 century in coal tar. Before 1950s, these compounds were considered as the main carcinogens. Nowadays, PAHs are still one of the most important classes of carcinogens owing to their ubiquity in the environment [13]. Due to their carcinogenicity as well as their persistence in the environment, they have been placed on the list of priority pollutants by the United States Environmental Protection Agency (US-EPA) and also the European Environment Agency [14]. It is therefore important that their concentrations in the environment have to be monitored [15]. In Fig. VI.1 are reported the structures of the 16 priority PAHs according to US-EPA.

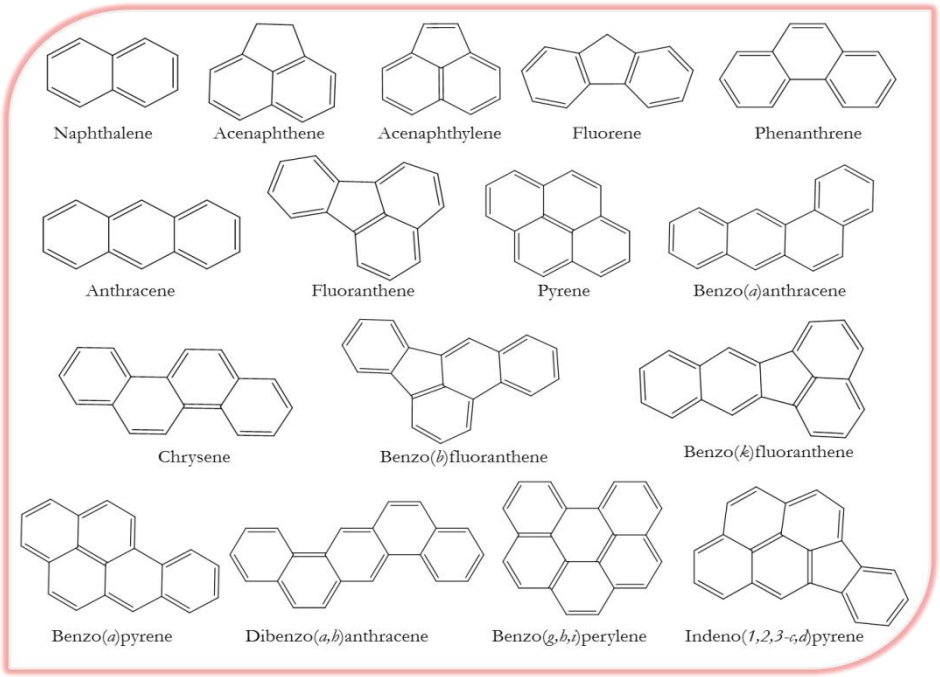

Fig. VI.1. Structures of the 16 priority PAHs according to US-EPA.

VI.1.1 PAHs physico-chemical characteristics

Chemically these compounds represent a large group with two or more aromatic (benzene) rings bonded in linear, cluster or angular arrangements [16]. PAHs, consisting of two or three rings (low-molecular weight), occur in the atmosphere principally in the vapor phase, while PAHs with five or more rings (high molecular weight), because of their low vapor pressure, tend rapidly to condense and to be adsorbed on the particle surfaces. Finally, PAHs with four rings (intermediate-molecular-weight) are partitioned between the vapor and particulate phases, depending on the atmospheric temperature [17]. The physical properties of PAHs vary with molecular weight and chemical structure. PAHs have high melting and boiling points (therefore they are solid), low vapor pressure, and very low aqueous solubility. These last two properties decrease increasing the molecular weight. They are soluble in most organic solvents and they are very lipophilic, thus they are subject to bioaccumulation [18].

VI.1.2 Toxicology

Many PAHs are classified as "probably carcinogenic to humans" or as "possibly carcinogenic to humans" [19] according to the International Agency for Research on Cancer (IARC) [20]. Typically, the PAHs show low acute toxicity, with No Observed Adverse Effect Level (NOAEL) for oral administration up to 100 mg/kg of body weight. They are a group of hydrocarbons that are mainly formed by the incomplete combustion of organic materials. There are several hundred PAHs, which usually occur as complex mixtures rather than as individual compounds.

Benzo(*a*)pyrene (B(*a*)P) is the most widely studied compound from a toxicological point of view and the most frequently determined in the various environmental and food matrices. It is often used as a biomarker of the PAHs class, for both the contamination levels and the carcinogenic risk [21]. B(*a*)P and all the PAHs with a molecular weight higher than one of fluoranthene, for their ability to accumulate in soils and sediments and their bio-concentration properties, are also classified as PBTs (Persistent, Bioaccumulable, and Toxic) according to EPA20-22 [22].

VI.1.3 Sources and pathways of exposure

Global human exposure to PAH occurs through several routes: these compounds can be released into the environment from both natural and anthropogenic sources (forest and bush fires) or man-made combustion sources (automobile emissions and cigarette smoke). PAHs are considered ubiquitous in the environment, therefore they are commonly detected in air, soil, and water [23, 24]. For lower-molecular-weight PAHs, the impact of indoor activities tends to be greater than the influence of the penetrating outdoor air. Indoor air is contaminated by PAHs, either from infiltration or intrusion of outdoor air or from indoor emission sources such as smoking, cooking, domestic heating with fuel stoves and open fireplaces, as well as from incense and candle emissions [25, 26]. On the other hand, for high molecular weight PAHs, the impact of outdoor activities predominates on the indoor one, especially for the compounds with four or more rings [27]. In conclusion the most relevant source contributing to the inhalation route would be indoor air since people spend 80-93% of their time indoor [28].

Air

PAHs are mainly adsorbed to airborne particulate matter. In the atmosphere, the PAHs pollution is mainly due to vehicle traffic, in the absence of other industrial sources of pollution. The levels of individual substances span several orders of magnitude and are generally in the range between 0.1 and 100 ng/m^3 [29]. The potential doses of carcinogenic PAHs were estimated using the standard EPA recommendation for an individual's respiration rate [30]. The daily intake dose due to inhalation was evaluated lying in the range of 0.15–32 ng/day. However, higher daily levels of inhaled B[*a*]P can be registered during exposure to specific indoor sources such as cooking with different fuels (91–2523 ng/day) or using stoves for heating (30–7448 ng/day) [31].

Food

PAHs have been detected in fresh vegetables, fruits, and cereals as a result of the deposition of airborne PAHs, particularly near industrial sources or in areas with high traffic [32-34]. They have also been found in mussels, snails, and fish from contaminated waters [35, 36] and, at high levels, in some vegetable oils and margarine [34, 37], probably formed during processing. PAHs are also

formed during some methods of food preparation, such as grilling, roasting, frying or baking. The highest levels were detected in smoked and grilled meat and fish samples (up to about 200 μg/kg) [29].

Soil

Carcinogenic PAHs are found in all surface soils [38]. Typical concentrations in forest soil range from 5 to 100 μg/kg. Considerable amounts of these compounds are transferred from vegetative litter to forest soil because the compounds are adsorbed from air onto organic matter such as leaves and pine needles. Rural soil contains carcinogenic PAHs at levels of 10–100 μg/kg, mainly originate from atmospheric fallout. For both forest and rural soil, values as high as 1000 μg/kg may occasionally be found [38-40]. Metropolitan areas have higher PAHs concentrations than forest and agricultural areas because of the many sources of fossil fuel combustion. The majority of urban soil concentrations fall in the 600–3000 μg/kg range [38, 41, 42]. Higher values near areas of heavy transportation and industrialization range from 8 to 336 mg/kg [38, 43]. Values in the order of 1000–3000 μg/kg are regarded as being in the upper range. Incidental ingestion of soil by adult males was estimated to be of the order of a few milligrams per day. Soil ingestion rates of the order of 100 mg/day are more typical for small children [44]. Therefore, the potential dose of carcinogenic PAHs for urban populations ranged from 0.2 to 96 ng/day (median 7 ng/day).

VI.1.4 Sources and occurrence of PAHs in natural waters

Contamination of aquatic ecosystems by PAHs has been known as a major public health risk [45]. Due to their low solubility and high affinity for particulate matter, PAHs are not usually found in water at high concentrations. Their presence in surface water or groundwater is an indication of a source of pollution.

Surface waters

PAHs, being semi-volatile organic compounds, exist in both the gaseous and the particulate phase in the air. Atmospheric deposition represents an important input of these compounds to surface waters. It has been estimated that 10-80% of PAHs contributions to the world's oceans is from atmospheric sources [46]. Sewers have also contributed to high levels of PAHs pollution in surface water through urban run-off. As a consequence, urban run-off contains these carcinogenic compounds deposited on surfaces, as well as mobile-related PAHs from gasoline and oil drips or spills, exhaust products, tyre particles, and road surfaces. Higher concentrations of PAHs in urban run-off were found during autumn and winter, due to the high incidence of vehicles in the streets, coupled with the use of heating systems [47]. Another source of PAHs to

surface waters is represented by industrial effluents. In general, industries that use oil or coal as raw material or fuel produce effluents with high concentration of PAHs [48]. Among 35 kinds of industrial effluents examined, a higher frequency of PAH occurrence was observed in the effluents of industries producing organic compounds and plastics, and the effluents of iron and steel manufactures [49]. Municipal wastewaters is another source of PAHs in surface waters. Concentrations of total PAHs in raw municipal wastewaters have been found in a number significantly variable, it depends on the amount of industrial effluents possibly co-treated with domestic wastewaters. Treated wastewaters usually contain these compounds at much lower concentrations due to their removal by adsorption on particles, biodegradation or volatilization [50]. Due to their hydrophobic nature, the solubility of PAHs in water is low and decreases with increasing molecular weight. Most surface waters contain individual PAHs at levels above 0.05 pg μL^{-1}, but highly polluted rivers can have concentrations of up to 6 pg μL^{-1} [51, 52].

Drinking water

The presence of PAHs in drinking water may be due to the surface or groundwater used as raw water sources, or to the use of coal tar-coated pipes in public water supply systems, as is permitted in certain countries [53]. It has been reported that higher PAHs levels must be expected in potable water from sources such as water treatment plants and rainwater collecting basins [54]. Regarding the chlorination of drinking water, it has been found that this disinfection technique may lead to formation of oxygenated and chlorinated PAHs, i.e. compounds that are more toxic than the parent PAHs. The main source of PAHs contamination in drinking-water is usually not the raw water sources but the coating of the drinking-water distribution pipes. In the past, coal tar was a common coating material for water pipes, used to give effective protection against corrosion. After the passage of drinking-water through those pipes or after repair work, significantly increased PAHs levels have been detected in the water [55, 56]. Even if WHO has ruled out the ban on using this practice, many countries still have a large amount of pipes lined with coal tar coating. PAHs levels in groundwater and drinking water range between 0.0002 and 0.0018 pg μL^{-1}, in rainwater from 0.01 to 0.2 pg μL^{-1} whereas, in highly urban areas, levels of up to 1 pg μL^{-1} were determined in snow and fog [51, 52]. This is probably a result of the adsorption of the compounds to air particulate matter, which is finely dispersed into the water during wet deposition. Assuming an average drinking-water consumption of 2 L/day, USEPA has developed ambient water quality criteria to protect human health from the carcinogenic effects of PAH exposure: the recommended maximum contaminant level (MCL) is 0.2 pg μL^{-1} in drinking water.

References

[1] Matsumpto G, Hanya T. Organic constituents in atmospheric fallout in the Tokyo area. Atmos. Environ. (1967) 1980;14:1409-19.
[2] Francis BM. Toxic substances in the environment: John Wiley and Sons, Inc.; 1994.
[3] Jones KC, De Voogt P. Persistent organic pollutants (POPs): state of the science. Environ. Pollut. 1999;100:209-21.
[4] Catoggio JA. Other organic toxic substances. Guidelines of lake management, toxic substances management in lakes and reservoirs 1991;4:113-26.
[5] Wania F, Mackay D. Peer reviewed: tracking the distribution of persistent organic pollutants. Environ. Sci. Technol. 1996;30:390A-6A.
[6] Wild SR, Jones KC. Polynuclear aromatic hydrocarbons in the United Kingdom environment: a preliminary source inventory and budget. Environ. Pollut. 1995;88:91-108.
[7] Kawamura K, Suzuki I, Fuji Y, Watanabe O. Ice core record of polycyclic aromatic hydrocarbons over the past 400 years. Naturwiss. 1994;81:502-5.
[8] Marlow M, Hurtubise RJ. Liquid–liquid–liquid microextraction for the enrichment of polycyclic aromatic hydrocarbon metabolites investigated with fluorescence spectroscopy and capillary electrophoresis. Anal. Chim. Acta 2004;526:41-9.
[9] Guo W, He M, Yang Z, Lin C, Quan X, Men B. Distribution, partitioning and sources of polycyclic aromatic hydrocarbons in Daliao River water system in dry season, China. J. Hazard. Mater. 2009;164:1379-85.
[10] Watson MD, Fechtenkötter A, Müllen K. Big is beautiful−"aromaticity" revisited from the viewpoint of macromolecular and supramolecular benzene chemistry. Chem. Rev. 2001;101:1267-300.
[11] Wu J, Pisula W, Müllen K. Graphenes as potential material for electronics. Chem. Rev. 2007;107:718-47.
[12] Clar E, Schoental R. Polycyclic hydrocarbons: Springer; 1964.
[13] Luch A. The carcinogenic effects of polycyclic aromatic hydrocarbons: World Scientific; 2005.
[14] Rawa-Adkonis M, Wolska L, Przyjazny A, Namieśnik J. Sources of errors associated with the determination of PAH and PCB analytes in water samples. Anal. Lett. 2006;39:2317-31.
[15] Charalabaki M, Psillakis E, Mantzavinos D, Kalogerakis N. Analysis of polycyclic aromatic hydrocarbons in wastewater treatment plant effluents using hollow fibre liquid-phase microextraction. Chemosphere 2005;60:690-8.
[16] Organization WH. Air quality guidelines for Europe. 1987.
[17] Srogi K. Monitoring of environmental exposure to polycyclic aromatic hydrocarbons: a review. Environ. Chem. Lett. 2007;5:169-95.
[18] Masih J, Singhvi R, Kumar K, Jain V, Taneja A. Seasonal variation and sources of polycyclic aromatic hydrocarbons (PAHs) in indoor and outdoor air in a semi arid tract of northern India. Aerosol Air Qual. Res. 2012;12:515-25.
[19] Grimmer G, Brune H, Dettbarn G, Jacob J, Misfeld J, Mohr U, et al. Relevance of polycyclic aromatic hydrocarbons as environmental carcinogens. Fresenius' J. Anal. Chem. 1991;339:792-5.
[20] Polycyclic SN-h. VOLUME 92 Some Non-heterocyclic Polycyclic Aromatic Hydrocarbons and Some Related Exposures.
[21] Leong M-I, Chang C-C, Fuh M-R, Huang S-D. Low toxic dispersive liquid–liquid microextraction using halosolvents for extraction of polycyclic aromatic hydrocarbons in water samples. J. Chromatogr. A 2010;1217:5455-61.
[22] Ying G-G, Yu X-Y, Kookana RS. Biological degradation of triclocarban and triclosan in a soil under aerobic and anaerobic conditions and comparison with environmental fate modelling. Environ. Pollut. 2007;150:300-5.

[23] Baklanov A, Hänninen O, Slørdal L, Kukkonen J, Bjergene N, Fay B, et al. Integrated systems for forecasting urban meteorology, air pollution and population exposure. Atmos. Chem. Phys. 2007;7:855-74.
[24] Latimer JS, Zheng J. and Fate of PAHs in the Marine Environment. PAHs: Ecotoxicol. Perspect. 2003:9.
[25] Baek S, Field R, Goldstone M, Kirk P, Lester J, Perry R. A review of atmospheric polycyclic aromatic hydrocarbons: sources, fate and behavior. Water, Air, Soil Pollut. 1991;60:279-300.
[26] Lau C, Fiedler H, Hutzinger O, Schwind K-H, Hosseinpour J. Levels of selected organic compounds in materials for candle production and human exposure to candle emissions. Chemosphere 1997;34:1623-30.
[27] Li A, Schoonover TM, Zou Q, Norlock F, Conroy LM, Scheff PA, et al. Polycyclic aromatic hydrocarbons in residential air of ten Chicago area homes: concentrations and influencing factors. Atmos. Environ. 2005;39:3491-501.
[28] Brunekreef B, Janssen N, de Hartog JJ, Oldenwening M, Meliefste K, Hoek G, et al. Personal, indoor, and outdoor exposures to PM2. 5 and its components for groups of cardiovascular patients in Amsterdam and Helsinki. Research report (Health Effects Institute) 2005:1-70; discussion 1-9.
[29] Organization WH. Selected non-heterocyclic polycyclic aromatic hydrocarbons. 1998.
[30] USEPA U. Exposure factors handbook. Office Res. Dev., Washington 1997.
[31] Raiyani C, Jani J, Desai N, Shah S, Shah P, Kashyap S. Assessment of indoor exposure to polycyclic aromatic hydrocarbons for urban poor using various types of cooking fuels. Bull. Environ. Contam. Toxicol. 1993;50:757-63.
[32] Tuominen JP, Pyysalo HS, Sauri M. Cereal products as a source of polycyclic aromatic hydrocarbons. J. Agric. Food Chem. 1988;36:118-20.
[33] De Vos R, Van Dokkum W, Schouten A, de Jong-Berkhout P. Polycyclic aromatic hydrocarbons in Dutch total diet samples (1984–1986). Food Chem. Toxicol. 1990;28:263-8.
[34] Dennis M, Massey R, Cripps G, Venn I, Howarth N, Lee G. Factors affecting the polycyclic aromatic hydrocarbon content of cereals, fats and other food products. Food Addit. Contam. 1991;8:517-30.
[35] Rostad CE, Pereira WE. Creosote compounds in snails obtained from Pensacola Bay, Florida, near an onshore hazardous-waste site. Chemosphere 1987;16:2397-404.
[36] Speer K, Steeg E, Horstmann P, Kühn T, Montag A. Determination and distribution of polycyclic aromatic hydrocarbons in native vegetable oils, smoked fish products, mussels and oysters, and bream from the river Elbe. J. Sep. Sci. 1990;13:104-11.
[37] Thomson B, Lake R, Lill R. The contribution of margarine to cancer risk from polycyclic aromatic hydrocarbons in the New Zealand diet. 1996.
[38] Menzie CA, Potocki BB, Santodonato J. Exposure to carcinogenic PAHs in the environment. Environ. Sci. Technol. 1992;26:1278-84.
[39] Nam J, Song B, Eom K, Lee S, Smith A. Distribution of polycyclic aromatic hydrocarbons in agricultural soils in South Korea. Chemosphere 2003;50:1281-9.
[40] Smith D, Harrison RM, Luhana L, Pio CA, Castro L, Tariq MN, et al. Concentrations of particulate airborne polycyclic aromatic hydrocarbons and metals collected in Lahore, Pakistan. Atmos. Environ. 1996;30:4031-40.
[41] Trapido M. Polycyclic aromatic hydrocarbons in Estonian soil: contamination and profiles. Environ. Pollut. 1999;105:67-74.
[42] Mielke HW, Wang G, Gonzales C, Le B, Quach V, Mielke P. PAH and metal mixtures in New Orleans soils and sediments. Sci. Total Environ. 2001;281:217-27.
[43] Harrison RM, Smith D, Piou C, Castro L. Comparative receptor modelling study of airborne particulate pollutants in Birmingham (United Kingdom), Coimbra (Portugal) and Lahore (Pakistan). Atmos. Environ. 1997;31:3309-21.
[44] Jeffries J, Martin I. Updated technical background to the CLEA model: Environment Agency; 2009.

[45] Okafor EC, Opuene K. Preliminary assessment of trace metals and polycyclic aromatic hydrocarbons in the sediments. Int. J. of Environ. Sci. Technol. 2007;4:233-40.
[46] Moore JW, Ramamoorthy S. Organic chemicals in natural waters: applied monitoring and impact assessment: Springer Science & Business Media; 2012.
[47] Bomboi M, Hernandez A. Hydrocarbons in urban runoff: their contribution to the wastewaters. Water Res. 1991;25:557-65.
[48] Terashi A, Hanada Y, Kido A, Ishikawa S. Organic compounds found in Dokai Bay, Japan. Bull. Environ. Contam. Toxicol. 1993;50:348-55.
[49] Mills WB. Water quality assessment: A screening procedure for toxic and conventional pollutants in surface and ground water: Environmental Research Laboratory, Office of Research and Development, US Environmental Protection Agency; 1985.
[50] Manoli E, Samara C. Polycyclic aromatic hydrocarbons in natural waters: sources, occurrence and analysis. TrAC, Trends Anal. Chem. 1999;18:417-28.
[51] Environmental PAE. National primary drinking water regulations: Long Term 1 Enhanced Surface Water Treatment Rule. Final rule. Federal register 2002;67:1811.
[52] Prabhukumar G, Pagilla K. Polycyclic aromatic hydrocarbons in urban runoff–sources, sinks and treatment: A review. Department of Civil, Architectural and Environmental Engineering, Chicago 2010.
[53] Shiraishi H, Pilkington NH, Otsuki A, Fuwa K. Occurrence of chlorinated polynuclear aromatic hydrocarbons in tap water. Environ. Sci. Technol. 1985;19:585-90.
[54] Kveseth K, Sortland B, Bokn T. Polycyclic aromatic hydrocarbons in sewage, mussels and tap water. Chemosphere 1982;11:623-39.
[55] Vu DT, Huynh C. Organic micropollutants in water. Preliminary results on haloforms and polycyclic aromatic hydrocarbons. Sozial-und Praventivmedizin 1981;26:315.
[56] Basu D, Saxena J, Stoss F, Santodonato J, Neal M, Kopfler F. Comparison of drinking water mutagenicity with leaching of polycyclic aromatic hydrocarbons from water distribution pipes. Chemosphere 1987;16:2595-612.

Chapter VII

Analytical methods for organic compounds determination

The available literature indicates that, although there are excellent techniques for separation and detection of toxic and carcinogenic contaminants, e.g. Gas Chromatography (GC) and High Performance Liquid Chromatography (HPLC), a number of difficulties has been encountered in their determination [1]. Direct analysis of these compounds in different environmental matrices, such as water, soil, food and sediments, is difficult because they occur at a parts per billion or trillion level compared to the detection capabilities in chromatographic techniques. In order to be able to determine very low concentrations of chemicals in the environment, a sample preparation step has to precede the final determination. This phase plays a crucial role in environmental monitoring and consists of a series of operations: 1) isolation (extraction and separation) of the target chemicals from sample matrix, 2) separation and purification of the target chemical from co-extracted, non-target chemicals (sample clean-up), and 3) sample concentration. The aim of this phase of analysis is to provide a sample aliquot that (a) is relatively free of interferences, (b) will not damage the column or instrument and (c) is compatible with the intended analytical method. For this reason, a number of significant applications in the pollutant determination and removal field stress the importance of optimizing treatments by utilizing strategies that meet reliability, sensitivity and cost effectiveness [2-4].

Until recently, sample preparation was carried out using traditional techniques, such as liquid–liquid extraction (LLE), that uses large volumes of organic solvents and solid-phase extraction (SPE) that uses much less solvent than LLE, although the volume can still be significant. These preparation methods are expensive, time-consuming and environmental unfriendly. Recently, a great effort has been made to develop new analytical methodologies, based on the use of microextraction techniques, able to perform direct analyses using miniaturised equipment, thereby achieving high enrichment factors, minimising solvent consumption and production waste. These techniques are designed to improve the performance during sample preparation, particularly in complex water environmental samples, such as wastewaters, surface and ground

waters, tap waters, sea and river waters. Among the microextraction techniques, dispersive liquid–liquid microextraction (DLLME) has become a very popular environmental friendly sample-preparation technique, because it is fast, inexpensive, easy to operate with a high enrichment factor while using low volumes of organic solvents [5]. Environmental water samples have been the matrix field in which DLLME has found its major applications due to the basic configuration of DLLME, as well as the weak purification ability. The waters (mainly tap, river, well, lake, sea and even wastewater) could be directly performed by the DLLME procedure or just after simple pretreatment (like a centrifugation step). DLLME has been successfully and conveniently applied to the extraction and pre-concentration of a wide variety of organic compounds and metal ions from various water samples. DLLME was applied for the pesticides analysis from water [6-11]. In addition, several environmental pollutants, typically including PAHs [12-17] in various waters, were analysed using different DLLME procedures throughout almost the entire evaluation of the DLLME technique. Apart from waters, the DLLME applications have also been extended to other environmental samples, mainly soils [15, 18-24].

VII.1 Dispersive Liquid-Liquid Microextraction (DLLME)

The dispersive liquid–liquid microextraction (DLLME) method was proposed by Assadi and co-workers in 2006 [25] and immediately has gained considerable attention from researchers. As the name suggests, DLLME is equivalent to a miniaturised type of liquid-liquid extraction (LLE) that is generally established on a ternary component solvent systems made of an aqueous sample and a blend of an organic extractant and disperser solvent. An appropriate disperser solvent is introduced to help the dispersion of an organic extraction solvent into an aqueous sample and further achieve a highly efficient extraction. Briefly, a DLLME procedure is shown in Fig. VII.1 and can be outlined as follows: (a) a mixture of extraction and disperser solvents is rapidly injected into the samples by syringe; (b) the rapid injection produces a high turbulence and small droplets forming a cloudy solution (c) due to infinitely large surface area between extraction solvent and aqueous phase (sample), transition of analyte from aqueous to extraction phases is fast, subsequently equilibrium state is achieved quickly, resulting in a very short extraction time, (d) after extraction, phase separation is performed by centrifugation and the enriched analyte in the bottom layer is determined by analytical techniques (e.g. chromatography or spectrometry methods). Therefore, in the extraction technique, there are substantially two phases at different densities: usually a phase consists of the aqueous phase, while the other one, consisting of the extraction solvent, may have higher water density. Obviously, the advantages of DLLME are mainly the following: (a) the negligible consumption of extraction solvents (only microliter

volumes); (b) the short extraction time due to the rapid achievement of an equilibrium state; (c) the high enrichment factor (EF) due to the high phase ratio of the donor (aqueous sample) and the acceptor (extraction solvent). Accordingly, the DLLME technique is simple, quick, efficient, and simultaneously meets the development requirement of green chemistry.

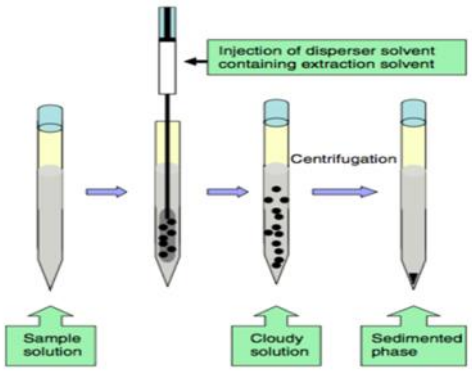

Figure VII.1. DLLME procedure

VII.1.2 Principles of DLLME

The applicability of dispersive liquid–liquid microextraction is mainly based upon the distribution coefficient (K) defined as the ratio between the analyte concentration in extraction solvent and sample solution, in other words, K should be greater than 500 to achieve suitable application of DLLME [26]. However, for the acidic or alkaline analytes, distribution coefficient could be increased by controlling the pH value of sample solution, making the analytes existing in nonionic state. Enrichment factor (EF) is defined as the ratio of analyte concentration in the sedimented phase to the initial concentration in the aqueous phase as shown in equation:

$$EF = \frac{C_{sed}}{C_0} \qquad \text{(VII.1)}$$

where C_{sed} and C_0 are the analyte concentration in sedimented phase obtained from a suitable calibration graph and the initial concentration in aqueous phase, respectively. The extraction recovery (R%) can be calculated as follows:

$$R\% = \frac{V_{sed}}{V_{aq}} \times EF \times 100 \qquad \text{(VII.2)}$$

where V_{sed} and V_{aq} are the volumes of sedimented phase and sample solution, respectively. On the other hand, the relative recovery (RR%) is obtained calculatedly from the following equation:

$$RR\% = (C_{found}) - (C_{real}) \times C_{added} \times 100 \qquad \text{(VII.3)}$$

where C_{found}, C_{real} and C_{added} are the concentration of analyte after the addition of known amount of standard into the sample, the real concentration of analyte found in sample, and the concentration of known amount of standard that is spiked to the sample, respectively [27].

VII.1.3 Parameters affecting the extraction efficiency of DLLME

The extraction efficiency for the target analyte by DLLME is influenced by many factors, such as the kind of extraction, disperser solvent and their volume, the extraction time and salt addition.

Selection of the extraction solvent

The distribution coefficient and selectivity are the most important parameters that govern extraction solvent selection. The extraction solvent, to be suitable as extractant, 1) must have the ability to extract the target analyte, 2) must have low solubility in the aqueous phase, and 3) must be compatible with the analytical instrumentation being used. In addition, it has also to satisfy some special requirements of the DLLME procedure, namely 1) to have a density greater than that of water for simple separation of the extraction phase after centrifugation, and 2) to form a cloudy solution in the presence of the disperser solvent. For this purpose, the number of extraction solvents available is limited, and the choice of the extraction solvent thus becomes the method's primary drawback. Of all the requirements listed, the most restrictive is the necessity of using an extraction solvent having a density greater than that of water, since the number of organic solvents meeting this requirement is relatively small. Halogenated hydrocarbon, such as chlorobenzene, chloroform, carbon tetrachloride, and tetrachloroethylene (tetrachloroethane), are usually selected as extraction solvents because of their high density. To overcome these various drawbacks, researchers have recently attempted to use solvents with a density lower than that of water (see paragraph VII.1.4). The volume of the extraction solvent should also be considered as well as the solvent type [25]. DLLME uses about 1.000.000 less solvent in comparison with conventional liquid-liquid extraction, so its volume has to be carefully optimized. The extraction solvent volume has great effects on the enrichment factor. With the increase of the extraction solvent volume, the final organic phase obtained by centrifugation is increased, resulting in a decrease of the target analyte concentration in organic phase. Although the extraction recovery keeps almost constant, the enrichment factor will be decreased, leading to a decrease of the determination sensitivity for the target compounds. Therefore, the optimal extraction solvent volume should ensure both the high enrichment factors and the enough volume for the subsequent determination after centrifugation. However, removing the sedimented phase without also transferring some of the aqueous phase can be difficult if the volume of the injected extraction solvent is very small [28]. The volume of sedimented phase is also dependent by the sample and the disperser solvent volumes, and by the water solubility of the extractant [5, 29]. In general, 5–100 µl of extraction solvent is selected.

Selection of disperser solvent

The disperser solvent has to be highly miscible with both water and the extraction solvent. The miscibility of disperser in both organic and water is the main point of selection for the extraction solvent emulsification. The extraction solvents with high interfacial tension make the formation of tiny droplets by shaking more difficult and the extraction efficiency would not be uniform [30]. Therefore, disperser solvent plays an important role in decreasing the interfacial tension between water and extracting solvent leading to the formation of smaller droplet size which facilitate the extraction. Acetone, methanol, acetonitrile, tetrahydrofuran, and ethanol are normally used as disperser solvents. The disperser solvent volume directly affects the formation of the cloudy solution, the dispersion degree of the extraction solvent in aqueous phase, and subsequently, the extraction efficiency. Low volumes of disperser solvent could not disperse the extraction solvent properly, and therefore, cloudy solution cannot be formed completely. Reversely, at high volumes, the solubility of analytes in water increases by increasing the volume of disperser solvent, thus, the extraction process is incomplete [31].

Effect of the extraction time

In contrast to most liquid extractions, DLLME is not particularly affected by the extraction time [28, 32-34] and it is therefore not always optimized [29, 35]. The extraction time is defined as the time between the injection and centrifugation phases [5]. A sufficient centrifugation time is important for the formation of phase separation and it is also the most time consuming step in DLLME. The centrifugation time is usually 5-10 minutes. An unnecessarily long centrifugation should be avoided because the centrifugation motion generates heat, which can cause the phase separation to dissolve [36, 37]. The sample volume is usually 5-10 mL which is easily handled in the laboratory.

Effect of ionic strength

The solubility of the target analyte and organic extraction solvent in aqueous phase is usually decreased with the increase of ionic strength due to the salting out effect [38]. On the other hand, the volume of obtained organic phase increases with increasing the salt concentration and therefore, both the target analyte concentration and the enrichment factor decrease. In some investigations, the electrolyte addition does not have effective influence on the efficiency of extraction.

VII.1.4 Evolution of DLLME

Since the invention of DLLME technology in 2006, many modifications have been proposed, aiming at making it faster, enable the extraction of more polar compounds, generate less toxic residue, decrease the analyst exposure to solvents and the solvent consumption.

Low density solvent dispersive liquid-liquid microextraction (LDS-DLLME)

Even though Rezaee et al. [25] limited DLLME to high density solvents, recently, low-density solvents have been used as extraction solvents in DLLME in order to increase the range of solvents compatible with the method. This mode is called low-density solvent based DLLME (LDS-DLLME) [39] and the extraction solvents, such as toluene, xylene, hexane, and heptane, are used. One possible way of enabling the application of low-density solvents in liquid–liquid based microextraction procedures is the use of special extraction devices. Farajzadeh et al. [40] designed a special vessel in which extraction is carried out in the usual way by rapid injection of the extraction and disperser solvent mixture and the formation of the cloudy state. After centrifugation, however, the extraction phase, which is lighter than water, is collected at the top of the aqueous phase, removed by a microsyringe and exposed to subsequent analysis. An advantage of LDS-DLLME is that, after centrifugation, any matrix components will be sedimented at the bottom of the extraction vessel while the extraction solvent will be floating on top. This will lead to a cleaner extract and potentially cleaner chromatography [41].

Ultrasound-assisted dispersive liquid-liquid microextraction (USA-DLLME)

Alternative methods have also been developed to enhance the dispersion of the extraction solvent throughout the aqueous sample. The use of ultrasound increases the number of microdroplets of extraction solvent resulting in an even larger surface area [45]. Thus, the dispersion of the extraction solvent in ultrasound-assisted dispersive liquid-liquid microextraction (USA-DLLME) is induced by ultrasound [42]. After injection of the extraction and disperser solvent, the samples are sonicated and thereafter left to stand for a suitable time, so that the analytes are extracted by the dispersed extractant droplets. Due to the effective dispersion by the sonication, a smaller amount of both extraction and disperser solvent can be used. Compared to the conventional DLLME, USA-DLLME requires also the optimisation of the ultrasound energy and sonication time [43].

Other DLLME techniques

In addition to USA-DLLME, ultrasound-vortex assisted dispersive liquid–liquid microextraction (USVADLLME) has also been developed to enhance the dispersion of the extraction solvent and, consequently reduce its amount in the extraction process. This technique is successfully

applied for the determination of phthalates esters (PAEs) in hydroalcoholic beverages. For such method, the small amount of extraction solvent makes the extraction and pre-concentration difficult despite the amount of energy supplied from vortex and ultrasound [44]. In another study, a microextraction based on a revised USVADLLME, supported by a double vortex treatment, is proposed for the determination of Bisphenol A (BPA) in hydroalcoholic solution and red wine. In particular, emphasis is given on the delicate parameters related to the preconcentration process such as the amount of the supplied extraction solvent.

Additional modifications to DLLME methods include the elimination of time-consuming centrifugation steps by the use of a de-emulsification solvent which causes phase separation of the emulsion upon its addition [41]. The solvent based de-emulsification dispersive liquid–liquid microextraction (SD-DLLME) [45] or solvent-terminated dispersive liquid-liquid microextraction (ST-DLLME) [8] are two examples. Solidified floating organic drop DLLME (SFO-DLLME) was developed by Melwanki et al. [39, 46] and involves the use of low-density extraction solvents having a melting point close to room temperature (typically 1-undecanol or 1-dodecanol). After phase separation, the floating extraction solvent is frozen and the formed frozen drop is easily collected into a separate vessel where it is usually diluted with a chromatographically suitable solvent prior to analysis [47]. While the use of a less toxic extraction solvent is advantageous, the choice of extraction solvent is limited to those that have a melting point at approximately room temperature [48]. Effervescence assisted DLLME involves the in situ generation of bubbles of CO_2 to assist the dispersion of the extraction solvent, removing the use of the dispersive solvent. The CO_2 is produced by adding a mixture of sodium carbonate and a weak acid (citric acid), usually in the form of a pressed tablet [49, 50]. This technique allows for the reduction in the use of organic solvents, potentially lowering the cost of the overall analysis. Air assisted dispersive liquid-liquid microextraction (AA-DLLME) removes the use of a dispersive solvent by repeatedly aspirating the aqueous phase and the extraction solvent into a glass syringe until a cloudy solution is formed [51]. Methods to allow easier recovery of the extraction solvent have also been developed. Hydrophobic magnetic nanoparticles interact with the extraction phase and can be sedimented by applying a magnet removing the centrifugation step [16]. The use of magnetic nanoparticles has also been combined with effervescence assisted dispersion, mentioned above [50]. Surfactant assisted DLLME (SA-DLLME) uses surfactants as dispersive solvents [52] whereas cloud point DLLME (CP-DLLME) uses surfactants as an extraction solvent to produce a surfactant rich sedimented phase after centrifugation [53]. Specifically, it involves heating the sample solution, containing the appropriate surfactant, past its cloud point. The cloud point is defined as the temperature at which phase separation occurs and the analytes are extracted into

the surfactant rich phase. Ionic liquids have been used as an alternative to traditional organic extraction solvents in ionic liquid DLLME (IL-DLLME) because they have tunable physicochemical properties. For example, ionic liquid miscibility in either water or organic solvents can be controlled by selecting the appropriate anion/cation combination and by incorporating the proper functional group within the IL. In addition, they exhibit lower toxicity than organic extraction solvents [54]. Ionic liquids have also been used as both dispersive and extraction solvents in combination with ultrasound assisted dispersion, referred to as ultrasound assisted ionic liquid/ionic liquid DLLME (UA-IL/IL-DLLME) [55]. In an effort to improve selectivity for polar or acidic/basic analytes, pH-controlled DLLME (pH-DLLME) has also been developed [56]. By performing two DLLME procedures it is possible to remove matrix interferences in the first extraction step, followed by a back extraction after appropriate pH adjustment.

VII.1.5 Applications of DLLME

DLLME combined with Gas-Chromatography (GC)

Since water-immiscible solvents are generally used in DLLME, the preferred technique for the analysis of extracts is gas-chromatography (GC). The versatility of DLLME-GC is seen in relation to the variety of applications in many areas. The application of DLLME was developed for extraction and determination of polycyclic aromatic hydrocarbons (PAHs) in water samples by Rezaee et al. [25]. Kozani et al. [34] described DLLME combined with GC-ECD for determining chlorobenzenes (CBs) in water samples. The results indicated that DLLME is a sensitive, rapid and reproducible technique that can be used for pre-concentration of CBs from water samples. DLLME-GC-ECD has also been used for determination of trihalomethanes (THMs) in drinking water [57]. Huang and co-worker [58] used DLLME in combination with gas chromatography–ion trap mass spectrometric detection (GC–MS) to pre-concentrate triazine herbicides in water and the LODs in the range of 0.021–0.12 μL^{-1} were obtained. For the strong polar and nonvolatile samples, which are unsuitable for analysis by GC, derivatization is necessary to increase the analytes volatility. Application of DLLME coupled with derivatization reaction provides a one-step derivatization and extraction technique, greatly simplifying the operation steps and shortening the analysis time. Huang et al. have also combined GC–MS with DLLME to determine the anilines in wastewater samples [59]. Besides, DLLME-GC combined with various detectors was applied to determine volatile phenols in red wines (MS) [60], and different compounds in water samples, such as phthalate esters (MS) [61], organophosphorus flame retardants and plasticizers (NPD) [6], amide herbicides (MS) [62], polychlorinated

biphenyls (ECD) [63], fatty acids after derivatization with ethyl chloroformate (FID) [64], pyrethroid pesticide (ECD) [65], nitroaromatic compounds (FID) [66], personal care products (MS) [67], organochlorine pesticides (MS) [68] and Polycyclic Aromatic Hydrocarbons (MS) [69, 70].

VII.2 Gas-Chromatography (GC)

Gas chromatography (GC) is a widely applied technique in many branches of science and technology. The development of GC as an analytical technique was originated by Martin and Synge in 1941; they suggested the use of gas-liquid partition chromatograms for analytical purposes [71]. GC describes the group of analytical separation techniques used to analyze volatile substances in the gas phase. In gas chromatography, the components of a sample are dissolved in a solvent and vaporized in order to separate the analytes by distributing the sample between two phases: a stationary phase and a mobile phase. The mobile phase is a chemically inert gas that serves to carry the analyte molecules through the heated column, while the stationary phase is either a solid adsorbent, named gas-solid chromatography (GSC), or a liquid on an inert support, called gas-liquid chromatography (GLC). The instrument used in Gas Chromatography is the Gas Chromatograph characterized by four principal sections: 1) introduction (injector), 2) separation (chromatographic column), 3) detection, and 4) data handling units. Each section has its own function and its responsibility for the quality of the analysis and the obtained results.

Sample injection

In a gas chromatographic system, the sample injection represents a critical step, especially for quantitative analysis. The main objective of this first phase is to transfer the sample to the chromatographic column in a rapid and quantitatively reproducible manner. Sample injection must be precise, accurate, reproducible, predictable and quantitative. During the transfer into the GC, the sample is volatilized by rapid exposure to a zone kept at relatively high temperature (200-300 °C) and mixed with a stream of carrier gas (Ar, He, N_2, H_2). The resulting gaseous mixture is swept toward the column by the carrier gas. For correct GC operation, among other conditions, this gateway to the column should remain unpolluted, clean, inert, and leak-free. The main requirement for an analyte in GC is that it should be volatile enough to be present in detectable amounts in the mobile phase. Substances with low vapor pressure will not enter the chromatographic column but will accumulate at the injection system, and may eventually clog its conduits. Among the different injection systems, Programmed Temperature Vaporized (PTV) injection is generally considered to be the most universal injection technique available. PTV inlet offers a mixture of injection possibilities, including cool sample introduction, split or splitless

modes, pyrolysis, thermal desorbtion, sample concentration (solvent elimination mode) and it is column protecting. Due to this flexibility, PTV inlets are good inlets for both general analysis and trace analysis [72].

Separation procedure

The separation mechanisms of the mixture components occur in the chromatographic column; it represents the heart of the GC. The chromatographic column, containing the stationary phase, is placed inside a thermostatic oven. The controlled variation of the oven temperature is proposed to improve the separation process of the analytes. One of the most important characteristics of the chromatographic column is its resolution, or the ability to separate components with very similar distribution constant between the mobile and stationary phases (K_D). Chromatographic resolution is a function of many operational parameters. Among them, the nature of the stationary phase, mobile phase, temperature, the size of the column, such as its length (L), inner diameter (ID) and the thickness of the stationary phase (d_f). The resolution, R, defines the degree of separation of two components according to the following expression:

$$R=\frac{\Delta t_R}{((W_A+W_B)/2)} \qquad \text{(VII.4)}$$

where Δt_R is the difference of retention time between two peaks (A and B), and W_A and W_B are the bases of the peaks A and B, respectively. They are specified in Fig. VII.2.

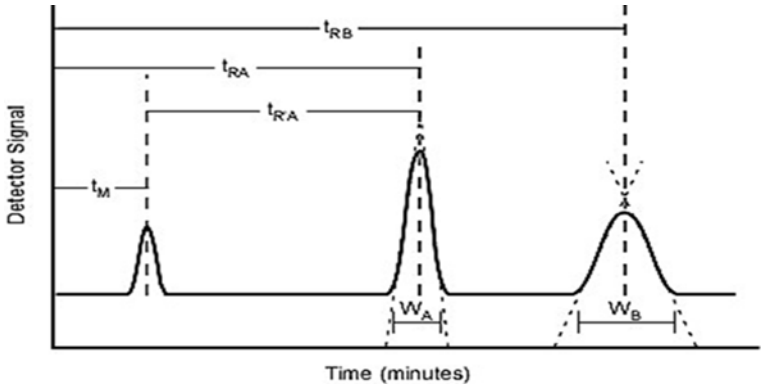

Fig. VII.2. Chromatogram resolution.

As can be seen in Fig. VII.2. the chromatographic peaks are perfectly solved if the parameter R is a large number. However, it is not convenient to have an R value too large otherwise the analysis times will prolong. The components that are more restrained, through their high chemical and physical interaction of solutes with the stationary phase, are moving more slowly with mobile phase flow. On the other hand, components that are weakly held by the stationary phase, they move faster. Columns vary in length and internal diameter depending on the application type and can be either packed or capillary. Packed columns (typical dimension 1.5 m x 4 mm) are packed

with a solid support coated with immobilized liquid stationary phase material (GLC). Capillary columns (typical dimension 30 m x 0.32 mm x 0.1 mm film thickness) are long hollow silica tubes with the inside wall of the column coated with immobilized liquid stationary phase material of various film thickness. Obviously, increasing the length of the column markedly increases the analysis time. The efficiency of a chromatographic column in the separation of a mixture components depends on the number of equilibrium between the stationary solid and the mobile gas phases. Efficiency is generally cited in terms of the Height Equivalent Theoretical Plate (HETP), which can be assumed as the minimum length required to establish the sample breakdown equilibrium between the stationary solid and the mobile gas phases. The number N of these plates depends either by the length of the column or by the flow rate of the carrier gas. The higher is the number of N and lower the value of HETP, the higher the resolution (efficiency) of the column. The number N is calculated from the observed retention time and peak width in a chromatogram (Eq. VII.5):

$$N=16\ (t_R/W)^2 \qquad \text{(VII.5)}$$

where t_R represents the retention time and W represents the basis of the triangle built on the chromatographic peak. These two values are also specified in Fig. VII.3.

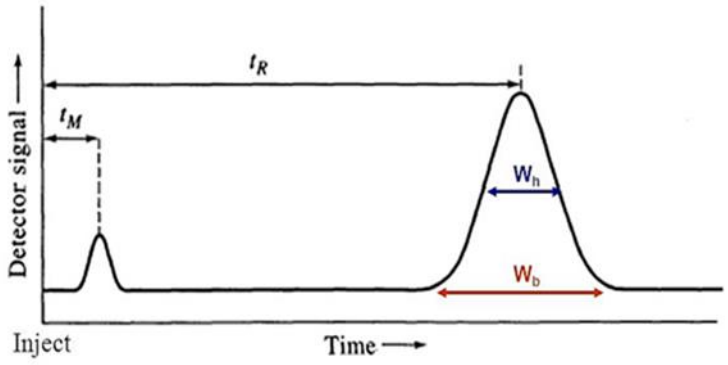

Fig. VII.3. Characteristic parameters of a chromatographic peak.

The final result of the elution of a substance is called chromatographic peak.
Each peak is characterized by:

- height peak: distance between the maximum point and the tangent to the baseline
- base width peak (W): segment length interpolated at intersection between Gaussian flange tangents and baseline
- mid-height width: width measured to half-height of the peak (W_{05})

- distance between the inflection points: segment interpolated between the two inflection points
- total area subtended: total area of the chromatographic peak, proportional to the concentration

In Fig. VII.4 are reported all the parts that characterize a chromatographic peak.

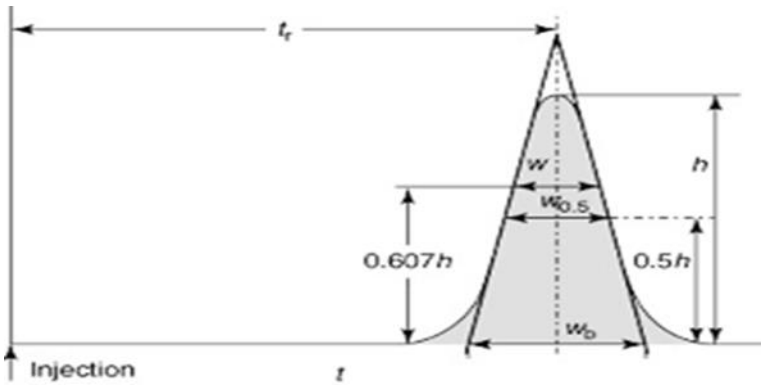

Fig. VII.4. Chromatographic peak.

Detector

At the end of the separation section, the molecules reach a detection system that differentiates the analyte molecules from the mobile phase, which is transparent to the detector. Detector response (signal) is based on measuring a physical property of the flow of analyte molecules (ionic current, thermal conductivity, fluorescence, refractive index, photon emission, electron capture, etc.). The signal should be proportional to the amount of analyte that exits from the column, thus carrying out a quantitative analysis, which is an essential part of a chromatographic determination. All detectors are distinguished by their sensitivity, minimum detection and quantitation levels, linearity, sensitivity to changes in gas flow, temperature or pressure. Detector choices include: 1) Flame Ionization (FID), 2) Electron Capture (ECD), 3) Flame Photometric (FPD), 4) Nitrogen Phosphorous (NPD), 5) Thermal Conductivity (TCD) and 6) Mass Spectrometer (MS). The latter is described in the paragraph VII.3.

Data system

The data system receives the analogue signal from the detector and digitizes it to form the record of the chromatographic separation known as the 'Chromatogram'. The data system can also be used to perform various quantitative and qualitative operations on the chromatogram – assisting with sample identification and quantitation.

VII.3 Gas Chromatography-Mass Spectrometry (GC-MS)

The need to unequivocally identify the components of complex mixtures was the motivation for the development of different instrumental coupling techniques (tandem). Gas chromatography-mass spectrometry (GC-MS) is an extremely favorable synergistic union of two different analytical techniques, Gas Chromatography (GC) and Mass Spectrometry (MS), to identify different substances within a test sample. GC can separate volatile and semi-volatile compounds with great resolution, but it cannot identify them. MS can provide detailed structural information on most compounds such that they can be exactly identified, but it cannot readily separate them. As the sample exits the end of the GC column, it is fragmented by ionization and the fragments are sorted by mass to form a fragmentation pattern. Like the retention time (t_R), the fragmentation pattern for a given component of sample is unique and therefore is an identifying characteristic of that component. It is so specific that it is often referred to as the molecular fingerprint. Spectra of compounds are collected as they exit a chromatographic column by the mass spectrometer, which identifies and quantifies the chemicals according their mass-to-charge ratio (m/z). These spectra can be then stored on the computer and analyzed [73]. The Fig. VII.5 shows a schematic representation of GC-MS. Its different parts and their functions are discussed below.

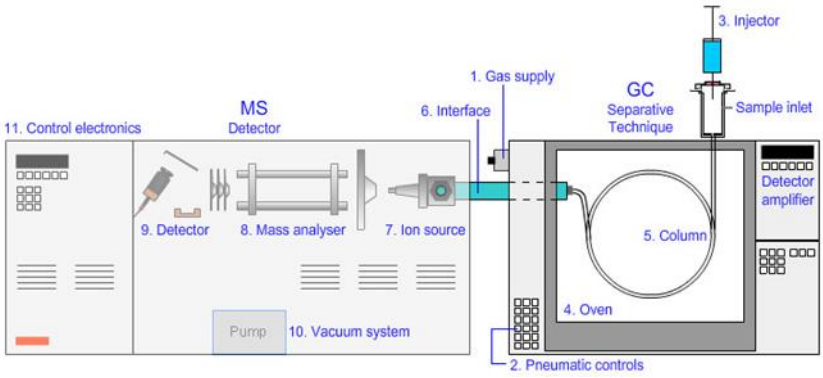

Fig. VII.5. Schematic representation of GC-MS.

The MS function is described as follows. When the individual analytes exit the GC column they enter the ionization area (ion source) of the MS [74] constituted by: 1) Ion source that ionizes the products prior to analysis in the mass spectrometer and 2) Mass analyzer that separates species on a mass-to-charge basis (Fig. VII.5). Mass analyzers require high levels of vacuum in order to operate in a predictable and efficient way. Finally, the ion beam that emerges from the mass analyzer, have to be detected and transformed into a usable signal. The detector is an important element of the mass spectrometer that generates a signal from incident ions either by generating secondary electrons, which are further amplified, or by inducing a current (generated by moving

charges). This data is then sent to a computer to be displayed and analyzed. The computer linked to the GC-MS has a library of samples to help in analyzing this data [73]. Data for the GC-MS is displayed in several ways. One is Full Scan mode that will monitor a range of masses know as mass to charge ratio (abbreviated m/z). A typical mass scan range will cover from 35-500 m/z four times per second and will detect compound fragments within that range over a set time period. Laboratories have extensive computer libraries containing mass-spectra of many different compounds to compare to the unknown analyte spectrum. The Full Scan mode is quite useful when identifying unknown compounds in a sample and providing confirmation of results from GC using other types of detectors. Another data acquisition way is SIM mode that allows for detection of specific analytes with increased sensitivity relative to full scan mode. In SIM mode the MS gathers data for masses of interest rather than looking for all masses over a wide range. Because the instrument is set to look for only masses of interest, it can be specific for a particular analyte of interest. Typically two to four ions are monitored per compound and the ratios of those ions will be unique to the analyte of interest. When properly setup and calibrated, GC/MS-SIM can increase sensitivity by a factor of 10 to 100 times that of GC/MS-Full Scan. Because unwanted ions are being filtered, the selectivity is greatly enhanced providing an additional tool to eliminate difficult matrix interferences. The ability of the mass spectrometer to identify unknowns in the full scan mode and quantitate know target analytes in the SIM mode, makes it one of the most powerful tools available for trace level quantitative analysis in the lab today [73].

References

[1] Rawa-Adkonis M, Wolska L, Przyjazny A, Namieśnik J. Sources of errors associated with the determination of PAH and PCB analytes in water samples. Anal. Lett. 2006;39:2317-31.
[2] Cinelli G, Cuomo F, Ambrosone L, Colella M, Ceglie A, Venditti F, et al. Photocatalytic degradation of a model textile dye using Carbon-doped titanium dioxide and visible light. J. Water Proc. Eng. 2017;20:71-7.
[3] Cuomo F, Venditti F, Ceglie A, De Leonardis A, Macciola V, Lopez F. Cleaning of olive mill wastewaters by visible light activated carbon doped titanium dioxide. RSC Adv. 2015;5:85586-91.
[4] Sungur Ş, Köroğlu M, Özkan A. Determinatıon of bisphenol a migrating from canned food and beverages in markets. Food Chem. 2014;142:87-91.
[5] Rezaee M, Yamini Y, Faraji M. Evolution of dispersive liquid–liquid microextraction method. J. Chromatogr. A 2010;1217:2342-57.
[6] García-López M, Rodriguez I, Cela R. Development of a dispersive liquid–liquid microextraction method for organophosphorus flame retardants and plasticizers determination in water samples. J. Chromatogr. A 2007;1166:9-15.
[7] Wei G, Li Y, Wang X. Application of dispersive liquid–liquid microextraction combined with high-performance liquid chromatography for the determination of methomyl in natural waters. J. Sep. Sci. 2007;30:3262-7.
[8] Chen H, Chen R, Li S. Low-density extraction solvent-based solvent terminated dispersive liquid–liquid microextraction combined with gas chromatography-tandem mass spectrometry for the determination of carbamate pesticides in water samples. J. Chromatogr. A 2010;1217:1244-8.
[9] Chang CC, Wei SY, Huang SD. Improved solvent collection system for a dispersive liquid–liquid microextraction of organochlorine pesticides from water using low-density organic solvent. J. Sep. Sci. 2011;34:837-43.
[10] Zhou Q, Zhang X, Xie G. Simultaneous analysis of phthalate esters and pyrethroid insecticides in water samples by temperature-controlled ionic liquid dispersive liquid-phase microextraction combined with high-performance liquid chromatography. Anal. Methods 2011;3:1815-20.
[11] Farajzadeh MA, Djozan D, Nouri N, Bamorowat M, Shalamzari MS. Coupling stir bar sorptive extraction-dispersive liquid–liquid microextraction for preconcentration of triazole pesticides from aqueous samples followed by GC-FID and GC-MS determinations. J. Sep. Sci. 2010;33:1816-28.
[12] Xu H, Ding Z, Lv L, Song D, Feng Y-Q. A novel dispersive liquid–liquid microextraction based on solidification of floating organic droplet method for determination of polycyclic aromatic hydrocarbons in aqueous samples. Anal. Chim. Acta 2009;636:28-33.
[13] Fatemi MH, Hadjmohammadi MR, Shakeri P, Biparva P. Extraction optimization of polycyclic aromatic hydrocarbons by alcoholic-assisted dispersive liquid–liquid microextraction and their determination by HPLC. J. Sep. Sci. 2012;35:86-92.
[14] Guo L, Lee HK. Low-density solvent-based solvent demulsification dispersive liquid–liquid microextraction for the fast determination of trace levels of sixteen priority polycyclic aromatic hydrocarbons in environmental water samples. J. Chromatogr. A 2011;1218:5040-6.
[15] Rezaee M, Yamini Y, Moradi M, Saleh A, Faraji M, Naeeni MH. Supercritical fluid extraction combined with dispersive liquid–liquid microextraction as a sensitive and efficient sample preparation method for determination of organic compounds in solid samples. J. Supercrit. Fluids 2010;55:161-8.
[16] Shi Z-G, Lee HK. Dispersive liquid− liquid microextraction coupled with dispersive μ-solid-phase extraction for the fast determination of polycyclic aromatic hydrocarbons in environmental water samples. Anal. Chem. 2010;82:1540-5.
[17] Leong M-I, Chang C-C, Fuh M-R, Huang S-D. Low toxic dispersive liquid–liquid microextraction using halosolvents for extraction of polycyclic aromatic hydrocarbons in water samples. J. Chromatogr. A 2010;1217:5455-61.

[18] Ying-Hong J, Yan H, Ting W, Jian-Lin L, ZHANG C, Yu L. Dispersive liquid-liquid microextraction based on solidification of floating organic drop with high performance liquid chromatography for determination of decabrominated diphenyl ether in surficial sediments. Chin. J. Anal. Chem. 2010;38:62-6.
[19] Wu Q, Wang C, Liu Z, Wu C, Zeng X, Wen J, et al. Dispersive solid-phase extraction followed by dispersive liquid–liquid microextraction for the determination of some sulfonylurea herbicides in soil by high-performance liquid chromatography. J. Chromatogr. A 2009;1216:5504-10.
[20] Wang H, Yan H, Qiao J. Miniaturized matrix solid-phase dispersion combined with ultrasound-assisted dispersive liquid–liquid microextraction for the determination of three pyrethroids in soil. J. Sep. Sci. 2012;35:292-8.
[21] Naeeni MH, Yamini Y, Rezaee M. Combination of supercritical fluid extraction with dispersive liquid–liquid microextraction for extraction of organophosphorus pesticides from soil and marine sediment samples. J. Supercrit. Fluids 2011;57:219-26.
[22] Çabuk H, Akyüz M, Ata Ş. A simple solvent collection technique for a dispersive liquid–liquid microextraction of parabens from aqueous samples using low-density organic solvent. J. Sep. Sci. 2012;35:2645-52.
[23] Hu J, Fu L, Zhao X, Liu X, Wang H, Wang X, et al. Dispersive liquid–liquid microextraction combined with gas chromatography–electron capture detection for the determination of polychlorinated biphenyls in soils. Anal. Chim. Acta 2009;640:100-5.
[24] Liang P, Zhang L, Zhao E. Displacement-dispersive liquid–liquid microextraction coupled with graphite furnace atomic absorption spectrometry for the selective determination of trace silver in environmental and geological samples. Talanta 2010;82:993-6.
[25] Rezaee M, Assadi Y, Hosseini M-RM, Aghaee E, Ahmadi F, Berijani S. Determination of organic compounds in water using dispersive liquid–liquid microextraction. J. Chromatogr. A 2006;1116:1-9.
[26] Xiao-Huan Z, Qiu-Hua W, ZHANG M-Y, Guo-Hong X, Zhi W. Developments of dispersive liquid-liquid microextraction technique. Chin. J. Anal. Chem. 2009;37:161-8.
[27] Retamal M, Ahumada I, Marican A, Fuentes E, Borie G, Richter P. Continuous pressurized solvent extraction of polycyclic aromatic hydrocarbons from biosolids. Assessment of their lability in soils amended with biosolids. Anal. Lett. 2010;43:2465-76.
[28] Chen H, Chen H, Ying J, Huang J, Liao L. Dispersive liquid–liquid microextraction followed by high-performance liquid chromatography as an efficient and sensitive technique for simultaneous determination of chloramphenicol and thiamphenicol in honey. Anal. Chim. Acta 2009;632:80-5.
[29] Melwanki MB, Fuh M-R. Partitioned dispersive liquid–liquid microextraction: an approach for polar organic compounds extraction from aqueous samples. J. Chromatogr. A 2008;1207:24-8.
[30] Tsai W-C, Huang S-D. Dispersive liquid–liquid microextraction with little solvent consumption combined with gas chromatography–mass spectrometry for the pretreatment of organochlorine pesticides in aqueous samples. J. Chromatogr. A 2009;1216:5171-5.
[31] Liang P, Sang H. Determination of trace lead in biological and water samples with dispersive liquid–liquid microextraction preconcentration. Anal. Biochem. 2008;380:21-5.
[32] Cunha S, Fernandes J, Oliveira M. Fast analysis of multiple pesticide residues in apple juice using dispersive liquid–liquid microextraction and multidimensional gas chromatography–mass spectrometry. J. Chromatogr. A 2009;1216:8835-44.
[33] Caldas SS, Costa FP, Primel EG. Validation of method for determination of different classes of pesticides in aqueous samples by dispersive liquid–liquid microextraction with liquid chromatography–tandem mass spectrometric detection. Anal. Chim. Acta 2010;665:55-62.
[34] Kozani RR, Assadi Y, Shemirani F, Hosseini M-RM, Jamali MR. Part-per-trillion determination of chlorobenzenes in water using dispersive liquid–liquid microextraction combined gas chromatography–electron capture detection. Talanta 2007;72:387-93.
[35] Chen H, Ying J, Chen H, Huang J, Liao L. LC determination of chloramphenicol in honey using dispersive liquid–liquid microextraction. Chromatographia 2008;68:629-34.

[36] Leong M-I, Huang S-D. Dispersive liquid–liquid microextraction method based on solidification of floating organic drop combined with gas chromatography with electron-capture or mass spectrometry detection. J. Chromatogr. A 2008;1211:8-12.
[37] Zhou Q, Bai H, Xie G, Xiao J. Temperature-controlled ionic liquid dispersive liquid phase micro-extraction. J. Chromatogr. A 2008;1177:43-9.
[38] Mirzaei M, Behzadi M, Abadi NM, Beizaei A. Simultaneous separation/preconcentration of ultra trace heavy metals in industrial wastewaters by dispersive liquid–liquid microextraction based on solidification of floating organic drop prior to determination by graphite furnace atomic absorption spectrometry. J. Hazard. Mater. 2011;186:1739-43.
[39] Kocúrová L, Balogh IS, Šandrejová J, Andruch V. Recent advances in dispersive liquid–liquid microextraction using organic solvents lighter than water. A review. Microchem. J. 2012;102:11-7.
[40] Farajzadeh MA, Seyedi SE, Shalamzari MS, Bamorowat M. Dispersive liquid–liquid microextraction using extraction solvent lighter than water. J. Sep. Sci. 2009;32:3191-200.
[41] Barrett CA, Orban DA, Seebeck SE, Lowe LE, Owens JE. Development of a low-density-solvent dispersive liquid–liquid microextraction with gas chromatography and mass spectrometry method for the quantitation of tetrabromobisphenol-A from dust. J. Sep. Sci. 2015;38:2503-9.
[42] Zhou Q, Zhang X, Xiao J. Ultrasound-assisted ionic liquid dispersive liquid-phase micro-extraction: A novel approach for the sensitive determination of aromatic amines in water samples. J. Chromatogr. A 2009;1216:4361-5.
[43] Cortada C, Vidal L, Canals A. Determination of nitroaromatic explosives in water samples by direct ultrasound-assisted dispersive liquid–liquid microextraction followed by gas chromatography–mass spectrometry. Talanta 2011;85:2546-52.
[44] Cinelli G, Avino P, Notardonato I, Centola A, Russo MV. Rapid analysis of six phthalate esters in wine by ultrasound-vortex-assisted dispersive liquid–liquid micro-extraction coupled with gas chromatography-flame ionization detector or gas chromatography–ion trap mass spectrometry. Anal. Chim. Acta 2013;769:72-8.
[45] Zacharis CK, Tzanavaras PD, Roubos K, Dhima K. Solvent-based de-emulsification dispersive liquid–liquid microextraction combined with gas chromatography–mass spectrometry for determination of trace organochlorine pesticides in environmental water samples. J. Chromatogr. A 2010;1217:5896-900.
[46] Melwanki MB, Fuh M-R. Dispersive liquid–liquid microextraction combined with semi-automated in-syringe back extraction as a new approach for the sample preparation of ionizable organic compounds prior to liquid chromatography. J. Chromatogr. A 2008;1198:1-6.
[47] Viñas P, Campillo N, Andruch V. Recent achievements in solidified floating organic drop microextraction. TrAC, Trends Anal. Chem. 2015;68:48-77.
[48] Rahimi A, Hashemi P. Development of a dispersive liquid-liquid microextraction method based on solidification of a floating organic drop for the determination of beta-carotene in human serum. J. Anal. Chem. 2014;69.
[49] Seebunrueng K, Santaladchaiyakit Y, Srijaranai S. Vortex-assisted low density solvent liquid–liquid microextraction and salt-induced demulsification coupled to high performance liquid chromatography for the determination of five organophosphorus pesticide residues in fruits. Talanta 2015;132:769-74.
[50] Lasarte-Aragonés G, Lucena R, Cárdenas S, Valcárcel M. Effervescence assisted dispersive liquid–liquid microextraction with extractant removal by magnetic nanoparticles. Anal. Chim. Acta 2014;807:61-6.
[51] Farajzadeh MA, Mogaddam MRA. Air-assisted liquid–liquid microextraction method as a novel microextraction technique; Application in extraction and preconcentration of phthalate esters in aqueous sample followed by gas chromatography–flame ionization detection. Anal. Chim. Acta 2012;728:31-8.
[52] Amoli-Diva M, Taherimaslak Z, Allahyari M, Pourghazi K, Manafi MH. Application of dispersive liquid–liquid microextraction coupled with vortex-assisted hydrophobic magnetic nanoparticles based

solid-phase extraction for determination of aflatoxin M1 in milk samples by sensitive micelle enhanced spectrofluorimetry. Talanta 2015;134:98-104.
[53] Daneshfar A, Khezeli T. Cloud point-dispersive liquid–liquid microextraction for extraction of organic acids from biological samples. J. Surfactants Deterg. 2014;17:1259-67.
[54] Trujillo-Rodríguez MJ, Rocío-Bautista P, Pino V, Afonso AM. Ionic liquids in dispersive liquid-liquid microextraction. TrAC, Trends Anal. Chem. 2013;51:87-106.
[55] Zhao RS, Wang X, Li FW, Wang SS, Zhang LL, Cheng CG. Ionic liquid/ionic liquid dispersive liquid–liquid microextraction. J. Sep. Sci. 2011;34:830-6.
[56] Campone L, Piccinelli AL, Celano R, Rastrelli L. pH-controlled dispersive liquid–liquid microextraction for the analysis of ionisable compounds in complex matrices: Case study of ochratoxin A in cereals. Anal. Chim. Acta 2012;754:61-6.
[57] Kozani RR, Assadi Y, Shemirani F, Hosseini MM, Jamali M. Determination of trihalomethanes in drinking water by dispersive liquid–liquid microextraction then gas chromatography with electron-capture detection. Chromatographia 2007;66:81-6.
[58] Nagaraju D, Huang S-D. Determination of triazine herbicides in aqueous samples by dispersive liquid–liquid microextraction with gas chromatography–ion trap mass spectrometry. J. Chromatogr. A 2007;1161:89-97.
[59] Chiang J-S, Huang S-D. Simultaneous derivatization and extraction of anilines in waste water with dispersive liquid–liquid microextraction followed by gas chromatography–mass spectrometric detection. Talanta 2008;75:70-5.
[60] Farina L, Boido E, Carrau F, Dellacassa E. Determination of volatile phenols in red wines by dispersive liquid–liquid microextraction and gas chromatography–mass spectrometry detection. J. Chromatogr. A 2007;1157:46-50.
[61] Farahani H, Norouzi P, Dinarvand R, Ganjali MR. Development of dispersive liquid–liquid microextraction combined with gas chromatography–mass spectrometry as a simple, rapid and highly sensitive method for the determination of phthalate esters in water samples. J. Chromatogr. A 2007;1172:105-12.
[62] Zhao R-S, Diao C-P, Wang X, Jiang T, Yuan J-P. Rapid determination of amide herbicides in environmental water samples with dispersive liquid–liquid microextraction prior to gas chromatography–mass spectrometry. Anal. Bioanal. Chem. 2008;391:2915-21.
[63] Rezaei F, Bidari A, Birjandi AP, Hosseini MRM, Assadi Y. Development of a dispersive liquid–liquid microextraction method for the determination of polychlorinated biphenyls in water. J. Hazard. Mater. 2008;158:621-7.
[64] Pusvaskiene E, Januskevic B, Prichodko A, Vickackaite V. Simultaneous Derivatization and dispersive liquid–liquid microextraction for fatty acid GC determination in water. Chromatographia 2009;69:271-6.
[65] Cristina Henriques Alves A, Margarida Pontes Boavida Gonçalves M, Manuel Serrano Bernardo M, Simões Mendes B. Dispersive liquid–liquid microextraction of organophosphorous pesticides using nonhalogenated solvents. J. Sep. Sci. 2012;35:2653-8.
[66] Ebrahimzadeh H, Yamini Y, Kamarei F. Optimization of dispersive liquid–liquid microextraction combined with gas chromatography for the analysis of nitroaromatic compounds in water. Talanta 2009;79:1472-7.
[67] Panagiotou AN, Sakkas VA, Albanis TA. Application of chemometric assisted dispersive liquid–liquid microextraction to the determination of personal care products in natural waters. Anal. Chim. Acta 2009;649:135-40.
[68] Cortada C, Vidal L, Pastor R, Santiago N, Canals A. Determination of organochlorine pesticides in water samples by dispersive liquid–liquid microextraction coupled to gas chromatography–mass spectrometry. Anal. Chim. Acta 2009;649:218-21.

[69] Sadeghi R, Kobarfard F, Yazdanpanah H, Eslamizad S, Bayat M. Validation of an Analytical Method for Determination of 13 priority polycyclic aromatic hydrocarbons in mineral water using dispersive liquid-liquid microextraction and GC-MS. Iran. J. Pharm. Res.: IJPR 2016;15:157.
[70] Borges B, Melo A, Ferreira IM, Mansilha C. Dispersive Liquid–Liquid Microextraction for the Simultaneous Determination of Parent and Nitrated Polycyclic Aromatic Hydrocarbons in Water Samples. Acta Chromatogr. 2016:1-8.
[71] Nagy B. Review of the chromatographic "plate" theory with reference to fluid flow in rocks and sediments. Geochim. Cosmochim. Acta 1960;19:289-96.
[72] Stashenko E, Martínez JR. Gas Chromatography-Mass Spectrometry. Advances in Gas Chromatography: InTech; 2014.
[73] Hussain SZ, Maqbool K. GC-MS: Principle, Technique and its application in Food Science. J CURR Science 2014;13:116-26.
[74] Skoog DA, Holler FJ, Crouch SR. Principles of instrumental analysis: Cengage learning; 2017.

Chapter VIII

New protocol based on DLLME-GC-IT/MS for determining low-trace levels of PAHs in high volume of surface water

VIII.1 Introduction

Polycyclic aromatic hydrocarbons (PAHs) are ubiquitous pollutants found throughout the environment in soils, sediments and surface waters, as cited in Chapter VI. Atmospheric deposition of these compounds occurs from natural and anthropogenic sources, such as forest fires and burning of fossil fuels [1]. Sixteen PAHs are listed as priority pollutants (Fig. VI.1 Chapter VI) by the United States Environmental Protection Agency (US-EPA) and by the European Environment Agency [2]. The monitoring of PAHs concentrations in surface water of oil sand regions has become a critical part of water quality surveillance programs implemented by government agencies. PAH analysis is also an important tool in cases of environmental contamination or accidental oil spills, where the ability to rapidly characterize and determine the concentration of PAHs in surface water is vital to identify sources, ecological effects, and appropriate remediation efforts. During surface oil spill clean-up responses, surfactant containing dispersants may be used to enhance the formation of small oil droplets, allowing oil to be dispersed into the water column. Dispersants may also affect the bioavailability of chemicals from the oil, including toxic PAHs [3]. Presently, the two most common techniques used to determine PAHs are High Performance Liquid Chromatography (HPLC) with fluorescence, ultra-violet, or diode array detection and capillary Gas Chromatography coupled with Mass Spectrometry (GC/MS) detection in electron impact mode (EI^+) with selected ion monitored (SIM) [1, 4-6]. Although HPLC methods can be rapid, detection is less specific and sensitive and more subject to interference than a GC/MS procedure. Typical GC/MS methods, however, require extensive sample clean-up to remove matrix contaminants, large sample and solvent volume (such as humic acids in water) and a concentration step in order to detect the trace level of PAHs found in surface waters [7]. As already cited in Chapter VI, most surface waters contain individual PAHs at levels above 0.05 pg μL^{-1}, but highly polluted rivers can have concentrations

of up to 6 pg μL^{-1}. On the other hand PAHs levels in groundwater and drinking water range between 0.0002 and 0.0018 pg μL^{-1}, in rainwater from 0.01 to 0.2 pg μL^{-1} whereas, in highly urban areas, levels of up to 1 pg μL^{-1} were determined in snow and fog [8, 9]. United States Environmental Protection Agency (USEPA) has developed ambient water quality criteria to protect human health from the carcinogenic effects of PAHs exposure: the recommended maximum contaminant level (MCL) is 0.2 pg μL^{-1} in drinking water.

Therefore, it became necessary to have an analytical method for determining PAHs at very low concentrations. The larger aromatic ring of PAHs has very low water solubility and therefore extraction of large volumes of water is typically required to achieve trace level detection and quantitation with single quadrupole GC/MS instruments. Basically, liquid-liquid extraction (LLE) [10] and solid phase extraction (SPE) [11] are used as pre-concentration step for concentrating PAHs in aqueous environmental samples [12] using large volumes of organic solvents. A published example of liquid/liquid extraction (LLE) employed 1 liter of water with 200 mL of methylene chloride (EPA method 610) [13]. Another publication utilizing LLE required 800 mL of water with three extractions using a total of 200 mL of binary n-hexane and Dichloromethane DCM (1:1 v/v) [14]. The clean-up further required column separation and nitrogen blow down, all with the potential for loss of PAHs together with higher material costs and waste solvent disposal requirements [13, 14]. Furthermore, the traditional LLE process is labour intensive and can suffer from emulsion formation [15]. New techniques that have been introduced in an attempt to reduce these problems include Solid Phase Extraction (SPE) and Solid Phase Micro-Extraction (SPME). Despite being relatively efficient, rapid and selective, SPE and SPME can suffer from relatively low recoveries of PAHs, in addition to lengthy method development time, costly sorbents, variation in results from cross contamination and incomplete removal of interfering matrix compounds [16-18]. Liquid phase microextraction (LPME) [19] and its variants (single-drop microextraction SDME [20], hollow-fiber-protected liquid phase microextraction (HF-LPME) [21, 22] and solvent bar microextraction (SBME) [23]) require long extraction times for reaching good Limit of Detections (LOD) [12] or, at least, LODs able to detect these compounds in such matrices. Ten years ago Rezaee et al. [24] introduced the dispersive liquid-liquid microextraction (DLLME) and it has become a very popular environment friendly sample-preparation technique, because it is fast, inexpensive, easy to operate with a high enrichment factor and consumes low volume of organic solvent. Thus, DLLME has been frequently used for determination of organic contaminants in liquid samples, including of PAHs in water samples [24, 25]. In this procedure a suitable combination of dispersive and extraction solvents is rapidly injected with a microsyringe into an aqueous sample. After the formation of a cloudy solution

and the subsequent centrifugation step (as detailed described in Chapter VII), the content of the lower phase can be analyzed by an appropriate analytical method [24]. All the details about this techniques are described in chapter VII. The methodology described in the following paragraph (VIII.2.2) offers different advantages whereas some drawbacks are connected to the use of toxic halogenated compounds for the extraction procedure or to the large amount of dispersive solvent [12]. However, this study represents an important innovation in the DLLME method because the emulsification occurred without disperser solvent but by means of external mechanical energy. So, dispersive solvent has not been added whereas ultrasounds have been used for providing the sufficient energy for obtaining the finely dispersed phase required to extract quantitatively the solutes. The other important novelty in this work is the use of large volume sample of water: the analytical parameters have been studied for sampling till 1 L of water. Further, an interesting use of the large volume sampling is the improvement of detection limits in trace analysis and the time analysis reduction (e.g., avoiding laborious solvent evaporation step). This study aims to develop a simple, cost-effective, sensitive and reproducible analytical method for the PAHs determination in large volume of surface water. In particular, the goal is to introduce a new extraction procedure based on Dispersive Liquid Liquid Micro-extraction (DLLME) followed by GC-MS for minimizing the sample preparation time and simultaneously obtaining high levels of sensitivity, reproducibility and selectivity.

VIII.2 Materials and methods

Materials

Among the list of priority pollutants by USEPA, these are the following PAHs chosen for the study: Fluorene ($C_{13}H_{10}$; 166.222 Da; lethal dose 50% (LD_{50}) not available (N/A); IARC classification Group 3), Phenanthrene ($C_{14}H_{10}$; 178.233 Da; LD_{50} 700 mg kg^{-1} mouse; Group 3), Anthracene ($C_{14}H_{10}$; 178.233 Da; LD_{50} 3200 mg kg^{-1} mouse; Group 3), Fluoranthene ($C_{16}H_{10}$; 202.255 Da; LD_{50} 2000 mg kg^{-1} mouse; Group 3), Pyrene ($C_{16}H_{10}$; 202.255 Da; LD_{50} 16,000 mg kg^{-1} mouse; Group 3), Chrysene ($C_{18}H_{12}$; 228.2928 Da; LD_{50} N/A; Group 2A), Benzo(b)fluoranthene ($C_{20}H_{12}$; 252.315 Da; LD_{50} N/A; Group 2B), Benzo(a)pyrene (or 3,4-benzopyrene) ($C_{20}H_{12}$; 252.3148 Da; LD_{50} 50 mg kg^{-1} mouse; Group 1) and Benzoperylene ($C_{22}H_{12}$; 276.337 Da; LD_{50} N/A; Group 3). n-Octacosane (C_{28}) has been used as Internal Standard (I.S.). All chemicals were from Sigma-Aldrich. Water samples were collected from two regions of Southern Italy, Molise and Campania and filtered before analysis. Stock standard solutions of PAHs were individually prepared by dissolving 5 mg of each in 1 mL of solvent.

Calibration standards

Individual stock standard solutions (5 mg mL^{-1}) of the PAHs were prepared. Fluorene, Anthracene, Fluoranthene, Pyrene were dissolved in methanol, Phenanthrene, Chrysene, Benzoperylene in acetone, Benzo(b)fluoranthene and Benzo(a)pyrene in *iso*-octane. Finally, *n*-Octacosane (C_{28}) was dissolved in acetone.

A mixed standard solution of the PAHs at a concentration of 20 ng μL^{-1} was prepared by appropriate dilution of the stock solutions in acetone. This solution was used as a spiking solution for validation experiments.

Development of the extraction process using the DLLME methodology

The extraction method is based on the use of DLLME and it can be divided into three steps.

Starting from 100 mL (up to 1000 mL) of water sample, different experiments have been performed by adding 25 µL of PAHs mix solution (5 pg μL^{-1} of each PAHs) and 5 µL of I.S. (concentration 25 pg μL^{-1}). The first phase allows determining the best extraction solvent and the relative ratio between the aqueous phase and the solvent. Different volumes of three extraction solvents were tested, all with a lower density than water in order to carry out a surface extraction: *n*-hexane (0.66 g cm^{-3}), *iso*-octane (0.69 g cm^{-3}) and toluene (0.87 g cm^{-3}). The tests were performed on blank water samples (ultrapure water samples) without the addition of the dispersive solvent. After this first step, it has been investigated the best way to obtain an effective emulsification with the only presence of the extraction solvent. Among the different methods used, the more stable and homogeneous emulsion has been obtained using ultrasounds: the solution, kept for 2 min in the ultrasound bath, allows the formation of a perfectly stable and homogeneous emulsion. This allows affirming that the DLLME extraction methodology can be performed without the use of the dispersive solvent. A second phase, a very sensitive step of the procedure, regarded how to break the emulsion, trying simultaneously to keep the short mixing times and obtain quantitative and reproducible recovery rates. In order to break the emulsion various tests have been carried out adding NaCl at different concentrations, i.e. 2, 5, 10, 15 and 25 g L^{-1}. After NaCl addition, the solution is kept under agitation for 30 min in order to break the emulsion and allow the separation of the two phases. In this way the drop is obtained: 1 µL withdrawn by syringe was injected in the GC-MS instrument.

GC-MS instrumentation

The GC-IT/MS system used for analysis was a Trace gas chromatograph coupled with a Polaris Q mass spectrometer (ThermFinnigan, Bremen, Germany). Data acquisition and analysis were performed using standard software supplied by the manufacturer (Xcalibur 1.4.1). A gas chromatograph Finnigan Trace GC Ultra-equipped with an Ion Trap Mass Spectrometry detector

Polaris Q (Thermo Fisher Scientific, Waltham, MA), a Programmed Temperature Vaporizer (PTV) injector and a PC with a chromatography station Xcalibur (Thermo Fisher Scientific), was used. A fused-silica capillary column with chemically bonded phase (SE-54, 5% phenyl-95% dimethylpolisiloxane) was used with the following characteristics: 30 m × 250 μm i.d., N (theoretical plate number) 125,000 for n-dodecane at 90 °C; K' (capacity factor) 6.8; d_f (film thickness) 0.24 μm; u_{opt} (optimum linear velocity of carrier gas, hydrogen) 39.5 cm s^{-1}, and UTE% (utilization of theoretical efficiency) 94%. A 1 μL sample was injected into the programmable temperature vaporization injector in the splitless mode. Five seconds after the injection the vaporizer was heated from 50 to 290 °C at 14.5 °C min^{-1}; the splitter valve was opened after 240 s. The temperature of the GC-IT/MS transfer line was 270 °C and the temperature of the ion source was 250 °C. Helium (IP 5.5) was used as the carrier gas at a flow rate of 1.0 mL min^{-1}. The oven temperature program was as follows: 60 °C, held for 50 s, 20 °C min^{-1} up to 150 °C, held for 2 min and heated to 290 °C at 20 °C min^{-1} and held for 11 min. The IT/MS was operated in the electron ionization mode (70 eV) and the analytes were qualitatively identified in full-scan mode (m/z 100–400) and quantified in SIM mode. The retention time (t_r) and the Selected Ion Monitoring (SIM) are reported for each compounds as following: 1) Fluorene (t_r 9.75, SIM 166), 2) Phenanthrene (t_r 11.24, Se SIM 178) 3) Anthracene (t_r 11.32, SIM 178), 4) Fluoranthene (t_r 12.9, SIM 202), 5) Pyrene (t_r 13.19, SIM 202), 6) crysene (t_r 14.88, SIM 228), 7) I.S. (t_r 16.48, SIM 113), 8) benzo(b)fluoranthene (t_r 16.88, SIM 252), 9) 3,4-benzopyrene (t_r 17.7, SIM 252), 9) benzoperylene (t_r 22.66, SIM 276). The quantitative analysis was performed by calibration graphs of the ratio $Area_{(PAH)}/Area_{(IS,octosane)}$ plotted vs. each PAH concentration (pg μL^{-1}). All the samples were determined in triplicate.

VIII.3 Results and discussion

Each step of the whole procedure, described in the paragraph VIII.2.2, has been followed and investigated and all the analytical parameters have been studied. The preliminary evaluation of the methodology was performed using matrices as close as possible to real samples (blank solutions). The preliminary tests were carried out on 100 mL of volume sample. Due to large volume sample, centrifugation step was discarded and, in order to break the emulsion, NaCl was added to the emulsion. Important steps in the development of the analytical methodology regard the NaCl amount necessary for breaking the emulsion without affecting the sample and the recoveries as well. Table VIII.1 shows the recoveries obtained spiking 100 mL of blank solution with 5 pg μL^{-1} of each PAH and adding 5 μL of I.S. (C_{28} 25 pg μL^{-1}) in relation to the different NaCl amount (2,

5, 10, 15 and 25 g L^{-1}). As can be seen in Table VIII.1, the addition of 10 g L^{-1} of NaCl allows to obtain the best recoveries.

Table VIII.1. Recoveries (%) obtained on 100 mL of blank solution in relation to the NaCl amount (2, 5, 10, 15 and 25 g L^{-1}). In brackets are reported the RSDs (%).

PAHs	Recovery (%)				
	2 g L^{-1}	5 g L^{-1}	10 g L^{-1}	15 g L^{-1}	25 g L^{-1}
Fluorene	82.7 (6.0)	86.7 (3.6)	104.9 (8.7)	94.7 (5.8)	101.4 (5.0)
Phenanthrene	54.1 (9.2)	89.5 (3.0)	105.7 (5.4)	96.0 (2.1)	103.4 (4.7)
Anthracene	53.0 (9.1)	85.5 (3.1)	104.4 (6.9)	94.2 (8.5)	104.2 (2.5)
Fluoranthene	56.3 (7.6)	92.4 (3.5)	98.5 (5.4)	84.9 (2.9)	103.6 (7.7)
Pyrene	89.4 (4.4)	91.4 (3.6)	100.9 (4.3)	100.1 (2.2)	104.8 (7.0)
Chrysene	64.6 (3.8)	80.0 (5.0)	100.8 (3.9)	81.9 (3.5)	117.4 (6.5)
Benzo(b)fluoranthene	80.9 (6.9)	85.4 (3.8)	102.4 (4.2)	88.2 (9.7)	103.8 (1.2)
Benzo(a)pyrene	73.7 (7.3)	79.7 (3.4)	99.6 (5.5)	80.4 (2.8)	105.7 (9.8)
Benzoperylene	62.6 (8.4)	69.0 (2.7)	103.8 (6.7)	69.5 (6.9)	104.4 (6.0)

Another important steps in the development of the analytical methodology regards the choice of the extraction solvent. For identifying the more reliable and effective extraction solvent, three solvents have been tested, such as *n*-hexane, *iso*-octane and toluene. 500 µL of *n*-hexane or *iso*-octane were able to form a cloudy solution and a final drop, after NaCl addition, of about 200 µL and 300 µL, respectively whereas for toluene 1000 µL were necessary for having a very small drop of about 50 µL. In Table VIII.2 are reported the recoveries (%) obtained spiking 100 mL of blank solution with 5 pg μL^{-1} of each PAH, adding 5 µL of I.S. (C_{28}, 25pg μL^{-1}), 10 g L^{-1} of NaCl and 500 µL volume of *n*-hexane or *iso*-octane and 1000 µL of toluene as extraction solvents, respectively. Looking at the data in Table VIII.2, *n*-hexane and *iso*-octane could be considered candidates as extraction solvent whereas toluene was discharged because a large volume was necessary for obtaining the emulsion.

After verifying the possible candidate solvents to be used in the extraction procedure, experiments for reducing the solvent extraction volume were carried out. The tests were made for verifying the influence of such parameter on the PAHs recoveries and were performed using 300 µL of n-hexane and 300, 250 and 200 µL of *iso*-octane. In this case, the two solvents have shown a different behavior: the experiments with *iso*-octane as extraction solvent manage to form a stable emulsion and consequently the separation of two phases; on the contrary tests adding 300 µL of *n*-hexane to 100 mL of water sample does not manage to make an emulsion. Table 8.3 shows the recoveries (%) of each PAH in relationship with different volume of *iso*-octane (300, 250 and 200 µL) as extraction solvent. 100 mL of blank solution were spiked with 5 pg μL^{-1} of each PAH and added with 5 µL of I.S. (C_{28}, 25 pg μL^{-1}) and 10 g L^{-1} of NaCl.

Table VIII.2. Recoveries (%) obtained on 100 mL of blank solution in relation to three different extraction solvents (*n*-hexane, *iso*-octane and toluene). In brackets are reported the RSDs (%).

PAHs	Recovery (%)		
	n-Hexane	*iso*-Octane	Toluene
Fluorene	94.8 (5.0)	98.8 (4.8)	81.3 (6.3)
Phenanthrene	99.7 (3.5)	101.6 (1.9)	96.7 (7.5)
Anthracene	91.1 (8.5)	98.1 (1.8)	75.8 (5.1)
Fluoranthene	105.8 (2.4)	100.1 (0.3)	99.8 (3.4)
Pyrene	106.3 (2.8)	99.4 (0.5)	99.7 (2.5)
Chrysene	107.7 (1.2)	100.4 (3.4)	96.8 (5.0)
Benzo(b)fluoranthene	108.6 (3.0)	101.8 (2.6)	103.1 (4.4)
Benzo(a)pyrene	106.4 (7.4)	100.0 (6.2)	88.2 (9.7)
Benzoperylene	105.5 (1.8)	102.6 (6.2)	102.9 (3.5)

As can be seen in Table VIII.3, 300 µL of *iso*-octane are sufficient for obtaining PAHs recoveries ranging between 99 and 103% with a good RSD (<9.5%) whereas 250 µL allow to obtain good PAHs recoveries (84–94%) with a very poor RSD (<16.1%).

Table VIII.3. Recoveries (%) of each PAH in relationship with different volume of *iso*-octane as extraction solvent (300, 250 and 200 µL). In brackets are reported the RSDs (%).

PAHs	Recovery (%)		
	300 µL	250 µL	200 µL
Fluorene	102.8 (2.9)	89.8 (12.1)	73.6 (15.7)
Phenanthrene	102.0 (2.2)	91.0 (13.0)	74.6 (16.3)
Anthracene	101.0 (3.1)	84.0 (15.6)	68.1 (21.8)
Fluoranthene	102.1 (3.6)	93.9 (7.5)	73.6 (8.5)
Pyrene	101.9 (3.6)	93.3 (5.0)	74.4 (5.5)
Chrysene	100.4 (2.3)	83.0 (14.7)	62.5 (21.0)
Benzo(b)fluoranthene	102.9 (7.9)	90.5 (12.0)	72.2 (11.6)
Benzo(a)pyrene	99.3 (3.8)	93.8 (12.0)	68.5 (15.1)
Benzoperylene	102.9 (9.5)	86.7 (16.1)	75.8 (21.2)

All the experiments have been carried out using 10 g L^{-1} of NaCl and 300 µL of iso-octane as extraction solvent: 100 µL are recovered at the end of the extraction procedure.

Another parameter investigated has been the temperature of the ultrasound bath: experiments were performed at ambient temperature (25 °C) and at other 4 different temperatures slightly lower and higher than the ambient temperature, such as 20, 22, 27 and 31 °C. No relevant changes has been detected (data not shown), so 25 °C temperature has been chosen for making the emulsion in the ultrasound bath. The other important novelty in this study regards the sampling volume: basically, in surface (and environmental as well) water samples PAHs are present at ultra-trace levels to be significantly below to the detection limit of the analytical instruments. So, it is generally necessary to perform long and sensitive clean-up procedures for

enriching such compounds, or to sample a more large-volume water samples for having good enrichment factors. This second possibility is really interesting for the implications reported in: some studies are oriented in this direction but they use complicated methodology for this aim [12]. This part of my work investigates the application of the entire procedure with increasing water sample volumes from 100 mL to 1000 mL in order to investigate the effect of the sample volume on PAH recoveries. In detail, the tests were performed on four different volume samples (100, 250, 500 and 1000 mL). Table VIII.4 shows the recoveries obtained spiking different water sample volumes with 5 pg μL^{-1} of each PAH and adding 5 µL of I.S. (C_{28}, 25 pg L^{-1}), 10 g L^{-1} of NaCl and 300 µL of iso-octane as extraction solvent. As can be seen in Table VIII.4, the PAH recoveries are higher than 90% with sample volume increasing from 100 to 1000 mL: considering the low level of PAH loading (each water sample was spiked with 25 µL of the standard solution containing 5 pg μL^{-1} of each PAH) the effect of the sample volume on the PAH recoveries is small.

Table VIII.4. Recoveries (%) of each PAH in relation to different water sample volumes (100, 250, 500 and 1000 mL). In brackets are reported the RSDs (%).

PAHs	Recovery (%)			
	100 mL	250 mL	500 mL	1000 mL
Fluorene	102.8 (2.9)	97.5 (8.5)	104.8 (8.8)	100.5 (4.6)
Phenanthrene	102.0 (2.2)	98.5 (6.5)	102.2 (8.7)	102.0 (2.2)
Anthracene	101.0 (3.1)	99.9 (7.5)	102.7 (8.1)	103.7 (3.9)
Fluoranthene	102.1 (3.6)	97.4 (4.6)	101.3 (8.3)	104.1 (1.5)
Pyrene	101.9 (3.6)	96.2 (4.9)	99.1 (8.5)	103.9 (1.4)
Chrysene	100.4 (2.3)	103.2 (4.9)	100.1 (2.0)	100.4 (2.3)
Benzo(b)fluoranthene	102.9 (7.9)	98.7 (2.7)	101.0 (6.9)	104.2 (5.4)
Benzo(a)pyrene	99.3 (3.8)	101.8 (3.8)	102.9 (4.7)	99.8 (3.6)
Benzoperylene	102.9 (9.5)	97.6 (8.6)	100.4 (4.5)	102.9 (9.5)

The effect of the sample volume (i.e. the increase from 100 to 1000 mL) in the size of the floating phase after breaking down the emulsion, is unimportant: experiments performed in this way have confirmed that the procedure is not affected by the sample volume. In brackets in Table 8.4 are reported the RSDs, the values obtained are good in all the cases: RSD ranges between 2.2 and 9.5%, 2.7–8.6%, 2.0–8.8% and 1.4–9.5% for sampling volumes of 100 mL, 250 mL, 500 mL and 1000 mL, respectively. The recoveries remain high also when 1000 mL of water is sampled. As the extraction process is not conditioned by the sample volume and because we want to achieve a high enrichment factor, the sample volume of 1000 mL has been adopted in this work. A main consideration could be drawn: the entire procedure is able to reach high extraction ability probably due to the synergic effect of the extraction solvent and the breaking

emulsion. So, under the optimized conditions (i.e., sampling volume 1 L; extraction solvent 300 µL *iso*-octane; 2 min of ultrasound bath at 25 °C; NaCl 10 g L^{-1} and 30 min of stirring), the mean recoveries of the 9 PAHs investigated in water samples ranges between 99% and 103% with a RSD below 9.5 (Table VIII.4): this shows that the optimized extraction conditions are appropriate for PAH extraction and analysis from large-volume water samples. The extraction process is shown in Fig. VIII.1, where it is possible to see that, starting from 1-L of water samples, a very small final volume (100 µL), is obtained and an enrichment factor (EF) of 10^4 times is achieved.

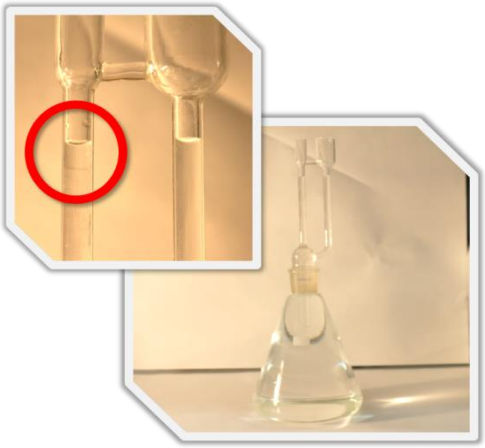

Fig. VIII.1. Extraction procedure; picture on the right side shows the starting water sample volume (1 L), the picture on the left shows the final volume of extraction solvent at the end of the extraction process (100 µL).

Method validation

In Table VIII.5 the equations of the calibration curves with relative R^2, the Limit of Detections (LODs) and Limit of quantifications (LOQs), the reproducibility of the extraction process and the intra-day and inter-day precisions have been reported. All the data are obtained spiking 1 L-water sample with PAH standard solutions at different concentrations and addition of 5 µL of I.S. (C_{28}, 25 pg μL^{-1}), 10 g L^{-1} of NaCl and 300 µL of iso-octane as extraction solvent.

The results, obtained spiking 1 L water samples with PAHs standard solutions at different increasing concentrations, i.e. 0.01, 0.1, 1, 10, 100 e 500 pg μL^{-1}, and adding 50 µL of I.S. in each, show R^2 always above 0.991 and a good linearity range in the investigated range. Further, the Limit of Detections (LODs) and Limit of quantifications (LOQs) ranging between 0.001 and 0.009 pg μL^{-1} and 0.003–0.022 pg μL^{-1}, respectively. These values were determined according to the Knoll's definition [26], i.e., an analyte concentration that produces a chromatographic peak equal to three times (LOD) and ten times (LOQ) the standard deviation of the baseline noise. It should be noted that this determination could give cross-contamination problems due to sorption of lipophilic PAHs on glass material at such LOQs and linearity range: this issue was deeply investigated by authors in previous papers [27, 28] and it is neglected in this procedure. Table

VIII.5 also shows the reproducibility obtained spiking 1000 mL of water samples with different PAHs standard solution concentrations, i.e. 0.1, 10 and 50 pg μL^{-1}, and 5 µL of I.S.: it ranges between 97 and 107% (RSD < 12.1), 99–104% (RSD < 9.5) and 99–105% (RSD < 6.3), respectively. As expected, the reproducibility improves as the concentration increases but it is also very good at low PAH concentrations. Finally, the inter- and intra-day precisions determined on 1-L water sample, at two different concentrations (5 pg μL^{-1} and 50 pg μL^{-1}) and evaluated as RSD, are below 6.0% and 8.2%, respectively.

Table VIII.5. Linear equations and correlation coefficient (R^2), LODs (pg μL^{-1}) and LOQs (pg μL^{-1}) of each PAH along with recoveries (%), intra-day and inter-day precisions (calculated as RSD, %) at different PAH concentrations. In brackets are reported the RSDs (%).

PAHs	Equation	R^2	LOD	LOQ	Recovery (%)			Intra-day		Inter-day	
					0.1 pg μL^{-1}	10 pg μL^{-1}	50 pg μL^{-1}	5 pg μL^{-1}	50 pg μL^{-1}	5 pg μL^{-1}	50 pg μL^{-1}
Fluorene	0.36x + 0.04	0.9911	0.002	0.004	97.4 (9.3)	103.8 (2.9)	101.9 (1.2)	4.6	3.2	3.8	6.9
Phenanthrene	0.51x + 0.29	0.9943	0.002	0.004	102.1 (10.1)	102.0 (6.4)	105.2 (2.2)	4.8	3.7	4.4	7.7
Anthracene	0.74x + 0.30	0.9947	0.001	0.003	106.5 (10.6)	101.0 (3.1)	100.8 (5.9)	6	3.5	6.2	8.2
Fluoranthene	0.87x + 0.62	0.9967	0.001	0.003	104.8 (11.4)	102.1 (3.6)	101.4 (4.7)	4.5	2.4	3.4	6.1
Pyrene	0.77x + 0.56	0.9963	0.001	0.004	106.9 (10.9)	101.9 (3.6)	102.5 (0.4)	2.9	3	2.7	5.9
Chrysene	0.99x + 0.78	0.9974	0.003	0.007	103.2 (12.1)	100.4 (2.3)	99.1 (3.7)	5	3.5	4.2	5.9
Benzo(b)fluoranthene	0.92x + 0.65	0.9987	0.003	0.007	101.6 (10.9)	102.9 (7.9)	103.6 (6.3)	4.8	2.4	4.2	5.1
Benzo(a)pyrene	0.56x + 0.18	0.9991	0.006	0.014	104.7 (9.0)	99.3 (3.8)	101.2 (1.9)	5.1	2.6	4.4	5.2
Benzoperylene	0.77x + 0.26	0.999	0.009	0.022	106.4 (8.8)	102.9 (9.5)	102.3 (3.8)	5.9	1.8	6.6	6.1

With the scope to evidence an eventual presence of matrix effect, a particular attention has been devoted to the comparison between the blank standard solution and the real sample. Table VIII.6 shows the comparison between blank and real (surface) 1 L-water samples spiking with standard solution containing 0.05 pg μL^{-1} (lowest level), 1 pg μL^{-1} (medium level) and 50 pg μL^{-1} (high level) of each PAH, respectively. First, the recoveries are quite similar for blank and real solutions: they range between 96 and 102% and 97–105% for spiking with 0.05 pg μL^{-1}, 99–104% and 99–106% for spiking with 1 pg μL^{-1} and between 98 and 104% and 99–105% for spiking with 50 pg μL^{-1}, respectively.

As can be seen in Table VIII.6, the RSDs are below 9.2% and 14.2%, below 6.5% and 13.5% and below 6.5% and 7.2% for standard and real solutions spiked with 0.05 pg μL^{-1}, 1 pg μL^{-1} and 50 pg μL^{-1}, respectively. In all cases, the matrix effect is not significant but the presence of interfering molecules increases the measurement error. These data evidence that the recoveries with PAHs spiked at 1 pg μL^{-1} and 50 pg μL^{-1} are quantitatively similar and significant: it means that the entire extraction procedure set up for standard solutions can also be successfully applied to real samples.

Table VIII.6. Comparison between blank and real (surface) 1 L-water samples spiking with standard solution containing 0.05 pg μL^{-1} (lowest level), 1 pg μL^{-1} (medium level) and 50 pg μL^{-1} (high level) of each PAH, respectively.

PAHs	Lowest levels		Medium levels		High levels	
	Blank	Real	Blank	Real	Blank	Real
Fluorene	97.5 (8.1)	99.4 (9.9)	101.3 (5.8)	101.6 (12.0)	100.5 (4.6)	105.1 (2.9)
Phenanthrene	96.8 (6.2)	98.4 (11.8)	100.8 (4.1)	102.7 (13.4)	102.0 (2.2)	104.3 (4.0)
Anthracene	99.2 (7.4)	102.4 (14.1)	102.6 (6.5)	104.6 (13.5)	103.7 (3.9)	102.4 (6.4)
Fluoranthene	101.3 (6.9)	104.5 (11.7)	99.3 (2.0)	106.1 (11.1)	104.1 (1.5)	104.0 (2.0)
Pyrene	98.6 (9.2)	97.1 (12.9)	100.6 (3.4)	104.0 (11.0)	103.9 (1.4)	103.4 (2.4)
Chrysene	97.1 (7.5)	101.6 (11.2)	101.7 (3.3)	105.9 (9.8)	100.4 (2.3)	105.0 (3.3)
Benzo(b)fluoranthene	102.0 (8.1)	99.1 (10.5)	102.9 (3.7)	99.3 (8.1)	106.2 (5.4)	103.5 (3.6)
Benzo(a)pyrene	96.2 (5.8)	98.7 (12.1)	104.4 (1.9)	101.5 (8.1)	98.3 (3.8)	99.1 (3.7)
Benzoperylene	98.7 (6.4)	101.6 (14.2)	102.2 (2.0)	103.3 (7.7)	102.3 (6.5)	105.1 (7.2)

Fig. VIII.2 shows the chromatograms of a surface water sample collected at the city water supply and water source PAH-spiked (5 pg μL^{-1}) (A): the peaks result well-separated and well-solved (for PAHs levels see sample F in Table VIII.8) and the same sample no spiked (B).

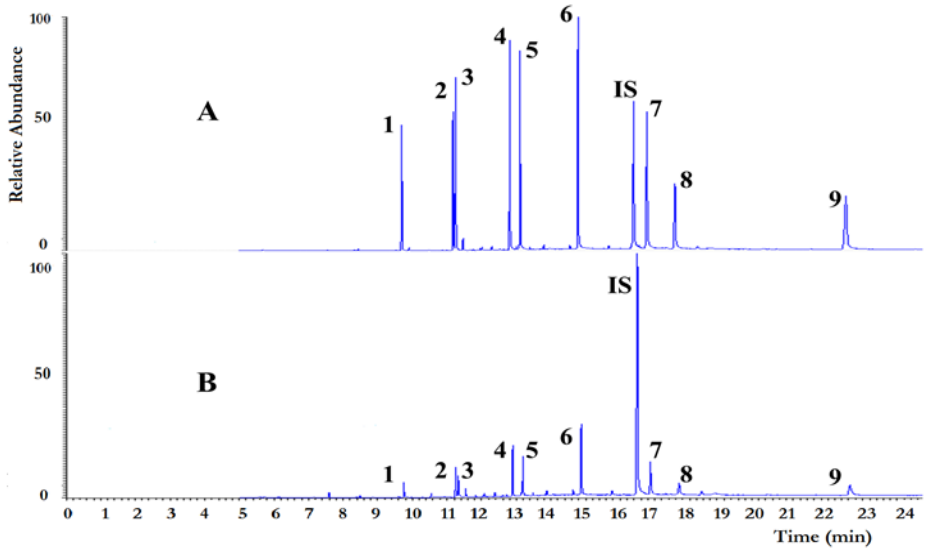

Fig. VIII.2. Chromatograms of (A), sample collected at the city water supply and water source spiked (5 pg μL^{-1})and (B) the same sample no spiked. Peaks: 1 Fluorene; 2 Phenanthrene; 3 Anthracene; 4 Fluoranthene; 5 Pyrene; 6 Chrysene; IS n-Octacosane (C_{28}); 7 Benzo(b)fluoranthene; 8 Benzo(a)pyrene; 9 Benzoperylene.

Finally, Table VIII.7 shows a comparison among different procedures reported in literature for determining PAHs in water samples at levels interesting for water quality evaluation (e.g., US-EPA,WHO) [29,30]: as it can be noted that the methodology developed in this study manages to investigate PAHs at levels lower than the other methods with a good linear range. Further, the use of *iso*-octane overcomes the toxicity problems related to using extraction solvents such as

toluene and carbon tetrachloride. The entire procedure is very easy and it does not require particular technology (e.g., use of hollow-fiber) or disperser solvent.

Table VIII.7. Comparison among different extraction methodologies for determining PAHs in water samples (a: solid-phase microextraction; b: headspace solid-phase microextraction; c: hollow-fiber liquid phase microextraction; d: dispersive liquid-liquid microextraction; e: dispersive liquid-liquid microextraction based on solidification of floating organic drop; f: ultrasound-assisted emulsification microextraction; g: up-and-down shaker-assisted dispersive liquid-liquid microextraction; h: water with low concentration of surfactant in dispersed solvent-assisted emulsion dispersive liquid-liquid microextraction; i: ultrasound-assisted dispersive liquid-liquid microextraction).

PAHs	Method	Solvent	Linear range ($\mu g\ L^{-1}$)	LOD ($\mu g\ L^{-1}$)	REF
16	SPME[a]-GC-MS	----	0.01-10	0.001-0.029	[25]
11	HSPME[b]-GC-FID	----	0.1-50	0.03-0.3	[26]
13	HF-LPME[c]-GC-MS	Toluene	10.0-2000	0.01-0.95	[27]
16	DLLME[d]-GC-FID	CCl_4	0.02-200	0.007-0.03	[17]
5	DLLME-SFO[e]-HPLC-VWD	1-Dodecanol	0.1-500	0.045-1.3	[28]
9	USAEME[f]-GC-FID	Toluene	0.05-100	0.02-0.05	[29]
11	UDSA-DLLME[g]-GC-MS	Heptanol	0.08-100	0.022-0.060	[9]
11	WLSEME[h]-GC-MS	Nonanol	0.08-100	0.022-0.060	[9]
9	USA-DLLE[i]-GC-IT/MS	*iso*-Octane	0.01-500	0.001-0.009	This study

Application to real surface water samples

The entire procedure has been applied to nine surface water samples collected in different areas of Molise and Campania regions. Table VIII.8 reports the PAH levels determined in the nine samples: five tap water samples, (A-E, *Molise and Campania*), two spring water samples (F,G, *Campania*), one surface river water sample (H, *Campania*) and one sample collected at the tap water vending machine (I, *Campania*).

Table VIII.8. PAH profile (pg μL^{-1}) determined in different real samples. A, B, C, D, E: tap water samples; F, G: spring water samples; H: surface river water; I: sample collected at the tap water vending machine (three replicates).

PAHs	A	B	C	D	E	F	G	H	I
Fluorene	0.12 ± 0.01	0.13 ± 0.02	0.07 ± 0.01	0.31 ± 0.05		0.08 ± 0.00	0.23 ± 0.03	0.06 ± 0.01	
Phenanthrene				0.16 ± 0.03			0.02 ± 0.00		
Anthracene	0.23 ± 0.02	0.13 ± 0.03	0.04 ± 0.00	0.12 ± 0.02		0.13 ± 0.01	0.27 ± 0.02		
Fluoranthene				0.06 ± 0.01					
Pyrene				0.02 ± 0.00					
Chrysene		0.06 ± 0.01		0.16 ± 0.05		0.55 ± 0.07		0.04 ± 0.00	
Benzo(b)fluoranthene		0.05 ± 0.00		0.07 ± 0.01		0.52 ± 0.08		0.03 ± 0.00	
Benzo(a)pyrene	0.17 ± 0.03	0.24 ± 0.03	0.18 ± 0.02	0.24 ± 0.03	0.12 ± 0.02	0.29 ± 0.03	0.26 ± 0.04	0.02 ± 0.00	0.08 ± 0.01
Benzoperylene	0.04 ± 0.00	0.31 ± 0.04	0.11 ± 0.03	0.30 ± 0.02	0.12 ± 0.03	0.58 ± 0.07	0.13 ± 0.03	0.10 ± 0.02	0.06 ± 0.01

As can be seen in Table VIII.8, only the tap water sample (D), shows the entire PAH profile (Fluorene, Anthracene, Phenanthrene, Fluoranthene, Pyrene, Chrysene, Benzo(b)fluoranthene, Benzo(a)pyrene, Benzoperylene) with levels ranging between 0.02 pg μL^{-1} (Pyrene) and 0.31 pg

μL^{-1} (Fluorene). As for the compounds Benzo(a)pyrene and Benzoperylene, they are present in all the samples at levels ranging between 0.02 and 0.29 pg μL^{-1} and 0.04–0.58 pg μL^{-1}, respectively, whereas Fluoranthene and Pyrene are present only in one sample (D) at 0.06 pg μL^{-1} and 0.02 pg μL^{-1}, respectively. The PAH carcinogenicity is expressed as a function of the Benzo(a)pyrene level, the more toxic compounds: considering that the Benzo(a)pyrene LD_{50} is 50 mg kg^{-1}, the BaP concentrations found in the nine samples are not toxicologically relevant (below 0.29 pg μL^{-1}).

VIII.4 Conclusions

The important aspects of the proposed method are: 1) the occurring emulsification, in the extraction technique, without the addition of a dispersive solvent but by means of ultrasound, 2) the breaking emulsion occurring without the use of centrifuge to separate the two phases but with the addition of NaCl and 3) the high sensitivity that we managed to reach. The developed method is very sensitive; it allows performing PAHs determinations with a very high pre-concentration factor, up to 10,000 times. Starting from a 1 L surface water sample and reaching a final volume of 100 µL, the method allows the PAHs determination at very low concentrations. Further, it should be considered that large volume sampling can be encountered in the on-line combination of sample pre-treatment and chromatographic analysis with different and high advantages of coupling of sample pre-treatment and chromatographic analysis. Moreover, the method is simple, reproducible and cost-effective; therefore it can be proposed as methodological analysis protocol for analyzing such compounds in water matrix. As a whole this study permits to provides very good correlation coefficients ($R^2 > 0.99$) in the range investigated, LODs and LOQs able to analyze such compounds in any water matrix (0.001–0.009 pg μL^{-1} and 0.003–0.022 pg μL^{-1}, respectively), recoveries between 97 and 106%, inter- and intra-day precisions below 6.0% and 8.2%, respectively, for all PAHs [31]. An important future perspective is to extend the proposed approach to other micro-pollutants as well as to other food matrices.

References

[1] Hawthorne SB, Azzolina NA, Neuhauser EF, Kreitinger JP. Predicting bioavailability of sediment polycyclic aromatic hydrocarbons to Hyalella azteca using equilibrium partitioning, supercritical fluid extraction, and pore water concentrations. Environ. Sci. Technol. 2007;41:6297-304.

[2] Rawa-Adkonis M, Wolska L, Przyjazny A, Namieśnik J. Sources of errors associated with the determination of PAH and PCB analytes in water samples. Anal. Lett. 2006;39:2317-31.

[3] Lee K-W, Shim WJ, Yim UH, Kang J-H. Acute and chronic toxicity study of the water accommodated fraction (WAF), chemically enhanced WAF (CEWAF) of crude oil and dispersant in the rock pool copepod Tigriopus japonicus. Chemosphere 2013;92:1161-8.

[4] Burkhardt MR, ReVello RC, Smith SG, Zaugg SD. Pressurized liquid extraction using water/isopropanol coupled with solid-phase extraction cleanup for industrial and anthropogenic waste-indicator compounds in sediment. Anal. Chim. Acta 2005;534:89-100.

[5] Hawthorne SB, Miller DJ, Kreitinger JP. Measurement of total polycyclic aromatic hydrocarbon concentrations in sediments and toxic units used for estimating risk to benthic invertebrates at manufactured gas plant sites. Environ. Toxicol. Chem. 2006;25:287-96.

[6] Yang C, Zhang G, Wang Z, Yang Z, Hollebone B, Landriault M, et al. Development of a methodology for accurate quantitation of alkylated polycyclic aromatic hydrocarbons in petroleum and oil contaminated environmental samples. Anal. Methods 2014;6:7760-71.

[7] Eichelberger J, Behymer T, Budde W. Determination of organic compounds in drinking water by liquid–solid extraction and capillary column gas chromatography/mass spectrometry. US EPA Method 1988;525:325-56.

[8] Environmental PAE. National primary drinking water regulations: Long Term 1 Enhanced Surface Water Treatment Rule. Final rule. Fed. Regist. 2002;67:1811.

[9] Prabhukumar G, Pagilla K. Polycyclic aromatic hydrocarbons in urban runoff–sources, sinks and treatment: A review. Department of Civil, Architectural and Environmental Engineering, Chicago 2010.

[10] Brum DM, Cassella RJ, Netto ADP. Multivariate optimization of a liquid–liquid extraction of the EPA-PAHs from natural contaminated waters prior to determination by liquid chromatography with fluorescence detection. Talanta 2008;74:1392-9.

[11] Marcé R, Borrull F. Solid-phase extraction of polycyclic aromatic compounds. J. Chromatogr. A 2000;885:273-90.

[12] Tseng W-C, Chen P-S, Huang S-D. Optimization of two different dispersive liquid–liquid microextraction methods followed by gas chromatography–mass spectrometry determination for polycyclic aromatic hydrocarbons (PAHs) analysis in water. Talanta 2014;120:425-32.

[13] Yan J, Kim M, Haberl M, Kwok H, Brunswick P, MacInnis C, et al. Determination of polycyclic aromatic hydrocarbons in surface water using simplified liquid–liquid micro-extraction and pseudo-MRM GC/MS/MS. Anal. Methods 2018.

[14] Kafilzadeh F, Shiva AH, Malekpour R. Determination of polycyclic aromatic hydrocarbons (PAHs) in water and sediments of the Kor River, Iran. Middle-East J. Sci. Res. 2011;10:01-7.

[15] Manoli E, Samara C. Polycyclic aromatic hydrocarbons in waste waters and sewage sludge: extraction and clean-up for HPLC analysis with fluorescence detection. Chromatographia 1996;43:135-42.

[16] Ma J, Xiao R, Li J, Yu J, Zhang Y, Chen L. Determination of 16 polycyclic aromatic hydrocarbons in environmental water samples by solid-phase extraction using multi-walled carbon nanotubes as adsorbent coupled with gas chromatography–mass spectrometry. J. Chromatogr. A 2010;1217:5462-9.

[17] King A, Readman J, Zhou J. Determination of polycyclic aromatic hydrocarbons in water by solid-phase microextraction–gas chromatography–mass spectrometry. Anal. Chim. Acta 2004;523:259-67.

[18] Kurek J, Kirk JL, Muir DC, Wang X, Evans MS, Smol JP. Legacy of a half century of Athabasca oil sands development recorded by lake ecosystems. Proc. Natl. Acad. Sci. 2013;110:1761-6.

[19] Liu J-f, Jiang G-b, Chi Y-g, Cai Y-q, Zhou Q-x, Hu J-T. Use of ionic liquids for liquid-phase microextraction of polycyclic aromatic hydrocarbons. Anal. Chem. 2003;75:5870-6.
[20] Jeannot MA, Cantwell FF. Solvent microextraction into a single drop. Anal. Chem. 1996;68:2236-40.
[21] Zhao L, Lee HK. Liquid-phase microextraction combined with hollow fiber as a sample preparation technique prior to gas chromatography/mass spectrometry. Anal. Chem. 2002;74:2486-92.
[22] Sanagi MM, Loh SH, Wan Ibrahim WA, Hasan MN, Aboul Enein HY. Determination of polycyclic aromatic hydrocarbons in fresh milk by hollow fiber liquid-phase microextraction–gas chromatography mass spectrometry. J. Chromatogr. Sci. 2012;51:112-6.
[23] Jiang X, Lee HK. Solvent bar microextraction. Anal. Chem. 2004;76:5591-6.
[24] Rezaee M, Assadi Y, Hosseini M-RM, Aghaee E, Ahmadi F, Berijani S. Determination of organic compounds in water using dispersive liquid–liquid microextraction. J. Chromatogr. A 2006;1116:1-9.
[25] Pena MT, Casais MC, Mejuto MC, Cela R. Development of an ionic liquid based dispersive liquid–liquid microextraction method for the analysis of polycyclic aromatic hydrocarbons in water samples. J. Chromatogr. A 2009;1216:6356-64.
[26] Knoll JE. Estimation of the limit of detection in chromatography. J. Chromatogr. Sci. 1985;23:422-5.
[27] Russo MV, Notardonato I, Avino P, Cinelli G. Fast determination of phthalate ester residues in soft drinks and light alcoholic beverages by ultrasound/vortex assisted dispersive liquid–liquid microextraction followed by gas chromatography-ion trap mass spectrometry. RSC Adv. 2014;4:59655-63.
[28] Russo MV, Avino P, Perugini L, Notardonato I. Extraction and GC-MS analysis of phthalate esters in food matrices: a review. RSC Adv. 2015;5:37023-43.
[29] USEPA U. Environmental Protection Agency, National primary drinking water regulation. Fed. Regist. 2001;66:69-85.
[30] Orecchio S, Papuzza V. Levels, fingerprint and daily intake of polycyclic aromatic hydrocarbons (PAHs) in bread baked using wood as fuel. J. Hazard. Mater. 2009;164:876-83.
[31] Avino P, Notardonato I, Perugini L, Russo MV. New protocol based on high-volume sampling followed by DLLME-GC-IT/MS for determining PAHs at ultra-trace levels in surface water samples. Microchem. J. 2017;133:251-7.

Acknowledgements

This thesis work has involved me for a period of about three years so there are many people I would like to thank.

Firstly, I would like to express my sincere gratitude to my supervisor, Prof. Francesco Lopez, and my co-supervisor, Dr. Francesca Cuomo. They were the people who guided me during my PhD course and the people who allowed me to grow up, not only on a professional level but also on a personal one. Thanks to their enthusiasm, constant availability and positive energy with which they work, they transmitted me the passion and love for the research sector in which I hope I can continue to work.

Besides my supervisor and co-supervisor, I would like to thank Prof. Mario Vincenzo Russo for introducing me to the PhD course and my coordinator, Prof. Giuseppe Maiorano, for his patience and availability.

My sincere thanks also goes to other people who work in the laboratory, particularly Martina Cofelice, friend and colleague, and Dr. Giuseppe Cinelli for his valuable advice.

Last but not the least, I would like to thank my family. This thesis work is dedicated to them: to my sister for always encouraging me and to my father and my mother for moral and economic support they offered me throughout my university career.

List of papers regarding the thesis

- Extraction and GC-MS analysis of phtalate esters in food matrices: a review.
  Mario V. Russo, Pasquale Avino, **Luisa Perugini**, Ivan Notardonato
  RSC Advances (2015) Volume 5, pages 37023-37043.

- New protocol based on high-volume sampling followed by DLLME-GC-IT/MS for determining PAHs at ultra-trace levels in surface water samples.
  Pasquale Avino, Ivan Notardonato, **Luisa Perugini**, Mario V. Russo
  Microchemical Journal (2017) Volume 133, pages 251-257.

- Effect of the coexistence of sodium caseinate and Tween 20 as stabilizers of food emulsions at acidic pH.
  Luisa Perugini, Giuseppe Cinelli, Martina Cofelice, Andrea Ceglie, Francesco Lopez, Francesca Cuomo
  Colloids and surfaces B (2018), 10.1016/j.colsurfb.2018.02.003.

- Effect of nanoemulsion stabilizers on the in vitro digestion of curcumin.
  Luisa Perugini, Francesco Lopez, Emanuele Marconi, Maria Cristina Messia, Francesca Cuomo
  Food Research International*, submitted.*

Other papers

- Fast analysis of nine PAHs in beer by Ultrasound-Vortex-Assisted Dispersive Liquid Liquid Micro-extraction coupled with Gas Chromatography-Ion Trap Mass Spectrometry.
  Mario V. Russo, Pasquale Avino, **Luisa Perugini**, Ivan Notardonato
  RSC Advances (2016) Volume 6, pages 13920-13927.